Bordered Heegaard Floer Homology and Graph Manifolds

Jonathan Hanselman

Submitted in partial fulfillment of the
requirements for the degree
of Doctor of Philosophy
in the Graduate School of Arts and Sciences

COLUMBIA UNIVERSITY

2014

ABSTRACT

Bordered Heegaard Floer Homology and Graph Manifolds

Jonathan Hanselman

We use the techniques of bordered Heegaard Floer homology to investigate the Heegaard Floer homology of graph manifolds. Bordered Heegaard Floer homology allows us to split a graph manifold into pieces and perform computations for each piece separately. The resulting invariants can then be combined by a simple algebraic procedure to recover $\widehat{HF}$. Graph manifolds by definition decompose into pieces which are S^1-bundles over surfaces. This decomposition makes them particularly well suited to the divide-and-conquer techniques of bordered Heegaard Floer homology. In fact, the problem reduces to computing bordered Heegaard Floer invariants of just two pieces. The first invariant is the type D trimodule associated to the trivial S^1-bundle over the pair of pants $\mathcal{P}$. The second is a bimodule that is necessary for self-gluing, when two torus boundary components of a bordered manifold are glued to each other. We explicitly compute both of these multimodules. We then describe an algorithm for computing $\widehat{HF}$ of any graph manifold using these results. The algorithm has been implemented in Python, and we give some example computations. We also use this algorithm to inductively prove that the bordered invariants of graph manifolds with torus boundary have a particularly simple form when the plumbing graphs are trees with no bad vertices.

Table of Contents

List of Figures

List of Tables

Acknowledgements

To begin, I would like express my sincerest thanks to my advisor Robert Lipshitz for his continual support and guidance. He selflessly made himself available to me no matter how busy or far away he was. I have learned much more with his help than I could have on my own. I thank him for suggesting this research project, and for many helpful suggestions along the way. I am also thankful for his feedback on drafts of this thesis. Most of all I am thankful for his consistent encouragement, which helped me to maintain my excitement for mathematics through the challenges of grad school.

I thank Peter Ozsváth, Walter Neumann, Mohammed Abouzaid, and Jen Hom for their interest in my work and for serving on my thesis committee. I am grateful for their helpful comments and questions.

I have had the pleasure of working with a vibrant topology group at Columbia University. I have learned a great deal of mathematics here, largely because those around me were always pleased to share their knowledge patiently. Particular thanks go to Dylan Thurston, Adam Knapp, Peter Horn, Shea Vela-Vick, Ben Elias, Rumen Zarev, Harold Sultan, Ina Petkova, Kristen Hendricks, Andre Carneiro, Corrin Clarkson, Krzysztof Putyra, Rob Castellano, Jingyu Zhao, and Mike Wong. I am also very grateful to Adam Levine, Matt Hedden, Liam Watson, John Baldwin, Tye Lidman, and others who took an interest in my work, and with whom I have had helpful mathematical conversations.

I thank my parents, Paul and Cheryl Hanselman, and my brother Paul for their unwavering love, support and encouragement throughout my education. Finally, I thank my wife Emily, who has continually encouraged me and infused my life with joy.

To my parents

Chapter 1

Introduction

Heegaard Floer homology is a collection of invariants for closed 3-manifolds introduced by Ozsváth and Szabó [23]. In its simplest form, Heegaard Floer homology associates to a closed 3-manifold Y a graded $\mathbb{Z}_2$ vector space $\widehat{HF}(Y)$. The package also contains invariants for 4-dimensional cobordisms and for knots and links [22, 24, 30]. Heegaard Floer homology has proved to be a powerful tool for understanding 3-manifolds. However, in general it is difficult to compute. The definition involves a chain complex whose generators are combinatorial but whose differential requires counting pseudo-holomorphic curves.

In principle Heegaard Floer homology is algorithmically computable. Sarkar and Wang developed an algorithm using sufficiently well behaved Heegaard diagrams, called *nice diagrams* [31]; this method has since been refined and extended [3, 20, 28]. Any Heegaard diagram can be isotoped to a nice diagram, and for such a diagram computing the differential in the Heegaard Floer chain complex is combinatorial. However, making a diagram nice comes at the cost of introducing many additional generators. In practice, the large number of generators often makes computation intractable. Another approach uses grid diagrams, which simplify the computation of Heegaard Floer invariants for knots and links. Using surgery formulas and an appropriate grid diagram, Heegaard Floer homology can be computed by realizing a 3-manifold as surgery on a link [13–15].

A third algorithm is based on computing the bordered Heegaard Floer invariant for the surface diffeomorphism associated with a Heegaard splitting [10]. Of these algorithms, only the third is practical enough to have been implemented on a computer, and in its current form it can only compute for Heegaard splittings of genus at most 2. This allows computations for many interesting manifolds, but ultimately the class of 3-manifolds which admit genus 2 Heegaard splittings is small. Efficiently computing Heegaard Floer homology for general 3-manifolds remains a difficult problem.

If we restrict to particular classes of 3-manifolds, computing Heegaard Floer homology becomes easier. For example, much is known about the Heegaard Floer homology of manifolds which are obtained by plumbing circle bundles according to a negative definite tree Γ. Ozsváth and Szabó gave a combinatorial description of HF^+ of these manifolds when the tree Γ has at most one "bad" vertex [21]. This class of manifolds includes all Seifert fibered rational homology spheres. Their algorithm for computing HF^+ has been useful, for instance, in determining the existence of tight contact structures on Seifert fibered spaces [12]. Nemethi introduced another invariant for negative definite plumbings, *lattice homology*, which is combinatorially computable and conjecturally equivalent to HF^+ [17]. Recent work has explored this conjectured equivalence; there is a spectral sequence from lattice cohomology to HF^+, and they are known to be isomorphic for plumbings with at most two bad vertices [25–27].

There has been significant interest in understanding L-spaces, manifolds with minimal Heegaard Floer homology. It is conjectured that the non-minimality of Heegaard Floer homology for a manifold is equivalent to the existence of taut foliations and to left orderability of the fundamental group; this relationship is known to hold for particular classes of 3-manifolds, including Seifert fibered manifolds [1, 29]. These geometric conditions can help us determine the L-space condition of a manifold even if we can not compute $\widehat{HF}$ directly. Mauricio used lattice homology and the existence of taut foliations to give sufficient conditions on the weights of a negative definite tree Γ under which a plumbing is or is not an L-space [16].

The plumbings of negative definite trees mentioned above are a special case of graph manifolds. A *graph manifold* is a 3-manifold whose JSJ decomposition contains only Seifert fibered pieces. The non-Seifert fibered pieces in a JSJ decomposition are hyperbolic, so with respect to geometrization a graph manifold is a manifold with no hyperbolic pieces in its geometric decomposition. For a brief overview of graph manifolds and their place in 3-manifold topology, see [19]. In this thesis we present a method for computing $\widehat{HF}$ of any graph manifold.

The key to our approach is bordered Heegaard Floer homology, an extension of Heegaard Floer homology to manifolds with boundary developed by Lipshitz, Ozsváth, and Thurston in [8] and [9]. Bordered Heegaard Floer homology allows us to break a closed 3-manifold Y into pieces and compute invariants for each piece. $\widehat{HF}(Y)$ can be recovered from the respective bordered invariants through a straightforward operation, the box tensor product. In fact, for graph manifolds computing $\widehat{HF}$ reduces to computing bordered invariants for just two pieces. Along with mapping cylinders of Dehn twists, whose bordered invariants are already known, these pieces can be combined to make any graph manifold.

This method finds a middle ground between the approaches mentioned above. It is more general than results restricted to negative definite plumbing trees, since it works for arbitrary graph manifolds. At the same time, it is more computationally practical than current algorithms for general 3-manfiolds. There is a computer implementation of this algorithm that is capable of handling quite complicated manifolds; it can been used, for instance, to see that the rank of $\widehat{HF}$ of the graph manifold represented by the weighted tree in Figure 20 is 213,312.

We recall here some important facts and terminology concerning graph manifolds; we will follow the notation found in [18]. A graph manifold can be encoded by a decorated graph:

Definition 1.0.1. A *connected closed plumbing graph* is a finite connected graph Γ dec-

orated as follows:

- each vertex i carries two integer weights g_i and e_i;
- each edge carries a sign, $+$ or $-$.

We allow Γ to have multiple edges connecting two vertices or edges connecting a vertex to itself.

A connected closed plumbing graph Γ specifies a (prime) graph manifold $M(\Gamma)$ as follows: For each vertex i of Γ, let d_i be the degree of the vertex. Let F_i be the compact surface of genus g_i with d_i boundary components, where if $g_i < 0$ we mean that F_i is nonorientable of genus $|g_i|$. Let E_i be the circle bundle with orientable total space over F_i with a chosen trivialization on the boundary and euler number e_i (the euler number is well defined once the trivialization on the boundary is chosen). The edges of Γ dictate how the E_i are glued together. For each edge connecting vertices i and j, a component $S^1 \times S^1$ of ∂E_i is glued to a component $S^1 \times S^1$ of ∂E_j. The gluing always exchanges base and fiber directions; for $(+)$-edges the gluing map is $\begin{pmatrix} 0 & 1 \\ 1 & 0 \end{pmatrix}$, and for $(-)$-edges the gluing map is $\begin{pmatrix} 0 & -1 \\ -1 & 0 \end{pmatrix}$. In either case the gluing map is orientation reversing, and so $M(\Gamma)$ inherits consistent orientations from all of the E_i. For each edge connecting a vertex i to itself, two components of ∂E_i are glued with the appropriate gluing map.

Every prime graph manifold can be represented by a connected closed plumbing graph (for non-prime graph manifolds we allow disconnected graphs). The representation is not unique, but [18, Section 4] gives a well developed calculus for manipulating plumbing graphs. In particular, plumbing graphs can be reduced to a normal form, and graphs of this form represent manifolds uniquely. A few additional facts are worth mentioning here:

- Changing the sign of an edge often does not change the resulting 3-manifold. In fact, all that matters is the total sign around each loop in Γ. In particular, for acyclic graphs we may ignore the decoration on the edges.

- It is possible to represent any graph manifold with a plumbing graph such that no vertex is assigned a negative genus.

- We can describe graph manifolds with boundary by adding an additional weight b_i to each vertex i. In the construction, F_i is the genus g_i surface with $b_i + d_i$ boundary components. E_i is the appropriate circle bundle over F_i, and b_i components of ∂E_i are not glued to anything.

Because graph manifolds decompose so nicely, bordered Heegaard Floer homology provides a natural approach for computing their $\widehat{HF}$. The key ingredient is to compute the bordered invariants for arbitrary S^1-bundles over surfaces, the building blocks of graph manifolds. Changing the euler number of one of these bundles is equivalent to changing the parametrization of the boundary, which can be accomplished by tensoring with the well understood bimodules for mapping classes of the torus [9, Section 10.2]. As a result, we only need to compute invariants for trivial bundles over surfaces. As noted above, it is sufficient to consider bundles over orientable surfaces. Furthermore, any orientable surface has a pants decomposition—it can be obtained by gluing together copies of the pair of pants $\mathcal{P} = S^3 \backslash \{\text{three open disks}\}$. The trivial S^1-bundle over the surface can be obtained by gluing copies of the trivial S^1-bundle over $\mathcal{P}$. Thus we see that the trivial bundle $\mathcal{Y}_\mathcal{P} = \mathcal{P} \times S^1$ is the fundamental building block for graph manifolds.

In Chapter 2 we will review the relevant background from bordered Heegaard Floer homology. In Section 2.7, in particular, we collect several lemmas that will be used for the the computations in the following chapters. The trimodule $\widehat{CFD^3}(\mathcal{Y}_\mathcal{P})$ will be explicitly computed in Chapter 3, proving the following:

Theorem 1. *The summand of the type D trimodule $\widehat{CFD^3}(\mathcal{Y}_\mathcal{P})$ in the middle spin^c-structure has five generators as a projective module: v, w, x, y, and z. Up to quasi-isomorphism, the differential is given by the following diagram:*

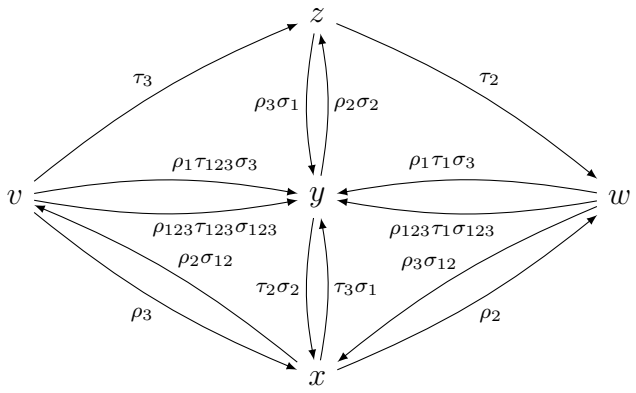

$\widehat{CFD^3}(\mathcal{Y}_\mathcal{P})$ in the other spin^c-structures will also be computed. For acyclic plumbing graphs with only genus zero vertices, $\widehat{HF}$ of the corresponding graph manifold can be obtained from the trimodule in Theorem 1 and bimodules for mapping classes of the torus. If the graph has a cycle or some vertex has genus $g_i > 0$, then an additional bimodule is needed. A bordered Heegaard diagram for this bimodule was described in [11, Section 4.4], but the bimodule was not computed. In Chapter 4 we explicitly compute this bimodule, using the bordered Heegaard diagram $\mathcal{H}_{SG}$ in Figure 11.

Theorem 2. *The bimodule $\widehat{CFDD}(\mathcal{H}_{SG})$ in the middle spin^c-structure is given by Figure 16. In the extremal spin^c-structures, it is quasi-isomorphic to zero.*

Given an arbitrary plumbing graph, Chapter 5 will describe the procedure for piecing together the relevant bordered invariants to obtain $\widehat{HF}$ of the corresponding graph manifold. We give the results of a few example computations performed by a computer implementation of this algorithm. Finally, we use this method to inductively prove a structure theorem for the bordered invariants of one-boundary graph manifolds satisfying certain conditions on their vertices. Specifically, we show that for graph manifolds with no bad vertices and with torus boundary, the bordered module $\widehat{CFD}$ breaks into loops that only contain the arrows ρ_1, ρ_3, and ρ_{23}.

Chapter 2

Bordered Heegaard Floer homology

We begin by recalling the essential definitions and properties concerning the bordered Heegaard Floer invariants developed by Lipshitz, Ozsváth, and Thurston. For a full treatment of these invariants, see [8], [9]. We discuss only the details that will be needed in the rest of this thesis. In particular, we restrict to the case of manifolds with toroidal boundary components, which simplifies many of the definitions.

2.1 Algebraic definitions

Let $(\mathcal{A}, d)$ be a unital differential algebra over $\mathbb{F}_2$, with a subring of idempotents $\mathcal{I}$, and let $\{\iota_i\}$ be an orthogonal basis for $\mathcal{I}$, with $\mathbf{1} = \sum \iota_i$.

A *(left) type D structure over* $\mathcal{A}$ is a vector space N over $\mathbb{F}_2$ with a left action of $\mathcal{I}$ and a map

$$\delta_1 : N \to \mathcal{A} \otimes_{\mathcal{I}} N$$

satisfying the relation

$$(\mu \otimes id_N) \circ (id_{\mathcal{A}} \otimes \delta_1) \circ \delta_1 + (d \otimes id_N) \circ \delta_1 = 0, \tag{2.1}$$

where $\mu : \mathcal{A} \otimes \mathcal{A} \to \mathcal{A}$ is multiplication on $\mathcal{A}$. The tensor product $\mathcal{A} \otimes_{\mathcal{I}} N$ is a left differential $\mathcal{A}$ module, with module structure $a \cdot (b \otimes x) = ab \otimes x$ and differential given

by $\partial(a \otimes x) = a \cdot \delta_1(x) + d(a) \otimes x$. The relation (2.1) ensures that $\partial^2 = 0$. Given the map δ_1, define

$$\delta_k : N \to \underbrace{\mathcal{A} \otimes_{\mathcal{I}} \cdots \otimes_{\mathcal{I}} \mathcal{A}}_{\text{k times}} \otimes_{\mathcal{I}} N$$

inductively by $\delta_0 = \mathrm{id}_N$ and $\delta_k = (\mathrm{id}_{\mathcal{A}^{\otimes k-1}} \otimes \delta_1) \circ \delta_{k-1}$ for $k > 0$. We say that the type D structure N is *bounded* if $\delta_k = 0$ for all k sufficiently large.

We will need to work with modules with multiple left actions. Let $\mathcal{A}_1, \cdots, \mathcal{A}_k$ be differential algebras, with rings of idempotents $\mathcal{I}_1, \ldots, \mathcal{I}_k$. A *$k$-fold type D structure over $\mathcal{A}_1, \ldots, \mathcal{A}_k$* is a type D structure over $\mathcal{A}_1 \otimes \cdots \otimes \mathcal{A}_k$. We will call the module $(\mathcal{A}_1 \otimes \cdots \otimes \mathcal{A}_k) \otimes_{(\mathcal{I}_1 \otimes \cdots \otimes \mathcal{I}_k)} N$ a *type D multimodule over $\mathcal{A}$*.

A *(right) $\mathcal{A}_\infty$ module (or type A structure) over $\mathcal{A}$* is a vector space M over $\mathbb{F}_2$ with a right action of $\mathcal{I}$ and maps

$$m_{k+1} : M \otimes_{\mathcal{I}} \underbrace{\mathcal{A} \otimes_{\mathcal{I}} \cdots \otimes_{\mathcal{I}} \mathcal{A}}_{\text{k times}} \to M$$

satisyfing the folowing $\mathcal{A}_\infty$ relation for any $x \in M$ and any $a_1, \ldots a_n \in \mathcal{A}$:

$$\begin{aligned} 0 = &\sum_{i=0}^{n} m_{n-i+1}\big(m_{i+1}(x, a_1, \ldots, a_i), a_{i+1}, \ldots, a_n\big) \\ &+ \sum_{i=1}^{n-1} m_n\big(x, a_1, \ldots, a_{i-1}, \mu(a_i, a_{i+1}), a_{i+2}, \ldots, a_n\big) \\ &+ \sum_{i=1}^{n} m_{n+1}\big(x, a_1, \ldots, a_{i-1}, d(a_i), a_{i+1}, \ldots, a_n\big). \end{aligned} \tag{2.2}$$

An informal statement of the $\mathcal{A}_\infty$ relations may be easier to remember: for any ordered set of inputs, the sum of all ways of combining those inputs using two steps (where each step is μ, d, or some m_i) is zero. We also require that $m_2(x, \mathbf{1}) = x$ and $m_k(x, \ldots, \mathbf{1}, \ldots) = 0$ for all $k > 2$. If $m_k = 0$ for all sufficiently large k, we say that the $\mathcal{A}_\infty$ module M is *bounded*.

More generally, we can define an *$\mathcal{A}_\infty$ multimodule M over $\mathcal{A}_1, \ldots, \mathcal{A}_k$* as follows: M is a vector space over $\mathbb{F}_2$ with a right action of $\mathcal{I}_1 \otimes \cdots \otimes \mathcal{I}_k$. M is also equipped with

maps

$$m_{1,i_1,\dots,i_k} : M \bigotimes_{\mathcal{I}_1\otimes\cdots\otimes\mathcal{I}_k} \mathcal{A}_1^{\otimes i_1}\otimes\cdots\otimes\mathcal{A}_k^{\otimes i_k} \to M$$

satisfying an appropriate version of the $\mathcal{A}_\infty$ relation (we will generally suppress the subscripts on m from the notation). To define the relation, we introduce the following functions. For $\vec{a}_\ell = (a_\ell^1,\dots,a_\ell^k) \in \mathcal{A}_\ell^{\otimes k}$ and $0 \le j \le k$, define

$$\begin{aligned}
T_j(\vec{a}_\ell) &:= \left(a_\ell^1,\dots,a_\ell^j\right) \in \mathcal{A}_\ell^{\otimes j}\\
T^j(\vec{a}_\ell) &:= \left(a_\ell^{j+1},\dots,a_\ell^k\right) \in \mathcal{A}_\ell^{\otimes k-j}\\
\bar{\mu}(\vec{a}_\ell) &:= \sum_{j=1}^{k-1}\left(a_\ell^1,\dots,a_\ell^{j-1},a_\ell^j a_\ell^{j+1},a_\ell^{j+2},\dots,a_\ell^k\right) \in \mathcal{A}_\ell^{\otimes k-1}\\
\bar{d}(\vec{a}_\ell) &:= \sum_{j=1}^{k}\left(a_\ell^1,\dots,a_\ell^{j-1},d(a_\ell^j),a_\ell^{j+1},\dots,a_\ell^k\right) \in \mathcal{A}_\ell^{\otimes k}.
\end{aligned}$$

Now we can write down the $\mathcal{A}_\infty$ relation for multimodules. For any $x \in M$ and any $\vec{a}_1,\dots,\vec{a}_k$ in $\mathcal{A}^{\otimes i_1},\dots,\mathcal{A}^{\otimes i_k}$, we have

$$\begin{aligned}
0 = &\sum_{j_1,\dots,j_k} m\big(m(x,T_{j_1}(\vec{a}_1),\dots,T_{j_k}(\vec{a}_k)),T^{j_1}(\vec{a}_1),\dots,T^{j_k}(\vec{a}_k)\big)\\
&+\sum_{j=1}^{k} m(x,\vec{a}_1,\dots,\vec{a}_{j-1},\bar{\mu}(\vec{a}_j),\vec{a}_{j+1},\dots,\vec{a_k})\\
&+\sum_{j=1}^{k} m\big(x,\vec{a}_1,\dots,\vec{a}_{j-1},\bar{d}(\vec{a}_j),\vec{a}_{j+1},\dots,\vec{a_k}\big).
\end{aligned} \tag{2.3}$$

It is possible to define combination multimodules, with some type D actions and some type A actions. Such a multimodule N is equipped with maps

$$\delta_1^{1,i_{k+1},\dots,i_\ell} : N\otimes\mathcal{A}_1^{\otimes i_{k+1}}\otimes\cdots\otimes\mathcal{A}_k^{\otimes i_\ell} \longrightarrow \mathcal{A}_{k+1}\otimes\cdots\otimes\mathcal{A}_{k+\ell}\otimes N$$

satisfying the appropriate versions of (2.1) and (2.3). Type DD, AA, and DA bimodules are discussed in [9], and the generalization to more algebra actions is straightforward.

If M is an $\mathcal{A}_\infty$ module over $\mathcal{A}$ and N is a type D module over $\mathcal{A}$, and if at least one of them is bounded, we may define the *box tensor product* $M\boxtimes N$ to be the vector space

$M \otimes_{\mathcal{I}} N$ equipped with the differential

$$\partial^{\boxtimes}(x \otimes y) = \sum_{k=0}^{\infty} (m_{k+1} \otimes \mathrm{id}_N)(x \otimes \delta_k(y)).$$

If M is a multimodule over $\mathcal{A}_1, \cdots, \mathcal{A}_k$ such that the action of $\mathcal{A}_k$ is type A, and N is a multimodule over $\mathcal{A}_k, \mathcal{A}_{k+1}, \ldots, \mathcal{A}_{k+\ell}$ such that the action of $\mathcal{A}_k$ is type D, and either M or N is bounded, then a box tensor product with respect to $\mathcal{A}_k$ can be defined in a similar way (see [9, Section 2.3.2] for the case when N and M are bimodules). $M \boxtimes_{\mathcal{A}_k} N$ is a multimodule over $\mathcal{A}_1, \ldots, \mathcal{A}_{k-1}, \mathcal{A}_{k+1}, \ldots, \mathcal{A}_{k+l}$, and the operations on $M \boxtimes N$ are determined by pairing operations on M with sequences of operations in N such that the A_k outputs of the operations on N match the A_k inputs of the operation on M.

Remark 2.1.1. We will often represent a k-fold type D multimodule M as a labeled, directed graph, where vertices correspond to the generators of M, and there is an arrow from x_i to x_j labeled by a_{ij} if $a_{ij} \neq 0$ is the coefficient of x_j in $\partial(x_i)$. Here a_{ij} is an element of $\mathcal{A}_1 \otimes \cdots \otimes \mathcal{A}_k$, the tensor product of k copies of the torus algebra. We omit the edge label when $a_{ij} = 1$. We sometimes refer to an unlabeled arrow from x_i to x_j as a *differential* from x_i to x_j. Graphs with unlabeled edges can be simplified by a well known edge reduction algorithm [6, Section 2.6]: we eliminate the endpoints x_i and x_j of the unlabeled edge and all edges attached to these two vertices, and for each "zig-zag"

$$x_k \xrightarrow{a_{kj}} x_j \longleftarrow x_i \xrightarrow{a_{i\ell}} x_\ell$$

we add an edge

$$x_k \xrightarrow{a_{kj}a_{i\ell}} x_\ell,$$

or if there is already an edge from x_k to x_ℓ we add $a_{kj}a_{i\ell}$ to the label of that edge. The resulting graph represents a type D multimodule that is quasi-isomorphic to M.

2.2 The Torus Algebra

To define bordered Heegaard Floer invariants, we associate a differential algebra to each boundary component of a 3-manifold with boundary. The algebra associated to the torus

splits into a direct sum

$$\mathcal{A}(T^2) = \mathcal{A}(T^2, -1) \oplus \mathcal{A}(T^2, 0) \oplus \mathcal{A}(T^2, 1).$$

$\mathcal{A}(T^2, -1)$ is $\mathbb{F}_2$, and $\mathcal{A}(T^2, 1)$ is quasi-isomorphic to $\mathbb{F}_2$, so we need only discuss $\mathcal{A}(T^2, 0)$.

The algebra $\mathcal{A}(T^2, 0)$ is generated as a vector space over $\mathbb{F}_2$ by eight elements: two idempotents, ι_0 and ι_1, and six Reeb elements $\rho_1, \rho_2, \rho_3, \rho_{12}, \rho_{23}$, and ρ_{123}. The idempotents satisfy $\iota_i \iota_j = \delta_{ij} \iota_i$, and the identity element is $\mathbf{1} = \iota_0 + \iota_1$. The Reeb elements interact with idempotents on either side as follows:

$$\iota_0 \rho_1 = \rho_1 \iota_1 = \rho_1, \quad \iota_1 \rho_2 = \rho_2 \iota_0 = \rho_2, \quad \iota_0 \rho_3 = \rho_3 \iota_1 = \rho_3,$$

$$\iota_0 \rho_{12} = \rho_{12} \iota_0 = \rho_{12}, \quad \iota_1 \rho_{23} = \rho_{23} \iota_1 = \rho_{23}, \quad \iota_0 \rho_{123} = \rho_{123} \iota_1 = \rho_{123}.$$

The only nonzero products of Reeb elements are $\rho_1 \rho_2 = \rho_{12}$, $\rho_2 \rho_3 = \rho_{23}$, and $\rho_1 \rho_{23} = \rho_{12} \rho_3 = \rho_{123}$. Although $\mathcal{A}(T^2)$ is a differential algebra, the differential on $\mathcal{A}(T^2, 0)$ is zero. For more on the torus algebra and how it arises in bordered Heegaard Floer homology, see [8, Sec 11.1].

2.3 Bordered manifolds and bordered diagrams

A bordered 3-manifold with k torus boundary components is an oriented 3-manifold Y with ∂Y a disjoint union of k tori $F_1, \ldots, F_k$, along with diffeomorphisms $\phi_i : T^2 \to F_i$. If ϕ_i is orientation reversing, then the corresponding boundary component is said to be type D; otherwise it is said to be type A. In this thesis, we will deal almost exclusively with type D boundaries.

A bordered 3-manifold can be represented by an arced bordered Heegaard diagram.

Definition 2.3.1. An *arced bordered Heegaard diagram with k (torus) boundary components* is a quadruple $(\Sigma, \boldsymbol{\alpha}, \boldsymbol{\beta}, \mathbf{z})$, where

- Σ is a compact surface of genus g with k boundary components;

- $\boldsymbol{\alpha} = \{\alpha_1^1, \alpha_2^1, \alpha_1^2, \alpha_2^2, \ldots, \alpha_1^k, \alpha_2^k, \alpha_1, \alpha_2, \ldots, \alpha_{g-k}\}$, where α_1^i and α_2^i are arcs embedded in Σ with boundary on the ith component of $\partial\Sigma$ and α_j is an embedded circle in Σ, and the α circles/arcs are pairwise disjoint;
- $\boldsymbol{\beta}$ is g-tuple of disjoint circles in Σ;
- $\mathbf{z}$ is a basepoint z in $\Sigma\backslash(\boldsymbol{\alpha} \cup \boldsymbol{\beta})$ together with arcs in $\Sigma\backslash(\boldsymbol{\alpha} \cup \boldsymbol{\beta})$ connecting z to each boundary component of Σ.

We also require that $\boldsymbol{\alpha}$ and $\boldsymbol{\beta}$ intersect transversely and $\Sigma\backslash\boldsymbol{\alpha}$ and $\Sigma\backslash\boldsymbol{\beta}$ are connected.

An arced bordered Heegaard diagram gives rise to a bordered 3-manifold by attaching 2-handles to a thickened version of the Heegaard surface Σ. The one and two boundary cases are described in Constructions 5.3 and 5.6 of [9], and the construction for more boundary components is completely analogous.

To define bordered invariants, we will also need to equip a bordered Heegaard diagram with labels on the boundary, as in Figure 1. Each component of $\partial\Sigma$ is divided into four segments by the arcs α_1^i and α_2^i, with one containing a basepoint, an endpoint of an arc in $\mathbf{z}$. Progressing from the basepointed segment in the direction which agrees with the boundary orientation on $\partial\Sigma$, we label the three remaining segments on the ith boundary component by ρ_1^i, ρ_2^i, and ρ_3^i for type A boundaries, or by ρ_3^i, ρ_2^i, and ρ_1^i for type D boundaries. In each case, ρ_{12}^i, ρ_{23}^i, and ρ_{123}^i refer to the relevant concatenations. We call these oriented arcs *Reeb chords*. The assumption that $\Sigma\backslash\boldsymbol{\alpha}$ is connected implies that the endpoints of α_1^i and α_2^i alternate. We assume that the first endpoint after the basepoint (following the boundary orientation) is α_1^i for type A boundaries and α_2^i for type D boundaries.

We can associate a copy of the torus algebra to each boundary component, so that the Reeb chords on $\partial\Sigma$ correspond directly to the Reeb elements of the algebra. By abuse of notation, we often use ρ_I^i to refer both to the Reeb chord on $\partial\Sigma$ and the corresponding algebra element in the corresponding copy of the torus algebra.

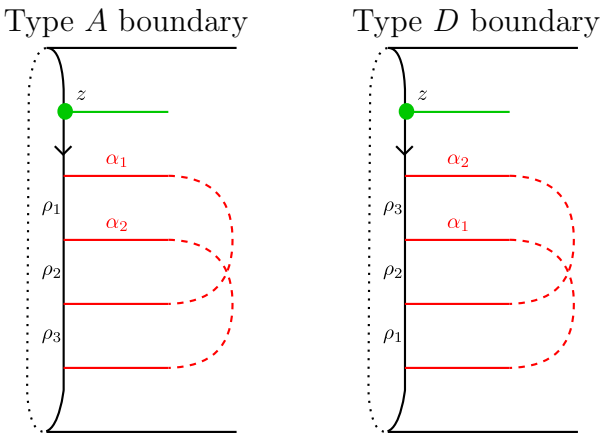

Figure 1: Boundary markings for type A and D boundaries on a bordered Heegaard diagram.

2.4 Type D invariants

Let Y be a borderd 3-manifold with k boundary components, and let $\mathcal{H}$ be an arced bordered Heegaard diagram representing Y which is provincially admissible in the sense of [8, Definition 4.23]. Choose a complex structure J on $\Sigma \times [0,1] \times \mathbb{R}$. To ensure transversality, the choice of J must be generic; however, for the computations in this thesis we may assume that J splits as $J_\Sigma \times J_D$, where J_Σ is a generic complex structure on Σ and J_D is a generic complex structure on $[0,1] \times \mathbb{R}$. Split complex structures provide enough flexibility for transversality when the projections to Σ of all curves being considered are somewhere injective [7, Proposition 3.9]. Given these choices, we will associate to $\mathcal{H}$ a type D multimodule $\widehat{CFD^k}(\mathcal{H}, J)$ over k copies of the torus algebra $\mathcal{A}(T^2)$. We will often suppress J from the notation.

Let $\mathfrak{S}(\mathcal{H})$ be the set of unordered g-tuples $\mathbf{x} = (x_1, \dots, x_g)$ which contain exactly one point on each β curve, exactly one point on each α curve, and at most one point on each α arc. Elements of $\mathfrak{S}(\mathcal{H})$ fall into different spin^c-structures according to how many α arcs are occupied on each boundary. As a vector space over $\mathbb{F}_2$, $\widehat{CFD^k}(\mathcal{H})$ is generated by $\mathfrak{S}(\mathcal{H})$, and it splits as a direct sum over spin^c-structures on Y [8, Lemma 4.21]. Each

generator $\mathbf{x} \in \mathfrak{S}(\mathcal{H})$ comes equipped with an idempotent in the algebra associated to each boundary component; if $\mathbf{x}$ has exactly one α^i arc occupied, then the corresponding idempotent in $\mathcal{A}_i = \mathcal{A}(T^2)$ is ι_1^i if $\mathbf{x}$ contains a point on α_1^i and ι_0^i if $\mathbf{x}$ contains a point on α_2^i.

The differential on $\widehat{CFD^k}(\mathcal{H})$ counts J-holomorphic curves in $\Sigma \times [0,1] \times \mathbb{R}$ with appropriate boundary conditions (for precise statements of these conditions, see [8, Section 5.2]). These curves can be sorted into relative homology classes. For any $\mathbf{x}, \mathbf{y} \in \mathfrak{S}(\mathcal{H})$, let $\pi_2(\mathbf{x}, \mathbf{y})$ denote the set of homology classes of curves in $\Sigma \times [0,1] \times \mathbb{R}$ with boundary conditions consistent with a differential connecting $\mathbf{x}$ to $\mathbf{y}$. Computing the differential involves counting the holomorphic representatives for each homology class.

Under the projection $\Sigma \times [0,1] \times \mathbb{R} \to \Sigma$, a homology class $B \in \pi_2(\mathbf{x}, \mathbf{y})$ projects to an element of $H_2(\Sigma, \boldsymbol{\alpha} \cup \boldsymbol{\beta} \cup \partial\Sigma)$, called the *domain* of B. B is determined by its domain. A domain is a linear combination of components of $\Sigma \backslash (\boldsymbol{\alpha} \cup \boldsymbol{\beta})$, which we call *regions*. Furthermore, the domain of any $B \in \pi_2(\mathbf{x}, \mathbf{y})$ must satisfy the following conditions:

- the multiplicity of the region containing the basepoint z is 0;
- at each $p \in \boldsymbol{\alpha} \cap \boldsymbol{\beta}$, let $n_1(p), \ldots, n_4(p)$ be the multiplicities of the four regions with corners at p, counting counterclockwise starting from an α. Then

$$n_1(p) - n_2(p) + n_3(p) - n_4(p) = \begin{cases} 1 & p \in \mathbf{x} \backslash \mathbf{y} \\ -1 & p \in \mathbf{y} \backslash \mathbf{x} \\ 0 & \text{else.} \end{cases} \tag{2.4}$$

A domain is called *positive* if every region has non-negative multiplicity. Only positive domains can support holomorphic representatives. Because the Heegaard diagram $\mathcal{H}$ is provincially admissible, there are a finite number of positive domains with multiplicity at most 1 in the regions adjacent to $\partial\Sigma$ (we will see that only these are relevant for computing $\widehat{CFD^k}$). Finding them is a simple matter of linear algebra.

In addition to its domain B, a holomorphic curve that contributes to the differential of $\mathbf{x}$ also specifies a sequence of Reeb chords $\vec{\rho} = (\vec{\rho}^{\,1}, \ldots, \vec{\rho}^{\,k})$, where $\vec{\rho}^{\,i} = (\rho^i_{I_1}, \ldots, \rho^i_{I_n})$ are sequences corresponding to each boundary component of Σ. For each boundary component with one α^i arc occupied by $\mathbf{x}$, the pair $(B, \vec{\rho}^{\,i})$ will satisfy the following conditions:

- the initial point (with respect to the boundary orientation) of $\rho^i_{I_1}$ lies on the same α^i arc as $\mathbf{x}$;
- for each $m > 1$, the initial point of $\rho^i_{I_m}$ lies on the same α^i arc as the terminal point of $\rho^i_{I_{m-1}}$.

A pair $(B, \vec{\rho}^{\,i})$ satisfying the above conditions is called *strongly boundary monotonic*. For each boundary component with zero or two α^i arcs occupied by $\mathbf{x}$, we may assume that $\vec{\rho}^{\,i} = ()$. The pair $(B, \vec{\rho}\,)$ coming from a holomorphic curve will also satisfy the following property:

- the intersection of B with the ith component of $\partial\Sigma$ is equal to the sum of the Reeb chords in $\vec{\rho}^{\,i}$ as elements of $H_1(\partial\Sigma, \boldsymbol{\alpha} \cap \partial\Sigma)$.

We say that the pair $(B, \vec{\rho}\,)$ is *compatible* if it satisfies this condition and each $(B, \vec{\rho}^{\,i})$ is strongly boundary monotonic (compare [8, Definition 5.61]).

Given generators $\mathbf{x}, \mathbf{y} \in \mathfrak{S}(\mathcal{H})$, a homology class $B \in \pi_2(\mathbf{x}, \mathbf{y})$, and a sequence of Reeb chords $\vec{\rho}$ such that $(B, \vec{\rho}\,)$ is compatible, we can define $\mathcal{M}^B(\mathbf{x}, \mathbf{y}, \vec{\rho}\,)$ to be the moduli space of J-holomorphic curves in $\Sigma \times [0,1] \times \mathbb{R}$ with domain B and whose asymptotics specify the initial generator $\mathbf{x}$, the final generator $\mathbf{y}$, and the sequence of Reeb chords $\vec{\rho}$ (for the full definition, see [8, Section 5]).

The dimension of the moduli space $\mathcal{M}^B(\mathbf{x}, \mathbf{y}, \vec{\rho}\,)$ is one less than the index $\mathrm{ind}(B, \vec{\rho}\,)$, defined in [8, Definition 5.61]. In the special case of toroidal boundary, the index is given by

$$\mathrm{ind}(B, \vec{\rho}\,) = e(B) + n_{\mathbf{x}}(B) + n_{\mathbf{y}}(B) + \sum_{1 \le i \le k} \left[\frac{1}{2} \left| \vec{\rho}^{\,i} \right| + \sum_{j<l} L(\rho^i_{I_j}, \rho^i_{I_l}) \right], \tag{2.5}$$

where

$$e(B) = \chi(B) - \frac{\#\text{ acute corners}}{4} + \frac{\#\text{ obtuse corners}}{4}$$

is the Euler measure of B, $n_{\mathbf{x}}(B)$ (respectively $n_{\mathbf{y}}(B)$) is the sum over $x_i \in \mathbf{x}$ (respectively $y_i \in \mathbf{y}$) of the average multiplicity in B of the four regions incident to x_i (respectively y_i), $|\vec{\rho}^{\,i}|$ is the number of Reeb chords in the part of $\vec{\rho}$ associated to the ith component of $\partial\Sigma$, and $L(\rho_{I_j}, \rho_{I_l})$ is a linking term for Reeb chords defined as follows:

$$\begin{aligned}
L(\rho_1,\rho_2) = L(\rho_2,\rho_3) = L(\rho_{12},\rho_3) = L(\rho_1,\rho_{23}) &= \tfrac{1}{2}\\
L(\rho_2,\rho_1) = L(\rho_3,\rho_2) = L(\rho_3,\rho_{12}) = L(\rho_{23},\rho_1) &= -\tfrac{1}{2}\\
L(\rho_{12},\rho_{23}) &= 1\\
L(\rho_{23},\rho_{12}) &= -1\\
L(\rho_{I_j},\rho_{I_l}) &= 0 \text{ for all other pairs of } I_j \text{ and } I_l.
\end{aligned}$$

The differential counts J-holomorphic curves in moduli spaces with dimension 0, so we only need to consider domains and Reeb chords with $\mathrm{ind}(B,\vec{\rho}) = 1$.

To define the differential we need one more piece of notation. If ρ^i_I represents a Reeb chord on the ith boundary component of Σ, let $a(\rho^i_I)$ denote the corresponding element of $\mathcal{A}_i$, the copy of the torus algebra associated to the ith boundary component. If $\vec{\rho}^{\,i} = (\rho^i_{I_1}, \ldots, \rho^i_{I_n})$ is a sequence of Reeb chords on the ith boundary, let $a(\vec{\rho}^{\,i})$ denote the element $\rho^i_{I_1}\rho^i_{I_2}\cdots\rho^i_{I_n} \in \mathcal{A}_i$, and if $\vec{\rho} = (\vec{\rho}^{\,1}, \ldots, \vec{\rho}^{\,k})$, let $a(\vec{\rho})$ denote the element $a(\vec{\rho}^{\,1}) \otimes \cdots \otimes a(\vec{\rho}^{\,k}) \in \mathcal{A}_1 \otimes \cdots \otimes \mathcal{A}_k$. We now define the differential on $\widehat{CFD^k}$ as follows: For any $\mathbf{x} \in \mathfrak{S}(\mathcal{H})$,

$$\partial(\mathbf{x}) = \sum_{\mathbf{y}\in\mathfrak{S}(\mathcal{H})} \sum_{B\in\pi_2(\mathbf{x},\mathbf{y})} \sum_{\substack{\{\vec{\rho}\,|\,\mathrm{ind}(B,\vec{\rho})=1,\\ (B,\vec{\rho})\text{is compatible}\}}} \Big(\#\mathcal{M}^B(\mathbf{x},\mathbf{y},\vec{\rho})\Big) a(\vec{\rho}) \otimes \mathbf{y},$$

where the count of a moduli space is taken mod 2.

Note that the multimodule $\widehat{CFD^k}(\mathcal{H}, J)$ depends on the choices of $\mathcal{H}$ and J. However, its quasi-isomorphism type is an invariant of the bordered manifold Y. We denote this quasi-isomorphism class by $\widehat{CFD^k}(Y)$. We will deviate slightly from the notation

introduced here when $k \leq 2$ in order to agree with existing notation. That is, we will omit the superscript in $\widehat{CFD^1}$, and we will write $\widehat{CFDD}$ instead of $\widehat{CFD^2}$.

2.5 Type A Invariants

Let Y be a bordered 3-manifold with k boundary components and let $\mathcal{H}$ be a provincially admissible arced bordered Heegaard diagram representing Y and J a chosen complex structure, as before. We can define a type A multimodule over k copies of the torus algebra, denoted $\widehat{CFA^k}(\mathcal{H})$. In this thesis, we will never need to compute $\widehat{CFA^k}(\mathcal{H})$. However, as a computational trick we will make use of the relationship between $\widehat{CFA^k}(\mathcal{H})$ and $\widehat{CFD^k}(\mathcal{H})$, so it will be helpful to state the definition.

$\widehat{CFA^k}(\mathcal{H})$ is generated by the same set $\mathfrak{S}(\mathcal{H})$ that generates $\widehat{CFD^k}(\mathcal{H})$. The differential and higher multiplications are defined by counting the same J-holomorphic curves that appear in the definition of $\widehat{CFD^k}(\mathcal{H})$. We will assume for the sake of comparison that the Reeb chords on the boundary are labeled the same as if we were computing $\widehat{CFD^k}(\mathcal{H})$, so that for a given domain the compatible sequences of Reeb chords $\vec{\rho}$ and the moduli spaces $\mathcal{M}^B(\mathbf{x}, \mathbf{y}, \vec{\rho}\,)$ are exactly the same. However, with this convention we must change the algebra elements in the $\mathcal{A}_\infty$ operation, since normally the Reeb chords are labeled in the opposite order for type A Heegaard diagrams. Let the function $\bar{a}$ be the same as a except that it also interchanges ρ_1^i with ρ_3^i and ρ_{12}^i with ρ_{23}^i. Then given a generator $\mathbf{x} \in \mathfrak{S}(\mathcal{H})$ and sequence of Reeb chords $\vec{\rho} = (\vec{\rho}^{\,1}, \ldots, \vec{\rho}^{\,k})$,

$$m(\mathbf{x}, \bar{a}(\vec{\rho}^{\,1}), \ldots, \bar{a}(\vec{\rho}^{\,k})) = \sum_{\mathbf{y} \in \mathfrak{S}(\mathcal{H})} \sum_{\substack{\{B \in \pi_2(\mathbf{x},\mathbf{y}) | \\ \mathrm{ind}(B,\vec{\rho}\,)=1, \\ (B,\vec{\rho}\,) \text{ compatible}\}}} \Big(\#\mathcal{M}^B(\mathbf{x}, \mathbf{y}, \vec{\rho}\,)\Big)\mathbf{y},$$

where we think of $\bar{a}(\vec{\rho}^{\,i})$ as an element of $\mathcal{A}_i^{\otimes |\vec{\rho}^{\,i}|}$, and where the moduli space counts are taken mod 2.

2.6 Tensor Products and the Pairing Theorem

For a bordered manifold with many boundary components, we can define bordered invariants which are type D with respect to some boundaries and type A with respect to others. These invariants can be obtained from $\widehat{CFD^k}$ by taking the box tensor product with the bimodule $\widehat{CFAA}(\mathbb{I})$, which can be found in [9, Figure 21]. An alternative shorthand algorithm for converting to type D boundaries to type A is described in [4, Section 2.3].

Bordered invariants satisfy a pairing theorem [9, Theorem 11]. Given a bordered invariant for Y_1 which is type A with respect to the ith boundary component and a bordered invariant for Y_2 which is type D with respect to the jth boundary component, we can compute the box tensor product of the two multimodules with respect to the corresponding copies of the torus algebra, assuming the modules are appropriately bounded. The pairing theorem states that up to $\mathcal{A}_\infty$-homotopy equivalence, the result is the bordered invariant for the manifold obtained by gluing the ith boundary of Y_1 to the jth boundary of Y_2.

In this thesis, we will work primarily with type D modules, and convert only one boundary component at a time to type A in order to tensor with another type D module.

2.7 Useful Results for Computation

This section collects a handful of results that are useful when explicitly computing a type D bordered invariant.

The first is a slight rephrasing of [6, Proposition 2.1]:

Proposition 2.7.1.

(a) For a given boundary component, the only non-empty sequences of Reeb chords which can contribute nonzero terms to the differential in $\widehat{CFD^k}$ *are* (ρ_1^i), (ρ_2^i), (ρ_3^i), (ρ_1^i, ρ_2^i), (ρ_2^i, ρ_3^i), $(\rho_1^i, \rho_2^i, \rho_3^i)$, *and* (ρ_{123}^i).

(b) Furthermore, if $B \in \pi_2(\mathbf{x}, \mathbf{y})$ contributes with $\vec{\rho}^{\,i} = (\rho_2^i)$ or $\vec{\rho}^{\,i} = (\rho_1^i, \rho_2^i)$, then $\mathbf{y}$ contains a point on α_2^i. If B contributes and $\vec{\rho}^{\,i}$ is (ρ_1^i), (ρ_3^i), (ρ_{123}^i), or (ρ_2^i, ρ_3^i), then $\mathbf{y}$ contains a point on α_1^i.

In particular, this proposition implies that only domains with multiplicity 0 or 1 in every region that intersects $\partial\Sigma$ can contribute nontrivially to the differential in $\widehat{CFD^k}$. For provincially admissible Heegaard diagrams this ensures that there is a finite number of positive domains to consider.

Another implication of Proposition 2.7.1 is that Equation (2.5) can be simplified for type D computations.

Lemma 2.7.2. *If the pair $(B, \vec{\rho}\,)$ contributes a nonzero term to the differential of $\widehat{CFD^k}$, then the index of the pair is given by*

$$\mathrm{ind}(B, \vec{\rho}\,) = \mathrm{ind}(B) = e(B) + n_{\mathbf{x}}(B) + n_{\mathbf{y}}(B) + \frac{\#\{Z \in \pi_0(\partial\Sigma) | Z \cap B \neq \emptyset\}}{2}. \tag{2.6}$$

In particular the index depends only on B.

Proof. We examine the term in brackets in Eq. 2.5. For the ith component of $\partial\Sigma$, there is a contribution to the index of

$$\left[\frac{1}{2}\left|\vec{\rho}^{\,i}\right| + \sum_{j<l} L(\rho_{I_j}^i, \rho_{I_l}^i)\right].$$

We can evaluate this term for each of the sequences of Reeb chords allowed by Proposition 2.7.1. If $\vec{\rho}^{\,i}$ is (ρ_1^i), (ρ_2^i), (ρ_3^i), or (ρ_{123}^i), then $|\vec{\rho}^{\,i}| = 1$ and there are no linking terms. If $\vec{\rho}^{\,i}$ is (ρ_1^i, ρ_2^i) or (ρ_2^i, ρ_3^i), then $|\vec{\rho}^{\,i}| = 2$, and there is one linking term, with a value of $-\frac{1}{2}$. If $\vec{\rho}^{\,i}$ is $(\rho_1^i, \rho_2^i, \rho_3^i)$, then $|\vec{\rho}^{\,i}| = 3$, and the two nonzero linking terms $L(\rho_1^i, \rho_2^i)$ and $L(\rho_2^i, \rho_3^i)$ evaluate to $-\frac{1}{2}$. In any of these cases, the total contribution to the index is $\frac{1}{2}$. The only other possibility is that $\vec{\rho}^{\,i} = ()$, which happens when B does not contain any regions adjacent to the ith boundary component of Σ. In this case, the contribution of $\vec{\rho}^{\,i}$ to the index is 0. Summing over all boundary components yields

$$\sum_{1\leq i\leq k}\left[\frac{1}{2}\left|\vec{\rho}^{\,i}\right|+\sum_{j<l}L(\rho^i_{I_j},\rho^i_{I_l})\right]=\frac{\#\{Z\in\pi_0(\partial\Sigma)|Z\cap B\neq\emptyset\}}{2}.$$

□

Lemma 2.7.2 allows us to exclude a domain B from consideration in computing $\widehat{CFD^k}$ if $\mathrm{ind}(B)\neq 1$, without needing to consider all sequences of Reeb chords compatible with B.

In practice, computing $\widehat{CFD^k}$ from a Heegaard diagram begins by writing down all positive domains $B\in\pi_2(\mathbf{x},\mathbf{y})$ for each pair of generators $\mathbf{x}$ and $\mathbf{y}$, and then eliminating as many domains as possible using Proposition 2.7.1 and Lemma 2.7.2. At some point, however, it is necessary to prove that a given domain/Reeb chord pair *does* contribute to the differential. The following proposition asserts that a domain which can be realized as an immersed polygon always contributes.

Proposition 2.7.3. *Let P be a $2n$-gon, with edges numbered consecutively, and suppose that there is map $P\xrightarrow{u}\Sigma$ satisfying the following conditions:*

- *$u|_{\partial P}$ takes even edges of P to $\boldsymbol{\beta}$, odd edges of P to $\boldsymbol{\alpha}\cup\partial\Sigma$, and corners to acute corners;*
- *u is an immersion, except at the preimages of $\boldsymbol{\alpha}\cap\partial\Sigma$;*
- *for each boundary component of Σ, at most one edge of P maps to $\alpha^i_1\cup\alpha^i_2$, and for each $\beta\in\boldsymbol{\beta}$, at most one edge of P maps to β.*

The image of u covers each region in Σ with a certain multiplicity; let $B(u)$ be the corresponding positive domain. The image of ∂P determines a sequence of Reeb chords $\vec{\rho}\,(u)$, with the chords in the image of a single edge ordered according to the boundary orientation on ∂P. If $B(u)\in\pi_2(\mathbf{x},\mathbf{y})$ for some generators $\mathbf{x}$ and $\mathbf{y}$ in the middle spin^c-structure, then $(B(u),\vec{\rho}\,(u))$ is compatible, and $\left(\#\mathcal{M}^B(\mathbf{x},\mathbf{y},\vec{\rho}\,)\right)\equiv 1$ (mod 2).

Proof. A holomorphic curve in $\Sigma \times [0,1] \times \mathbb{R}$ is equivalent to a holomorphic map of a Riemann surface with boundary into Σ along with a branched covering map of that surface over the unit disk $D^2 \subset \mathbb{C}$ (see [23, Lemma 3.6]). For a specific domain, we look at Riemann surfaces which map onto the given domain in Σ, such that the preimages of the α arcs (together with boundary Reeb chords) and β arcs map to the right and left boundaries, respectively, in the projection to D^2, and the preimages of the $\mathbf{x}$ and $\mathbf{y}$ corners map to $-i$ and i, respectively.

In this case, we already have a map from the polygon P to Σ. There is a unique choice of complex structure on P that makes u holomorphic (induced by pulling back the complex structure on Σ). So we need to show that with this fixed complex structure, there is a unique n-fold branched covering map to D^2 up to an $\mathbb{R}$ action.

First choose a biholomorphic map from P to the upper half plane $\mathbb{H}$, which takes one of the $\mathbf{y}$ corners to ∞, and the other corners to points $x_1, x_2, \dots, x_{2n-1}$ along the real axis. We now want to find a degree n map $\mathbb{H} \to \mathbb{H}$ which takes x_i to 0 for i odd and to ∞ for i even, and takes ∞ to ∞. Such a map is given by

$$z \to \frac{(z-x_1)(z-x_3)\cdots(z-x_{2n-1})}{(z-x_2)(z-x_4)\cdots(z-x_{2n-2})}.$$

This map is unique up to scaling. Finally we can find a biholomorphic map from $\mathbb{H}$ to D^2 which takes 0 to $-i$ and ∞ to $+i$. Composing these three maps gives the desired k-fold branched cover $P \to D^2$. □

Another common situation in which the moduli space of holomorphic curves can be understood is pictured in Figure 2. The following is [6, Lemma 3.2], but we recall the proof here in order to introduce notation and reasoning that will be useful later.

Proposition 2.7.4. *Suppose a Heegaard diagram contains an annulus A as in Figure 2 and one or more of the bigons $B_1, \dots, B_4$, where α arcs may contain segments of $\partial\Sigma$, and where the ends of α_1 and β_1 leave A through the opposite boundary component. Let D_i denote the domain corresponding to the union of A and B_i. Then either D_1 and D_3 count*

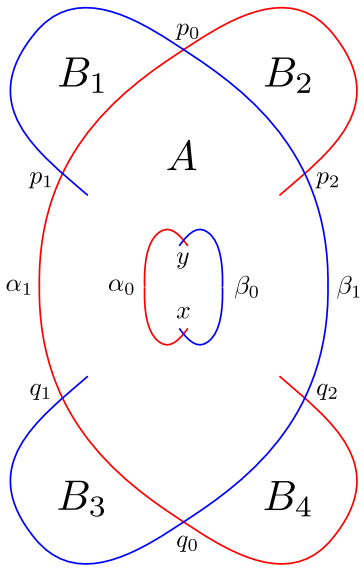

Figure 2: Index 0 annuli A with four attached bigons.

toward the differential and D_2 and D_4 do not, or vice versa, depending on the choice of complex structure J on Σ.

Proof. Let A_r denote the standard annulus, $S^1 \times [0, r]$ with a fixed complex structure. For a unique positive number r there is a holomorphic map $u : A_r \to A$ taking $S^1 \times \{0\}$ to the inner boundary of D, $D \cap (\alpha_0 \cup \beta_0)$, and taking $S^1 \times \{r\}$ to the outer boundary $D \cap (\alpha_1 \cup \beta_1)$. This map is unique up to rotation in the S^1 factor. Let a_0 and b_0 denote the inverse images in $S^1 \times \{0\}$ of α_0 and β_0, respectively. Let a_1 and b_1 denote the respective inverse images of α_1 and β_1 in $S^1 \times \{r\}$. Define $\Theta_A^{x,y}$ to be $l(a_0)/l(b_0)$, the ratio of the lengths of the preimages of the α and β arcs on the boundary of A which contains x and y. Similarly, define $\Theta_A^{p_0,q_0}$ to be $l(a_1)/l(b_1)$. The domain A will have a holomorphic representative if $\Theta_A^{x,y} = \Theta_A^{p_0,q_0}$ [23, Lemma 9.3], but for a generic choice of complex structure this will not be the case.

Now consider the domain D_1. It is an annulus with one obtuse corner at p_1. There is a one parameter family of conformal structures depending on how much we cut into the annulus along the α or β arc at the obtuse corner. We specify the length of this cut

by a parameter c, where $c < 0$ corresponds to cutting along α_1 and $c > 0$ corresponds to cutting along β_1. The cut approaches p_0 as $c \to -\infty$ and it approaches α_0 as $c \to \infty$. For any value of c there is a holomorphic map $U^c : A_r \to D_1$, unique up to rotation in the S^1 factor of A_r. We can define $\theta^{x,y}_{D_1}(c)$ and $\theta^{p_1,q_0}_{D_1}(c)$ analogously to $\Theta^{x,y}_A$ and Θ^{p_0,q_0}_A, as the ratio of the lengths of the α and β components on the corresponding boundary of D_1.

As the cutting parameter varies, D_1 will have a holomorphic representative each time $\theta^{x,y}_{D_1}(c) = \theta^{p_1,q_0}_{D_1}(c)$, and thus the number of holomorphic representatives is determined by the number of zeros of $\theta^{x,y}_{D_1} - \theta^{p_1,q_0}_{D_1}$. The mod 2 count of these zeros is determined by the end behavior of $\theta^{x,y}_{D_1} - \theta^{p_1,q_0}_{D_1}$. As c approaches ∞, the cut along β_1 from p_1 approaches α_0. In this limit $\theta^{x,y}_{D_1}$ becomes very large and $\theta^{p_1,q_0}_{D_1}$ becomes very small, so $\theta^{x,y}_{D_1} - \theta^{p_1,q_0}_{D_1} \to +\infty$. In the other extreme, we cut along α_1 from p_1 to p_0. The limit is a broken flow where the bigon B_1 is pinched off from the annulus A. In this limit $\theta^{x,y}_{D_1} = \Theta^{x,y}_A$ and $\theta^{p_1,q_0}_{D_1} = \Theta^{p_0,q_0}_A$. Therefore, the domain D_1 will contribute to the differential in $\widehat{CFD^k}$ if and only if $\Theta^{p_0,q_0}_A > \Theta^{x,y}_A$.

The domains D_2, D_3, and D_4 can be analyzed in the same way. For D_3 the results are the same: cutting along β_1 from q_1 to α_0 makes $\theta^{x,y}_{D_3} - \theta^{p_0,q_1}_{D_3}$ approach $+\infty$, and cutting along α_1 from q_1 to q_0 yields $\Theta^{x,y}_{D_3} - \theta^{p_0,q_1}_{D_3} = \Theta^{x,y}_A - \Theta^{p_0,q_0}_A$, so D_3 contributes if and only if $\Theta^{p_0,q_0}_A > \Theta^{x,y}_A$. The domains D_2 and D_4, on the other hand, contribute if and only if $\Theta^{x,y}_A > \Theta^{p_0,q_0}_A$. □

We will often encounter annular domains which fit the form of the annuli in Proposition 2.7.4 except that one boundary component has more than one α segment and more than one β segment. For instance, the bigon B_1 might be replaced with a quadrilateral. In practice, quadrilaterals behave like bigons in this context, but it is not immediately apparent how to extend the proof of Proposition 2.7.4 for more general annuli. Instead, we will use the following proposition to simplify a domain by pinching off an extra α or β arc.

Proposition 2.7.5. *Let γ be an arc in a domain D which is a small pushoff of one of the β segments or one of the α segments (possibly containing Reeb chords) in ∂D, as pictured below. Assume that γ only passes through regions with multiplicity 1 in D. Let D' be the domain which results from collapsing γ to a point and removing the bigon on the left. Then for an appropriate choice of complex structure, D contributes to $\widehat{CFD^k}$ if and only if D' would contribute.*

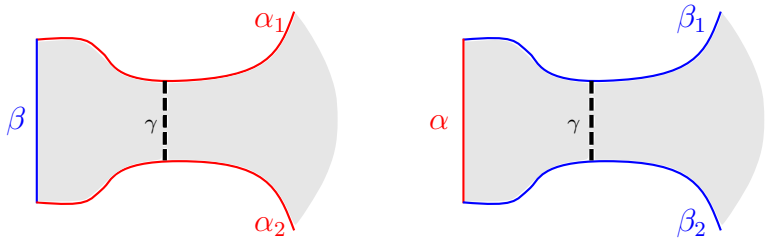

Proof. Given a complex structure J on D, identify a neighborhood of γ with $[0,1]\times(-\epsilon,\epsilon)$. Consider the one parameter family of complex structures J_t, $t > 0$, such that the same neighborhood of γ is identified with $[0,1] \times (-t,t)$ and J_t agrees with J outside that neighborhood. As t goes to infinity, the neighborhood of γ is pinched and stretched—effectively the arc γ becomes shorter. The limiting complex structure J_∞ corresponds to γ being pinched to a single point, resulting in a bigon B and the the domain D' joined at a point. A J_∞-holomorphic curve with domain D splits as a holomorphic map to the bigon and a holomorphic curve with domain D'. By the Riemann Mapping Theorem, there is an $\mathbb{R}$ family of holomorphic maps from the standard bigon to B, and precisely one once the point of contact with the preimage of D' is determined. Therefore the existence of J_∞-holomorphic curves with domain D is equivalent to the existence of J_∞-holomorphic curves with domain D'.

J_∞ is not a valid complex structure to choose when computing $\widehat{CFD^k}$, but we can choose J_t for arbitrarily large t, and standard compactness and gluing arguments show that for t sufficiently large, D has a J_t-holomorphic representative if and only if it has a J_∞-holomorphic representative. Thus for a complex structure with the arc γ sufficiently

pinched, the statement of the proposition holds.

□

Finally, we discuss how $\mathcal{A}_\infty$ relations can be used to deduce which domains count toward the differential, even if we are computing $\widehat{CFD^k}$. The key is the following observation:

Lemma 2.7.6. *A sequence of Reeb chords $\vec{\rho} = (\vec{\rho}^1, \dots, \vec{\rho}^k)$ contributes $a(\vec{\rho}) \otimes \mathbf{y}$ to the differential of $\mathbf{x}$ in $\widehat{CFD^k}$ if and only if $m(\mathbf{x}, \bar{a}(\vec{\rho}^1), \dots, \bar{a}(\vec{\rho}^k)) = \mathbf{y}$ in $\widehat{CFA^k}$.*

Proof. This follows directly from the definitions of $\widehat{CFD^k}$ and $\widehat{CFA^k}$, since both involve counts of the same moduli spaces. For a given domain $B \in \pi_2(\mathbf{x}, \mathbf{y})$ that is compatible with $\vec{\rho}$, the pair $(B, \vec{\rho})$ may contribute $a(\vec{\rho}) \otimes \mathbf{y}$ to $\partial\mathbf{x}$ in $\widehat{CFD^k}$, and it may contribute the operation $m(\mathbf{x}, \bar{a}(\vec{\rho}^1), \dots, \bar{a}(\vec{\rho}^k)) = \mathbf{y}$ to $\widehat{CFA^k}$. In both cases, the pair contributes if and only if $\#(\mathcal{M}^B(\mathbf{x}, \mathbf{y}, \vec{\rho})) \equiv 1 \pmod 2$.

□

Here we say that $\vec{\rho}$ *contributes* to $\widehat{CFD^k}$ if the relevant counts of moduli spaces are nonzero, even if the contribution $a(\vec{\rho}) \otimes \mathbf{y}$ may be zero. In comparison, notice that Proposition 2.7.1 and Lemma 2.7.2 discuss when a domain *contributes a nonzero term* to $\widehat{CFD^k}$. Thus a domain that is ruled out from consideration for $\widehat{CFD^k}$ by Proposition 2.7.1 or Lemma 2.7.2 might still contribute to $\widehat{CFA^k}$.

Lemma 2.7.6 is most useful for checking if domains contribute to $\widehat{CFD^k}$ when $\vec{\rho}$ contains the long chord ρ^i_{123} for some boundary component. For example, suppose in the one boundary case that $\vec{\rho} = (\rho_{123})$ is compatible with a domain B from $\mathbf{x}$ to $\mathbf{y}$. If the domain is too complicated to understand the moduli space $\mathcal{M}^B(\mathbf{x}, \mathbf{y}, \vec{\rho})$ directly, we can instead ask whether $(B, \vec{\rho})$ contributes the operation $m(\mathbf{x}, \rho_{123}) = \mathbf{y}$ to $\widehat{CFA}$. To answer this, we consider the $\mathcal{A}_\infty$ relation (Equation 2.3) corresponding to $\mathbf{x}$ and $\vec{\rho'} = (\rho_{12}, \rho_3)$. The relation says that

$$0 = m\Big(\mathbf{x}, \mu(\rho_{12}, \rho_3)\Big) + m\Big(m(\mathbf{x}, \rho_{12}), \rho_3\Big).$$

The first term is just $m(\mathbf{x}, \rho_{123})$, the operation we are interested in, and the second term might be easier to analyze. If $m(\mathbf{x}, \rho_{12}) = 0$, for instance, then the second term in the relation is 0, and thus $(B, \vec{\rho})$ does not contribute to $\widehat{CFA}$ or to $\widehat{CFD}$.

2.8 Gradings

Bordered Heegaard Floer invariants can be equipped with a relative grading on each spin^c-structure as described in [8, Chapter 10] and [9, Section 6.5]. We recall here the construction of these gradings for manifolds with only torus boundary components. We will only discuss the refined grading.

Let Y be a bordered manifold represented by a bordered Heegaard diagram $\mathcal{H}$. Let $\widehat{CF}(\mathcal{H})$ denote the relevant bordered Heegaard Floer invariant. The gradings for $\widehat{CF}(\mathcal{H})$ lie in a noncommutative group which depends on the number and type of boundary components. We will denote this group $G_{n,m}$ where n is the number of type D boundary components of Y and m is the number of type A boundary components. $G_{n,m}$ is generated by tuples $(j; a_1, b_1; a_2, b_2; \ldots; a_{n+m}, b_{n+m})$, where every entry is in $\frac{1}{2}\mathbb{Z}$, and $a_i + b_i \in \mathbb{Z}$ for each i. j is referred to as the *Maslov component* of the grading. Multiplication on this group is defined as follows:

$$(j; a_1, b_1; a_2, b_2; \ldots; a_{n+m}, b_{n+m}) \cdot (j'; a'_1, b'_1; a'_2, b'_2; \ldots; a'_{n+m}, b'_{n+m}) =$$
$$(j + j' + C; a_1 + a'_1, b_1 + b'_1; a_2 + a'_2, b_2 + b'_2; \ldots; a_{n+m} + a'_{n+m}, b_{n+m} + b'_{n+m}),$$

where the correction term C is given by

$$C = \begin{vmatrix} a_1 & a'_1 \\ b_1 & b'_1 \end{vmatrix} + \ldots + \begin{vmatrix} a_n & a'_n \\ b_n & b'_n \end{vmatrix} + \begin{vmatrix} a'_{n+1} & a_{n+1} \\ b'_{n+1} & b_{n+1} \end{vmatrix} + \ldots + \begin{vmatrix} a'_{n+m} & a_{n+m} \\ b'_{n+m} & b_{n+m} \end{vmatrix}.$$

Given generators $\mathbf{x}$ and $\mathbf{y}$, a domain in $B \in \pi_2(\mathbf{x}, \mathbf{y})$ can be given a grading in $G_{n,m}$ [8, Definition 10.1]. The Maslov component of $gr(B)$ is given by

$$-e(B) - n_{\mathbf{x}}(B) - n_{\mathbf{y}}(B),$$

where $e(B)$, $n_{\mathbf{x}}(B)$, and $n_{\mathbf{y}}(B)$ are are the same quantities that appear in the index formula, Equation 2.5. For each $1 \leq i \leq n+m$, let γ_i denote the intersection of ∂B with the ith boundary component of $\mathcal{H}$, which can be thought of as a linear combination of the Reeb chords ρ_1^i, ρ_2^i, and ρ_3^i. If $\gamma_i = c_1\rho_1^i + c_2\rho_2^i + c_3\rho_3^i$, then the ith pair of coefficients in $gr(B)$ is given by

$$a_i = \frac{c_1 + c_2 - c_3}{2}, \qquad b_i = \frac{-c_1 + c_2 + c_3}{2}.$$

To define the gradings on a bordered multimodule in a given spin^c-structure, we choose a base generator $\mathbf{x}$ in that spin^c-structure. Let $\mathcal{P}(\mathbf{x})$ be the subgroup of $G_{n,m}$ generated by $\{gr(B)|B \in \pi_2(\mathbf{x},\mathbf{x})\}$. $\widehat{CF}(\mathcal{H})$ then has a well defined grading by the set $G_{n,m}/\mathcal{P}(\mathbf{x})$. Up to canonical isomorphism, this grading set does not depend on the choice of $\mathbf{x}$. We define the relative grading by the following rule: if $\mathbf{y}$ is generator in the same spin^c-structure as $\mathbf{x}$ and B is a domain connecting $\mathbf{x}$ to $\mathbf{y}$, then $gr(\mathbf{y}) = gr(\mathbf{x})gr(B)$.

In many cases, gradings can be computed directly from the labeled graph representing $\widehat{CF}(\mathcal{H})$, without reference to the Heegaard diagram. To do this, we use the fact that elements of the torus algebra have gradings in $G_{n,m}$. Recall that $\widehat{CF}(\mathcal{H})$ is a module over $n+m$ copies of the torus algebra, one for each boundary of Y, and ρ_I^i denotes an element of the torus algebra associated to the ith boundary. The Maslov component of $gr(\rho_I^i)$ is $-\frac{1}{2}$ and the coefficients a_j and b_j are zero for all $j \neq i$. The coefficients a_i and b_i are determined by I as follows:

I	a_i	b_i
1	$\frac{1}{2}$	$-\frac{1}{2}$
2	$\frac{1}{2}$	$\frac{1}{2}$
3	$-\frac{1}{2}$	$\frac{1}{2}$
12	1	0
23	0	1
123	$\frac{1}{2}$	$\frac{1}{2}$

This grading respects the algebra product in the sense that $gr(\rho_{I_1}\rho_{I_2}) = gr(\rho_{I_1})gr(\rho_{I_2})$.

The grading on $\widehat{CF}(\mathcal{H})$ also respects the module structure in the sense that $gr(\rho_I x) = gr(\rho_I)gr(x)$, where the product on the right refers to the left action of the group $G_{n,m}$ on the set $G_{n,m}/\mathcal{P}(\mathbf{x})$. Finally, the grading on $\widehat{CF}(\mathcal{H})$ satisfies the following relation [9, Definition 2.5.2]:

$$gr(m_{k+1}(x, \rho_{I_1}, \dots, \rho_{I_k})) = \lambda^{k-1} gr(\rho_{I_k}) \cdots gr(\rho_{I_1}) gr(x). \tag{2.7}$$

Here $\lambda = (1; 0, 0; \dots; 0, 0)$ is the preferred central element of $G_{n,m}$. The same relation applies for both type D and type A modules if we think of the differential ∂ as an m_1 map. Thus $gr(\partial x) = \lambda^{-1} gr(x)$.

To compute the relative grading from the graph representing $\widehat{CF}(\mathcal{H})$, we choose a base generator $\mathbf{x}$ and assign it an arbitrary grading. The gradings of the remaining generators can be determined using Equation 2.7, as long as each generator is connected by $\mathbf{x}$ by a path of arrows (that is, as long as the graph is connected). A loop in the graph representing $\widehat{CF}(\mathcal{H})$, along with Equation 2.7, gives rise to a value for $gr(\mathbf{x})$ which may not be equal to the value initially chosen for $gr(\mathbf{x})$. The difference is $gr(B)$ for some periodic domain $B \in \pi_2(\mathbf{x}, \mathbf{x})$. If there are enough loops in the graph (there must be one independent periodic domain for each boundary component of Y), then we can determine $\mathcal{P}(\mathbf{x})$.

Chapter 3

Direct Computation of $\widehat{CFD^3}(\mathcal{Y}_\mathcal{P})$

In this section we explicitly compute the type D trimodule associated to $\mathcal{Y}_\mathcal{P}$, the trivial S^1-bundle over the pair of paints $\mathcal{P}$.

3.1 A borderded Heegaard diagram for $\mathcal{Y}_\mathcal{P}$

3.1.1 Choosing a Heegaard diagram

We obtain the Heegaard surface Σ from the boundary of $\mathcal{Y}_\mathcal{P}$ by drilling through $\mathcal{Y}_\mathcal{P}$ to connect each inner torus boundary component with the outer boundary component. This surface is pictured in Figure 3(a), where the front and back faces are identified by the identity map. To obtain the 3-manifold $\mathcal{Y}_\mathcal{P}$ from this surface, we attach three 2-handles to the inside along the β curves, and fill in the drilling tubes by attaching disks along the thick grey dotted lines. Filling in the interior with a 3-ball yields $\mathcal{Y}_\mathcal{P}$.

We decorate each boundary component of $\mathcal{Y}_\mathcal{P}$ with a pair of intersecting α curves to specify a parametrization of the boundary. There are many choices of parametrization, but it is natural and convenient to choose one α curve to lie in the base surface $\mathcal{P}$ and the other to be an S^1 fiber.

To finish the construction of $\mathcal{H}$ we must also remove a disk around each $\alpha - \alpha$ in-

Figure 3: Constructing the Heegaard diagram for $\mathcal{Y}_\mathcal{P}$.

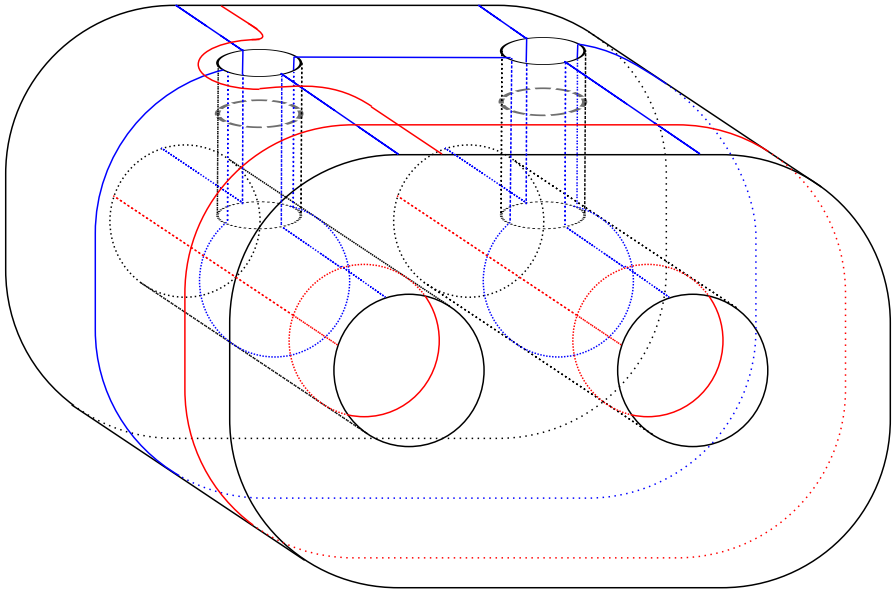

(a) The front and back faces are identified. Attaching 2-handles to the β curves (blue), capping off the drilling tubes along the dotted gray lines, and adding a 3-handle yields $\mathcal{Y}_\mathcal{P}$. Intersecting pairs of α curves (red) specify a parametrization of each boundary component of $\mathcal{Y}_\mathcal{P}$.

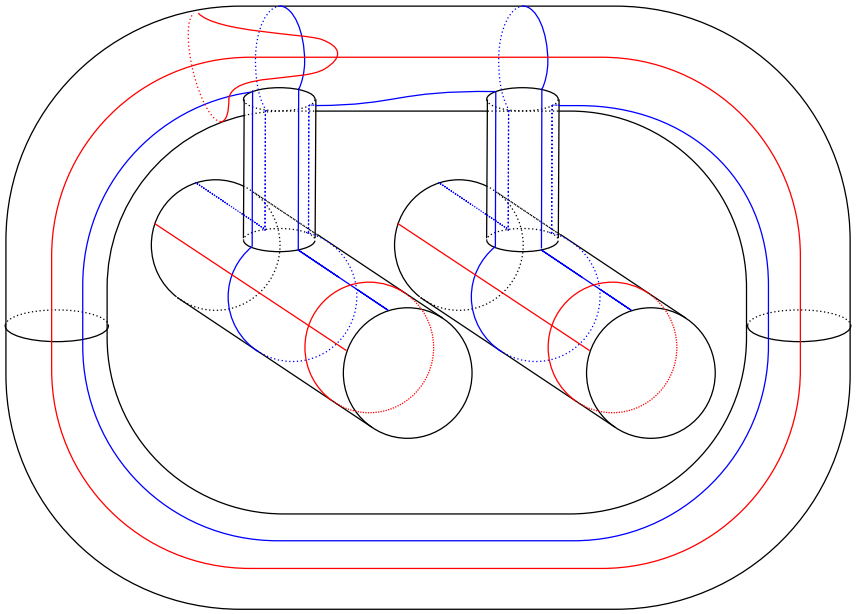

(b) The diagram is easier to read and manipulate if we redraw the outer torus.

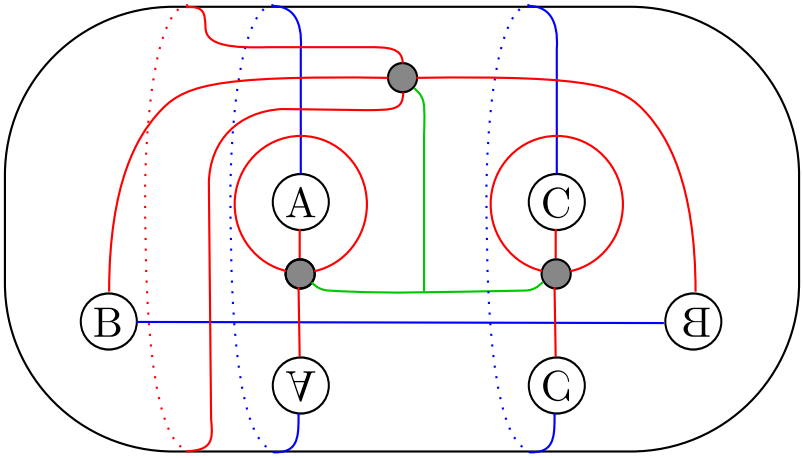

(c) An isotopy simplifies the diagram. Pairs of circles labeled by letters signify 1-handle attachment. We remove a small disk (shaded) around each intersection of α curves, resulting in the genus 3 Heegaard surface Σ with three boundary components. There is a basepoint z connected by arcs (green) to each boundary component.

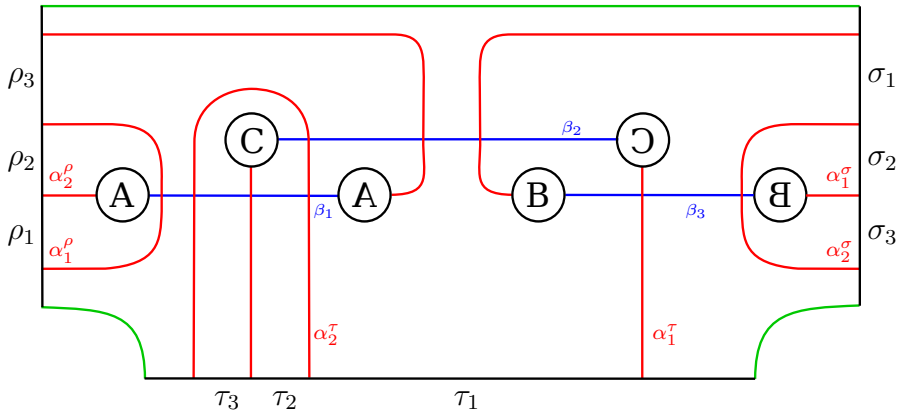

Figure 4: A bordered Heegaard diagram $\mathcal{H}$ for $\mathcal{Y}_\mathcal{P}$, with type D boundaries.

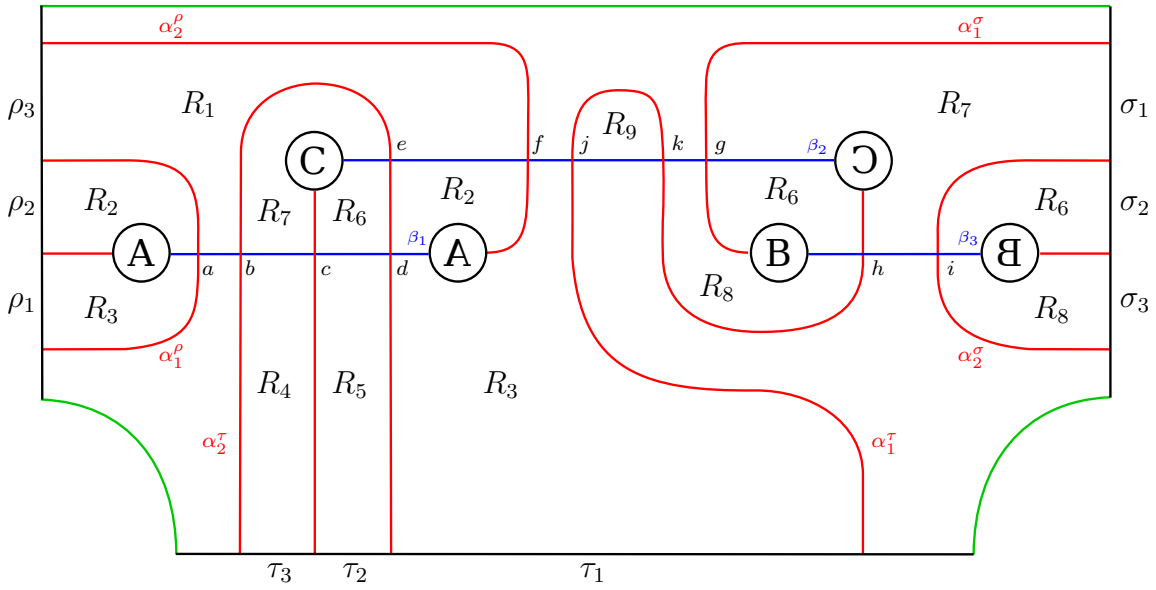

Figure 5: A slightly modified arced Heegaard diagram $\mathcal{Y}_\mathcal{P}$, $\mathcal{H}'$.

tersection point, turning the α curves into arcs and giving the surface Σ three boundary components, and we must chose a basepoint z connected by arcs to each component of $\partial\Sigma$. These features are not shown until after the surface has been simplified by isotopy in Figure 3(b) and (c). Notice the placement of the α curves relative to the drilling tunnels in Figure 3(a). This was to ensure that there is one component of $\Sigma\backslash(\boldsymbol{\alpha}\cup\boldsymbol{\beta})$ that meets all three components of $\partial\Sigma$.

The borderd Heegaard diagram $\mathcal{H}$ in 3(c) can be represented in the plane (except for the handles) by cutting Σ open along the arcs in $\mathbf{z}$. The result is shown in Figure 4, and some relevant labels have been added. The Reeb chords along the three boundary components are labeled in the order consistent with type D boundaries, and they are denoted by ρ, σ, and τ instead of ρ^1, ρ^2, and ρ^3. The α arcs are also labeled to correspond to type D boundaries. Tracing through the sequence in Figure 3 with α labels in mind, note that the arcs α_1^ρ, α_2^σ, and α_1^τ represent curves in the base surface $\mathcal{P}$ of the S^1-bundle $\mathcal{Y}_\mathcal{P}$, and the arcs α_2^ρ, α_1^σ, and α_2^τ represent S^1 fibers.

Before computing $\widehat{CFD^3}(\mathcal{Y}_\mathcal{P})$, we make one final adjustment to the Heegaard diagram

$\mathcal{H}$. Computing directly from $\mathcal{H}$ would involve a few large and complicated domains which are difficult to analyze. It will be convenient to perform an isotopy to produce the new Heegaard diagram $\mathcal{H}'$ shown in Figure 5. This change introduces a few extra generators, but it eliminates the trickiest domains and overall makes the computation easier.

3.1.2 Complex Structure

To compute $\widehat{CFD^3}$, we also must fix a generically chosen complex structure J on Σ. We collect here some relevant choices about J that will be used in the computation. Note that if J were chosen with different properties we would get a different, but quasi-isomorphic, trimodule.

As in the proof of Proposition 2.7.4, if the annulus A has one α and one β segment on each boundary component, let $\Theta_A^{p,q}$ denote the ratio of the lengths of the α and β segments on the boundary component which contains p and q. As shorthand we will use, for example, the subscript "67" for the annulus R_6R_7. We will assume that J satisfies:

- $\Theta_{67}^{d,b} > \Theta_{67}^{i,i}$
- $\Theta_{1267}^{a,a} > \Theta_{1267}^{i,i}$

We will also assume that the following arcs are arbitrarily short, as in Proposition 2.7.5:

- an arc in R_3 from α_2^ρ to α_1^τ;
- an arc in R_8 from α_1^σ to α_1^τ;
- an arc in $R_1 \cup R_2$ parallel to α_2^τ, from β_1 to itself.

It is straightforward to check that these choices are consistent with each other and that there are suitable complex structures satisfying all of these conditions.

3.2 Generators

The chain complex $\widehat{CFD}^3(\mathcal{H}')$ is generated by the set $\mathfrak{S}(\mathcal{H}')$ consisting of triples of intersection points with one point on each β circle and at most one point on each α arc. In total, there are 23 generators. These generators fall into seven different spin^c-structures, corresponding to how many α arcs are occupied on each boundary component.

We begin by computing the summand of $\widehat{CFD}^3(\mathcal{H}')$ corresponding to the middle spin^c-structure, with exactly one α arc occupied on each boundary (the other spin^c-structures are much easier and will be addressed at the end of this section). There are seven generators in the middle spin^c-structure: $x = (a, e, i)$, $y = (a, g, h)$, $z = (c, f, i)$, $v = (b, f, i)$, $w = (d, f, i)$, $s = (a, j, i)$, and $t = (a, k, i)$.

3.3 Possible Domains

We begin by listing domains in $\pi_2(\mathbf{x}, \mathbf{y})$ for any pair of generators $\mathbf{x}$ and $\mathbf{y}$. Recall that a domain connecting $\mathbf{x}$ and $\mathbf{y}$ is a linear combination of the regions $R_1, \dots, R_9$ in Figure 5 with the correct multiplicity at each corner (that is, satisfying Equation 2.4). We do not need to list every domain in $\pi_2(\mathbf{x}, \mathbf{y})$, since only positive domains can have holomorphic representatives, and by Proposition 2.7.1 we can assume that regions which intersect $\partial\Sigma$ have multiplicity 0 or 1. The only region which does not intersect the boundary is R_9. The multiplicity of R_9 is also limited; in fact, R_9 can not combine with any other regions because domains with holomorphic representatives must be connected in $\Sigma\backslash(\alpha \cap \beta)$. Thus we can restrict to linear combinations of $R_1, \dots, R_8$ with multiplicity 0 or 1 for each region, and the single domain R_9. All such domains which connect two generators are listed in Table 1.

Table 1: Domains which potentially contribute to the differential. All subsets of the regions $\{R_1, \ldots, R_8\}$ with the proper corner multiplicities, and the single domain R_9. We omit the R for the purposes of this table. Thus 56 refers to the domain R_5R_6, which connects y to x.

from to	x	y	z	w	v	s	t
x	1267 4567	56	1567	167	1 14567	-	568
y	47	1267 4567	17	-	147	-	8 12678 45678
z	2467	26	1267 4567	467	4 12467	-	268
w	2 24567	256	5 12567	1267 4567	12 45 124567	-	2568
v	267	-	567	67	1267 4567	-	-
s	23 234567	2356	35 123567	3 12367 34567	123 345 1234567	1267 4567	23568 9
t	-	-	-	-	-	-	1267 4567

3.4 Analysis of Domains

3.4.1 Compatibility and Idempotents

Several domains in Table 1 can be ruled out using Proposition 2.7.1. Consider for example the domain R_2R_3, which potentially contributes to the differential from x to s. By Proposition 2.7.1, this domain can only contribute with the Reeb chords (ρ_1, ρ_2), and then the contribution $a(\rho_{12}) \otimes s$ is zero unless s contains a point on α_2^ρ. Since s does not contain a point on α_2^ρ, the domain R_2R_3 has zero contribution to the differential.

In general, for a differential ending in s to be nontrivial, the algebra element for the ρ boundary can not be ρ_2 or ρ_{12}. This means that the domain associated with such a differential can not contain R_2 without containing R_1. In addition to R_2R_3, this line of reasoning eliminates the domains $R_2R_3R_4R_5R_6R_7$, $R_2R_3R_5R_6$, and $R_2R_3R_5R_6R_8$. A similar analysis on the other boundaries shows that domains contributing nontrivial differentials ending in s cannot contain R_5 without R_4, R_7 without R_6, or R_8. This further rules out the domains R_3R_5 and $R_1R_2R_3R_5R_6R_7$. Finally, applying the same technique to differentials ending in other generators rules out the following domains:

domains to x :	4567, 14567, 568
domains to y :	1267, 4567
domains to z :	1267, 12467, 268
domains to w :	24567, 12567, 1267, 4567, 12, 45, 124567, 2568
domains to v :	1267, 4567

3.4.2 Polygons

Of the remaining domains from Table 1, many are immersed polygons and therefore contribute to the differential by Proposition 2.7.3. The proposition depends on the sequence of Reeb chords $\vec{\rho}$, but each of the following domains has only one compatible sequence of Reeb chords, so Proposition 2.7.3 tells us the entire contribution of the domain to the differential:

R_1	contributes	$v \xrightarrow{\rho_3} x$	R_2	contributes	$x \xrightarrow{\rho_2} w$
R_3	contributes	$w \xrightarrow{\rho_1\tau_1} s$	R_4	contributes	$v \xrightarrow{\tau_3} z$
R_5	contributes	$z \xrightarrow{\tau_2} w$	R_8	contributes	$t \xrightarrow{\sigma_3} y$
R_9	contributes	$t \xrightarrow{1} s$	R_1R_7	contributes	$z \xrightarrow{\rho_3\sigma_1} y$
R_2R_6	contributes	$y \xrightarrow{\rho_2\sigma_2} z$	R_4R_7	contributes	$x \xrightarrow{\tau_3\sigma_1} y$
R_5R_6	contributes	$y \xrightarrow{\tau_2\sigma_2} x$			

Here the notation $\mathbf{x} \xrightarrow{a} \mathbf{y}$ means that there is an $a \otimes \mathbf{y}$ term in $\partial\mathbf{x}$.

3.4.3 Index

At this point there are 22 domains in Table 1 whose contribution to $\widehat{CFD^k}$ remain unknown. Of these, 11 can be ruled out by showing that $\mathrm{ind}(B) \neq 1$. In general computing the index is a good task for a computer, but because we have narrowed the list of domains down so much we can work out the index computations by hand.

The quantities $e(B)$ and $n_\mathbf{x}(B)$ for any generator $\mathbf{x}$ are additive, so it is helpful to record their values for individual regions (see Table 2). For instance, region R_1 has euler measure $e(R_1) = -\frac{1}{2}$, because it has euler characteristic $\chi(R_1) = 1$ and six acute corners. R_1 has a corner at the point a, which means that the average multiplicity of R_1 near a is $\frac{1}{4}$. R_1 also has corners at b, e, and f. For the generator $x = (a, e, i)$ we find that $n_x(R_1) = \frac{1}{4} + \frac{1}{4} + 0 = \frac{1}{2}$, and for $y = (a, g, h)$ we get $n_y(R_1) = \frac{1}{4} + 0 + 0 = \frac{1}{4}$. It is straightforward to fill in the rest of Table 2.

From this information, it is easy to compute the index as in Table 3. We add the euler measures of all of the regions in a given domain B to find $e(B)$. Similarly, we add the values of $n_\mathbf{x}$ and $n_\mathbf{y}$ for each region for the relevant generators $\mathbf{x}$ and $\mathbf{y}$ to find $n_\mathbf{x}(B)$ and $n_\mathbf{y}(B)$. Finally, we count how many of the three components of $\partial\Sigma$ are touched by B (that is, we find $\#\{Z \in \pi_0(\partial\Sigma) | Z \cap B \neq \emptyset\}$), and add half of this number to $e(B) + n_\mathbf{x}(B) + n_\mathbf{y}(B)$. By Equation 2.6, the result is $\mathrm{ind}(B)$. Table 3 only shows the computation for regions that are ruled out by this method. The index can be computed

Table 2: Values of e and $n_{\mathbf{x}}$ for each region and each generator $\mathbf{x}$.

	e	n_x	n_y	n_z	n_v	n_w	n_s	n_t
R_1	$-\frac{1}{2}$	$\frac{1}{2}$	$\frac{1}{4}$	$\frac{1}{4}$	$\frac{1}{2}$	$\frac{1}{4}$	$\frac{1}{4}$	$\frac{1}{4}$
R_2	$-\frac{1}{2}$	$\frac{1}{2}$	$\frac{1}{4}$	$\frac{1}{4}$	$\frac{1}{4}$	$\frac{1}{2}$	$\frac{1}{4}$	$\frac{1}{4}$
R_3	-1	$\frac{1}{4}$	$\frac{1}{4}$	$\frac{1}{4}$	$\frac{1}{4}$	$\frac{1}{2}$	$\frac{1}{2}$	$\frac{1}{4}$
R_4	0	0	0	$\frac{1}{4}$	$\frac{1}{4}$	0	0	0
R_5	0	0	0	$\frac{1}{4}$	0	$\frac{1}{4}$	0	0
R_6	-1	$\frac{1}{2}$	$\frac{1}{2}$	$\frac{1}{2}$	$\frac{1}{4}$	$\frac{1}{2}$	$\frac{1}{4}$	$\frac{1}{4}$
R_7	-1	$\frac{1}{2}$	$\frac{1}{2}$	$\frac{1}{2}$	$\frac{1}{2}$	$\frac{1}{4}$	$\frac{1}{4}$	$\frac{1}{4}$
R_8	$-\frac{1}{2}$	$\frac{1}{4}$	$\frac{1}{2}$	$\frac{1}{4}$	$\frac{1}{4}$	$\frac{1}{4}$	$\frac{1}{4}$	$\frac{1}{2}$

in the same way for the remaining 11 domains, but they all have $\mathrm{ind}(B) = 1$, so more work is needed to determine if they contribute to $\widehat{CFD^k}$.

3.4.4 Index Zero Annulus

R_6R_7 is an index 0 annulus of the same form as A in Proposition 2.7.4. The domains $R_2R_6R_7$, $R_5R_6R_7$, $R_1R_6R_7$, and $R_4R_6R_7$ in $\mathcal{H}'$ correspond to the domains D_1, D_2, D_3, and D_4, respectively, in Figure 2. By Proposition 2.7.4, the contribution of these four domains is determined by the choice of complex structure J on Σ, and in particular on the resulting ratios of lengths $\Theta^{i,i}_{67}$ and $\Theta^{d,b}_{67}$. Recall that we chose the complex structure on Σ so that $\Theta^{d,b}_{67} > \Theta^{i,i}_{67}$.

It follows directly from the proof of Proposition 2.7.4 that $R_4R_6R_7$ and $R_5R_6R_7$ do not contribute to the differential for our choice of J. It is also true that $R_1R_6R_7$ contributes $\rho_3\sigma_{12} \otimes x$ to ∂w and $R_2R_6R_7$ contributes $\rho_2\sigma_{12} \otimes v$ to ∂x, but for these domains the

Table 3: Computation of index for relevant domains.

Domain	$\mathbf{x} \to \mathbf{y}$	$e(B)$	$n_{\mathbf{x}}$	$n_{\mathbf{y}}$	bdys hit/2	ind(B)
1267	$x \to x$	-3	2	2	1	2
2467	$x \to z$	$-\frac{5}{2}$	$\frac{3}{2}$	$\frac{3}{2}$	$\frac{3}{2}$	2
256	$y \to w$	$-\frac{3}{2}$	$\frac{3}{4}$	$\frac{5}{4}$	$\frac{3}{2}$	2
1567	$z \to x$	$-\frac{5}{2}$	$\frac{3}{2}$	$\frac{3}{2}$	$\frac{3}{2}$	2
4567	$z \to z$	-2	$\frac{3}{2}$	$\frac{3}{2}$	1	2
147	$v \to y$	$-\frac{3}{2}$	$\frac{5}{4}$	$\frac{3}{4}$	$\frac{3}{2}$	2
67	$w \to v$	-2	$\frac{3}{4}$	$\frac{3}{4}$	$\frac{1}{2}$	0
1267	$s \to s$	-3	1	1	1	0
4567	$s \to s$	-2	$\frac{1}{2}$	$\frac{1}{2}$	1	0
1267	$t \to t$	-3	1	1	1	0
4567	$t \to t$	-2	$\frac{1}{2}$	$\frac{1}{2}$	1	0

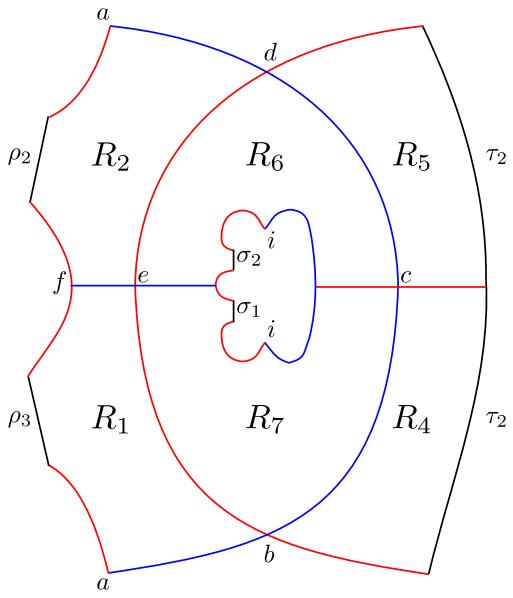

Figure 6: The index 0 annulus R_6R_7, with four surrounding regions.

outer boundary of the annulus has too many α and β segments to apply Proposition 2.7.4 directly. First we apply Proposition 2.7.5 and pinch along the arcs in R_1 or R_2 that are parallel to α_2^τ; recall that the complex structure was chosen to be consistent with pinching these arcs. The annuli that result from pinching the arcs completely have holomorphic representatives by Proposition 2.7.4, and so $R_1R_6R_7$ and $R_2R_6R_7$ contribute to the differential.

We need to perform a similar analysis on two more domains, which are obtained from adding regions to the index 0 annulus $R_1R_2R_6R_7$ (see Figure 7). If we let the inner boundary in Figure 7 correspond to the outer boundary in Figure 2, then R_8 is analogous to B_4. R_8 is not a bigon, however, so we must first use Proposition 2.7.5 to notice that the contribution of $R_1R_2R_6R_7R_8$ is the same as the contribution of the annulus which would result from collapsing an arc in R_8 which connects α_1^σ to α_1^τ. This pinched annulus would contribute *with the Reeb chords* $(\rho_2, \rho_3, \sigma_1, \sigma_2, \sigma_3)$ by Proposition 2.7.4, using the fact that $\Theta^{a,a}_{1267} > \Theta^{i,i}_{1267}$. Thus the pair $(R_1R_2R_6R_7, (\rho_2, \rho_3, \sigma_1, \sigma_2, \sigma_3))$ contributes to $\widehat{CFD}^k$. We emphasize however that this domain has a second compatible

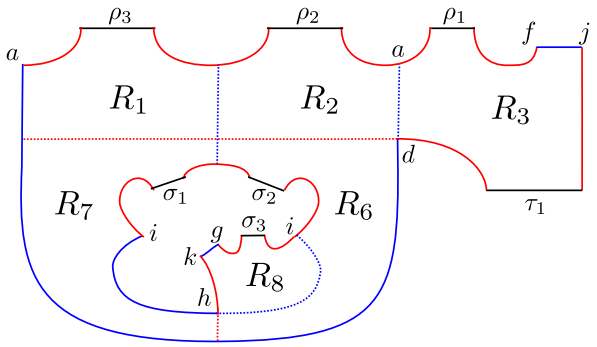

Figure 7: The annulus $R_1R_2R_6R_7R_8$ contributes to the differential, while $R_1R_2R_3R_6R_7$ does not.

sequence of Reeb chords, about which Proposition 2.7.4 says nothing. The contribution of this domain with $\vec{\rho} = (\rho_2, \rho_3, \sigma_{123})$ will be discussed in section 3.4.5.

The domain $R_1R_2R_3R_6R_7$, with Reeb chords $(\rho_1, \rho_2, \rho_3, \sigma_1, \sigma_2, \tau_1)$, can be analyzed in a similar way. By Propostion 2.7.5 we will treat R_3 as a bigon attached to $R_1R_2R_6R_7$, since the extra β segment can be removed by pinching along γ_3. In this case Proposition 2.7.4 does not apply, because the arc α_2^τ cutting into the annulus from the obtuse corner does not leave the annulus on the opposite boundary component, but the reasoning is similar. There is a one parameter family of cuts starting at d. We can define the ratios $\theta^{d,a}_{12367}$ and $\theta^{i,i}_{12367}$, which depend on the cutting parameter, as in the proof of Proposition 2.7.4. There is a holomorphic representative for each zero of $\theta^{d,a}_{12367} - \theta^{i,i}_{12367}$. Cutting along α_2^τ from d to b pinches off the annulus R_6R_7. In this extreme, $\theta^{d,a}_{12367} - \theta^{i,i}_{12367}$ approaches $\Theta^{d,b}_{67} - \Theta^{i,i}_{67}$, which is positive for our choice of complex structure. In the other extreme, cutting along β_1 from d to a pinches off the annulus $R_1R_2R_6R_7$, and $\theta^{d,a}_{12367} - \theta^{i,i}_{12367}$ becomes $\Theta^{a,a}_{1267} - \Theta^{i,i}_{1267} > 0$. Since $\theta^{d,a}_{12367} - \theta^{i,i}_{12367}$ has the same sign at both extremes, the number of zeros is even and the pair $(R_1R_2R_3R_6R_7, (\rho_1, \rho_2, \rho_3, \sigma_1, \sigma_2, \tau_1))$ does not contribute to the differential.

3.4.5 Decomposable Boundaries

We have determined the contribution of all domains in Table 1 except for the following seven:

$$\begin{array}{cccccc} R_1R_2R_3 & \text{from} & v & \text{to} & s \\ R_3R_4R_5 & \text{from} & v & \text{to} & s \\ R_1R_2R_3R_6R_7 & \text{from} & w & \text{to} & s \\ R_3R_4R_5R_6R_7 & \text{from} & w & \text{to} & s \\ R_1R_2R_6R_7R_8 & \text{from} & t & \text{to} & y \\ R_4R_5R_6R_7R_8 & \text{from} & t & \text{to} & y \\ R_1R_2R_3R_4R_5R_6R_7 & \text{from} & v & \text{to} & s \end{array}$$

Each of these domains is compatible with multiple Reeb chord sequences. The contribution of each domain/Reeb chord pair must be considered separately.

$\mathbf{R_1R_2R_3}$: The domain $R_1R_2R_3$ is compatible with both $\vec{\eta}_1 = (\rho_1, \rho_2, \rho_3, \tau_1)$ and $\vec{\eta}_2 = (\rho_{123}, \tau_1)$. By cutting along α arcs, the domain can be represented differently for each Reeb chord sequence (see Figure 8). Figure 8(a) is an immersed polygon; it is clear that the conditions of Propositions 2.7.3 are satisfied, and so the pair $(R_1, R_2, R_3, \vec{\eta}_1)$ contributes to the differential.

For $\vec{\eta}_2$, we use Lemma 2.7.6 and consider the $\mathcal{A}_\infty$ relation for $(v, \rho_1, \rho_{23}, \tau_3)$:

$$0 = m\left(v, \mu(\rho_1, \rho_{23}), \tau_3\right) + m\left(m(v, \rho_1), \rho_{23}, \tau_3\right).$$

There are no other nonzero terms in the relation. Note that it is impossible to have an $\mathcal{A}_\infty$ operation involving τ_3 and not ρ_3, since both Reeb chords are on the same region R_3. Thus the term $m\left(m(v, \rho_1, \tau_3), \rho_{23}\right)$ does not appear in the $\mathcal{A}_\infty$ relation. Since we use $\mathbb{F}_2$ coefficients, the relation above can be rewritten as

$$m(v, \rho_{123}, \tau_3) = m\left(m(v, \rho_1), \rho_{23}, \tau_3\right).$$

The inner operation on the right, $m(v, \rho_1)$, records the contribution of the domain R_1 with $\vec{\rho} = (\rho_1)$. We showed that this pair contributes in $\widehat{CFD}^3$, and so by Lemma 2.7.6

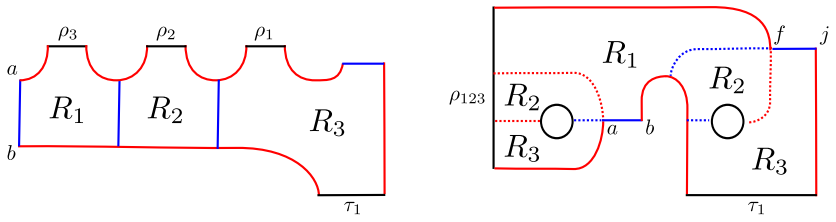

(a) (b)

Figure 8: Two versions of the domain $R_1R_2R_3$. (a) represents the sequence of Reeb chords $\vec{\eta}_1 = (\rho_3, \rho_2, \rho_1, \tau_1)$. This domain/Reeb chord pair is a polygon and contributes to the differential. (b) represents the sequence of Reeb chords $\vec{\eta}_2 = (\rho_{123}, \tau_1)$. This genus one domain also contributes to the differential

it also contributes to $\widehat{CFA}^{\beta}$. Thus $m(v, \rho_1) = x$. The outer operation is determined by the contribution of of the domain R_2R_3. This domain was eliminated from consideration for $\widehat{CFD}^{\beta}$, but it may still contribute to $\widehat{CFA}^{\beta}$. To find out if it does we use another $\mathcal{A}_\infty$ relation, this time for $(x, \rho_2, \rho_3, \tau_3)$. The relation implies that

$$m(x, \rho_{23}, \tau_3) = m\left(m(x, \rho_2), \rho_3, \tau_3\right).$$

Since R_2 and R_3 are known to contribute in $\widehat{CFD}^{k}$ (and thus in $\widehat{CFA}^{k}$), we find that $m(x, \rho_{23}, \tau_3) = m(w, \rho_3, \tau_3) = s$, and $m(v, \rho_{123}, \tau_3) = s$. By Lemma 2.7.6 the pair $(R_1R_2R_3), \vec{\eta}_2)$ contributes to $\widehat{CFD}^{k}$.

$(R_1R_2R_3, \vec{\eta}_1)$ and $(R_1R_2R_3, \vec{\eta}_2)$ both contribute the term $\rho_{123}\tau_1 s$ to $\partial(v)$ in $\widehat{CFD}^{k}$. Over $\mathbb{F}_2$, these contributions cancel, so the total contribution of $R_1R_2R_3$ to the differential is zero.

$\mathbf{R_3R_4R_5}$: The two compatible Reeb chord sequences are $\vec{\eta}_1 = (\rho_1, \tau_1, \tau_2, \tau_3)$ and $\vec{\eta}_2 = (\rho_1, \tau_{123})$. The first does not contribute, because a holomorphic representative consistent with $\vec{\eta}_1$ would project to $R_3R_4R_5$ with cuts along α_1^{τ} and α_2^{τ}, making the domain disconnected. If we do not cut the domain along α_1^{τ} and α_2^{τ}, we see that it is an immersed polygon compatible with $\vec{\eta}_2$, and Proposition 2.7.3 tells us that $(R_3R_4R_5, \vec{\eta}_2)$ contributes to the differential. Overall, the domain $R_3R_4R_5$ contributes $\rho_1\tau_{123}s$ to $\partial(v)$.

$\mathbf{R_1R_2R_3R_6R_7}$: This domain is compatible with $\vec{\eta}_1 = (\rho_1, \rho_2, \rho_3, \tau_1, \sigma_1, \sigma_2)$ and $\vec{\eta}_2 = (\rho_{123}, \tau_1, \sigma_1, \sigma_2)$. It was shown in the previous section that there is a contribution from $\vec{\eta}_1$. For the other case consider the A_∞ relation for $(w, \rho_1, \rho_{23}, \tau_3, \sigma_3, \sigma_2)$, which says that $m\left(w, \mu(\rho_1, \rho_{23}), \tau_3, \sigma_2, \sigma_1\right) = m\left(m(w, \rho_1, \sigma_3, \sigma_2), \rho_{23}, \tau_3\right)$. The inner operation on the right is nontrivial because we have shown that the domain $R_1R_6R_7$ contributes to $\widehat{CFD^3}$. The inner operation evaluates to x. The outer operation, $m(x, \rho_{23}, \tau_3)$, evaluates to s as shown above. Thus $m(w, \rho_{123}, \tau_3, \sigma_2, \sigma_1) = s$, and by Lemma 2.7.6 the pair $(R_1R_2R_3R_6R_7, \vec{\eta}_2)$ contributes to $\widehat{CFD^3}$. The total mod 2 contribution of $R_1R_2R_3R_6R_7$ is zero.

$\mathbf{R_3R_4R_5R_6R_7}$: This domain is compatible with $\vec{\eta}_1 = (\rho_1, \tau_1, \tau_2, \tau_3, \sigma_1, \sigma_2)$ and $\vec{\eta}_2 = (\rho_1, \tau_{123}, \sigma_1, \sigma_2)$. $\vec{\eta}_1$ does not contribute because realizing the domain with boundary Reeb chords $\vec{\eta}_1$ would involve cutting along α_2^τ, which leaves the domain disconnected. For the contribution of $\vec{\eta}_2$, consider the A_∞ relation for $(w, \rho_3, \tau_{12}, \tau_3, \sigma_3, \sigma_2)$. To find all terms of the relation, first note that any type A operation that involves $m(\mathbf{x}, \ldots, \tau_{12}, \tau_3, \ldots)$ will be trivial for boundary monotonicity reasons. As a result, any term in the $\mathcal{A}_\infty$ relation splits as an operation involving τ_{12} and an operation involving τ_3. We look in Table 1 for domains that connect w to another generator and involve R_4 and R_5, but not R_3, and some subset of $\{R_6, R_7\}$. The only option is the domain $R_4R_5R_6R_7$ connecting w to itself. The relation can be written as

$$m(w, \rho_3, \tau_{123}, \sigma_3, \sigma_2) = m\left(m(w, \tau_{12}, \sigma_3, \sigma_2), \rho_3, \tau_3\right).$$

To compute the inner operation on the right, we can use another $\mathcal{A}_\infty$ relation to show that

$$m(w, \tau_{12}, \sigma_3, \sigma_2) = m\left(m(w, \tau_1, \sigma_3, \sigma_2), \tau_2\right) = m(0, \tau_2) = 0,$$

where $m(w, \tau_1, \sigma_3, \sigma_2) = 0$ because the domain $R_4R_6R_7$ was shown not to contribute to $\widehat{CFD^3}$ based on the choice of complex structure J. Thus $(R_3R_4R_5R_6R_7, \vec{\eta}_2)$ does not contribute to $\widehat{CFA^3}$ or $\widehat{CFD^3}$, and overall the domain $R_3R_4R_5R_6R_7$ does not contribute.

$\mathbf{R_1R_2R_6R_7R_8}$: The compatible Reeb chord sequences are $\vec{\eta}_1 = (\rho_2, \rho_3, \tau_1, \sigma_1, \sigma_2, \sigma_3)$ and $\vec{\eta}_2 = (\rho_2, \rho_3, \tau_1, \sigma_{123})$. It has already been shown that there is no contribution with

$\vec{\eta}_1$. For the contribution of $\vec{\eta}_2$, use the $\mathcal{A}_\infty$ relation for $(t, \rho_2, \rho_1, \sigma_{12}, \sigma_3)$. Look for in Table 1 for domains starting at t which involve R_6 and R_8 but not R_7, and some subset of $\{R_1, R_2\}$; there is only one option. The $\mathcal{A}_\infty$ relation becomes

$$m(t, \rho_2, \rho_1, \mu(\sigma_{12}, \sigma_3)) = m(m(t, \rho_2, \sigma_{12}), \rho_1, \sigma_3) = m(z, \rho_1, \sigma_3) = y.$$

Thus by Lemma 2.7.6, the domain $R_1R_2R_6R_7R_8$ contributes $\rho_{23}\sigma_{123}y$ to $\partial(t)$.

$\mathbf{R_4R_5R_6R_7R_8}$: This domain is compatible with $\vec{\eta}_1 = (\tau_2, \tau_3, \sigma_1, \sigma_2, \sigma_3)$ and $\vec{\eta}_2 = (\tau_2, \tau_3, \sigma_{123})$. With $\vec{\eta}_1$, the $R_4R_5R_6R_7R_8$ is realized as an immersed polygon, so the pair contributes to the differential. With $\vec{\eta}_2$, the contribution of this domain is determined by the $\mathcal{A}_\infty$ relation

$$m(t, \tau_2, \tau_1, \mu(\sigma_{12}, \sigma_3)) = m(m(t, \tau_2, \sigma_{12}), \tau_1, \sigma_3) = m(x, \tau_1, \sigma_3) = y$$

and Lemma 2.7.6. The domain contributes with $\vec{\eta}_2$, and the total mod 2 contribution of the domain is zero.

$\mathbf{R_1R_2R_3R_4R_5R_6R_7}$: This domain has four compatible sequences of Reeb chords: $\vec{\eta}_1 = (\rho_1, \rho_2, \rho_3, \tau_1, \tau_2, \tau_3, \sigma_1, \sigma_2)$, $\vec{\eta}_2 = (\rho_1, \rho_2, \rho_3, \tau_{123}, \sigma_1, \sigma_2)$, $\vec{\eta}_3 = (\rho_{123}, \tau_1, \tau_2, \tau_3, \sigma_1, \sigma_2)$, and $\vec{\eta}_4 = (\rho_{123}, \tau_{123}, \sigma_1, \sigma_2)$. To obtain a boundary with Reeb chords $\vec{\eta}_1$, we must cut along all α arcs. This produces an immersed polygon, but there are too many edges and corners for Proposition 2.7.3 to apply. For instance, cutting along α_1^τ produces corners at h, but the generators v and s do not contain the point h. Therefore the domain does not contribute with $\vec{\eta}_1$. For the other sequences of Reeb chords, we can use Lemma 2.7.6 and appropriate $\mathcal{A}_\infty$ relations. We find that the domain contributes with $\vec{\eta}_2$ and $\vec{\eta}_4$, and not with $\vec{\eta}_3$. Overall with $\mathbb{F}_2$ coefficients the contribution of this domain is zero.

3.4.6 Canceling Differentials

Putting everything together, the differential on $\widehat{CFD^k}(\mathcal{Y}_\mathcal{P})$ is recorded in Figure 9. The unlabeled arrow from t to s is the differential corresponding to the bigon R_9. This

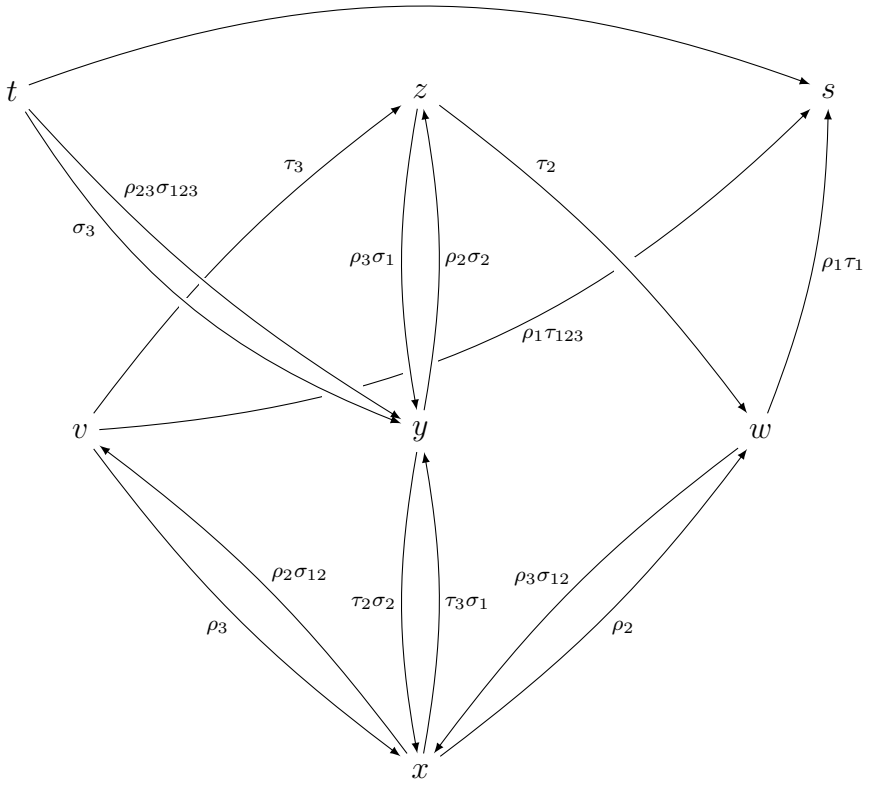

Figure 9: $\widehat{CFD^k}(\mathcal{H}')$ in the middle spin^c-structure, for the given choice of complex structure J.

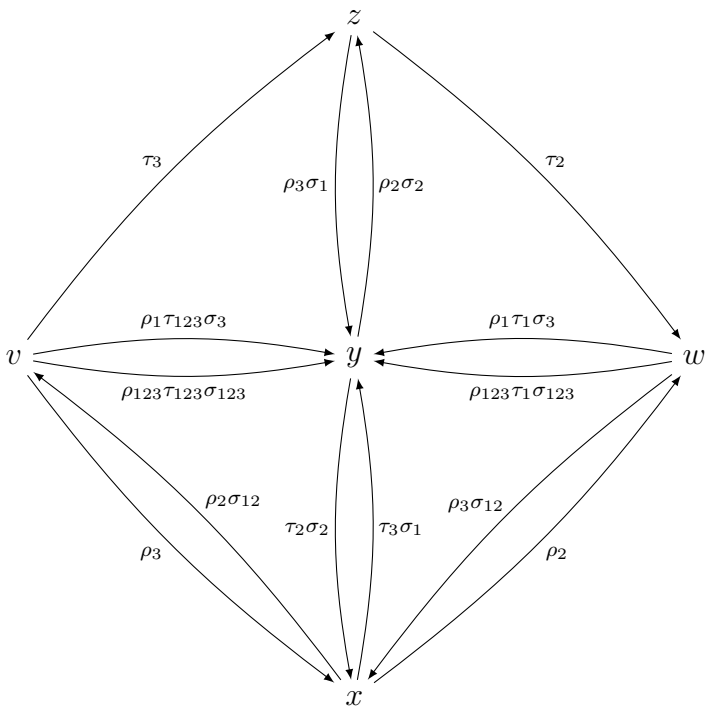

Figure 10: $\widehat{CFD}^3(\mathcal{Y}_\mathcal{P})$ in the middle spin^c-structure after canceling the differential from t to s in $\widehat{CFD}^3(\mathcal{H}')$.

unlabeled edge can be canceled using the edge reduction algorithm for type D structures described in Remark 2.1.1. We eliminate the arrow and the generators t and s, and for every "zig-zag"

$$\mathbf{x} \xrightarrow{a_1} s \longleftarrow t \xrightarrow{a_2} \mathbf{y}$$

we introduce the new arrow $\mathbf{x} \xrightarrow{a_1 \cdot a_2} \mathbf{y}$. The resulting simplified form of $\widehat{CFD}^k(\mathcal{Y}_\mathcal{P})$ (which is quasi-isomorphic to the first diagram) is given in Figure 10.

3.5 Extremal spin^c-structures

To complete the computation of $\widehat{CFD}^3(\mathcal{Y}_\mathcal{P})$, we must compute $\widehat{CFD}^3(\mathcal{Y}_\mathcal{P}, \mathfrak{s})$ for other spin^c-structures $\mathfrak{s}$.

(1, 2, 0): Consider first the spin^c-structure $\mathfrak{s}$ that has 1, 2, and 0 α arcs occupied on the ρ, σ, and τ boundaries, respectively. The only generator in this spin^c-structure is agi, so $\widehat{CFD^3}(\mathcal{Y}_\mathcal{P}, \mathfrak{s})$ has one generator and no differentials.

(2, 1, 0) and (2, 0, 1): The spin^c-structures with two arcs occupied on the ρ boundary each have only one generator, and no differentials. The generator with one α^σ arc is occupied is afi, and the generator with one α^τ arc occupied is afh.

(1, 0, 2): The spin^c-structure $\mathfrak{s}$ that has one α arc occupied on the ρ boundary, zero on the σ boundary, and two on the τ boundary has 3 generators: aeh, bfh, and dfh. Recall that domains connecting these generators may not touch the σ or τ boundaries, so we only need to consider the regions R_1, R_2, and R_9. It is easy to see that R_1 contributes a differential from bfh to aeh and R_2 contributes a differential from aeh to dfh (they are both polygons). None of the generators include the points i or j, so R_9 is not involved in any differentials. Finally, R_1R_2 does not contribute by Proposition 2.7.1; the corners make R_1R_2 a domain connecting bfh to dfh, but neither of these generators contain a point on α_1^ρ, which is required for a domain with Reeb chords (ρ_2, ρ_3) to contribute nontrivially. For this spin^c-structure, $\widehat{CFD^3}(\mathcal{Y}_\mathcal{P}, \mathfrak{s})$ is given by

$$bfh \xrightarrow{\rho_3} aeh \xrightarrow{\rho_2} dfh.$$

(0, 2, 1): This spin^c-structure has 3 generators: bgi, dgi, and dgi. Domains that contribute to the differential do not touch the ρ or σ boundaries. The only domains which connect two generators are R_4, R_5, and R_4R_5. It is clear that the polygons R_4 and R_5 contribute, but the contribution of R_4R_5 is zero. Thus $\widehat{CFD^3}(\mathcal{Y}_\mathcal{P}, \mathfrak{s})$ for this spin^c-structure is given by

$$bgi \xrightarrow{\tau_3} cgi \xrightarrow{\tau_2} dgi.$$

(0, 1, 2): This spin^c-structure has 7 generators: bgh, dgh, cei, bji, bki, djk, and dki. R_9 contributes differentials from bki to bji and from dki to dji. There can be no other differentials ending at bji or dji, so the edge reduction algorithm lets us cancel

these differentials and remove the generators bki, bji, dki, and dji without adding new differentials (it is worth noting that we could also compute $\widehat{CFD^3}(\mathcal{Y}_\mathcal{P}, \mathfrak{s})$ using the Heegaard diagram $\mathcal{H}$ in Figure 4 instead of $\mathcal{H}'$, and we would not have to deal with these four generators at all). The only domains connecting the remaining three generators are R_6, R_7, and R_6R_7. Once again, the individual regions contribute while R_6R_7 has zero contribution for idempotent reasons, and $\widehat{CFD^3}(\mathcal{Y}_\mathcal{P}, \mathfrak{s})$ is

$$dgh \xrightarrow{\sigma_2} cei \xrightarrow{\sigma_1} bgh.$$

3.6 Gradings

As described in Section 2.8, $\widehat{CFD^3}(\mathcal{Y}_\mathcal{P})$ is graded by a set which is a quotient of the noncommutative group $G_{3,0}$. We will compute this (relative) grading for the middle spin^c-structure, using the form of $\widehat{CFD^3}(\mathcal{Y}_\mathcal{P})$ depicted in Figure 10.

We choose x to be the preferred generator and assign it the grading $\vec{0} = (0; 0, 0; 0, 0; 0, 0)$. The arrow from x to w indicates that ∂x contains the term $\rho_2 w$, and thus $gr(\partial x) = gr(\rho_2 w)$. By the relation 2.7, we have

$$\lambda^{-1} gr(x) = gr(\partial x) = gr(\rho_2) gr(w),$$

and so

$$gr(w) = \lambda^{-1} gr(\rho_2)^{-1} gr(x) = \lambda^{-1} \left(\frac{1}{2}; -\frac{1}{2}, -\frac{1}{2}; 0, 0; 0, 0\right) \vec{0} = \left(-\frac{1}{2}; -\frac{1}{2}, -\frac{1}{2}; 0, 0; 0, 0\right).$$

Similarly, the arrow from z to w implies that $\lambda^{-1} gr(z) = gr(\partial z) = gr(\tau_2) gr(w)$, so

$$\begin{aligned} gr(z) &= \lambda \left(-\frac{1}{2}; 0, 0; 0, 0; \frac{1}{2}, \frac{1}{2}\right) \left(-\frac{1}{2}; -\frac{1}{2}, -\frac{1}{2}; 0, 0; 0, 0\right) \\ &= \left(0; -\frac{1}{2}, -\frac{1}{2}; 0, 0; \frac{1}{2}, \frac{1}{2}\right) \end{aligned}$$

The arrow from v to z implies that

$$\begin{aligned} gr(v) &= \lambda gr(\tau_3) gr(z) \\ &= \lambda \left(-\frac{1}{2}; 0, 0; 0, 0; -\frac{1}{2}, \frac{1}{2}\right) \left(0; -\frac{1}{2}, -\frac{1}{2}; 0, 0; \frac{1}{2}, \frac{1}{2}\right) \\ &= \left(0; -\frac{1}{2}, -\frac{1}{2}; 0, 0; 0, 1\right). \end{aligned}$$

Finally, the arrow from y to x implies that

$$\begin{aligned} gr(y) &= \lambda gr(\sigma_2) gr(\tau_2) gr(x) \\ &= \lambda \left(-\frac{1}{2}; 0, 0; \frac{1}{2}, \frac{1}{2}; 0, 0\right) \left(-\frac{1}{2}; 0, 0; 0, 0; \frac{1}{2}, \frac{1}{2}\right) \vec{0} \\ &= \left(0; 0, 0; \frac{1}{2}, \frac{1}{2}; \frac{1}{2}, \frac{1}{2}\right). \end{aligned}$$

We have now computed the gradings of each generator as elements of the group $G_{3,0}$. However, these gradings are only well defined modulo the action of $\mathcal{P}(x)$, the group generated by the gradings of periodic domains connecting x to itself. To finish the computation, we need to find $\mathcal{P}(x)$.

Consider the arrow from v to x, which implies that $\lambda^{-1} gr(v) = gr(\rho_3) gr(x)$. It follows that

$$\begin{aligned} gr(x) &= \lambda^{-1} gr(\rho_3)^{-1} gr(v) \\ &= \lambda^{-1} \left(\frac{1}{2}; \frac{1}{2}, -\frac{1}{2}; 0, 0; 0, 0\right) \left(0; -\frac{1}{2}, -\frac{1}{2}; 0, 0; 0, 1\right) \\ &= (-1; 0, -1; 0, 1; 0, 0). \end{aligned}$$

We have that $gr(x) = (-1; 0, -1; 0, 1; 0, 0)$, but also that $gr(x) = \vec{0}$. It follows that $(-1; 0, -1; 0, 1; 0, 0)$ and $\vec{0}$ are equivalent modulo $\mathcal{P}(x)$, and thus that $(-1; 0, -1; 0, 1; 0, 0) \in \mathcal{P}(x)$. In fact, since this nonzero value of $gr(x)$ was obtained from $\vec{0}$ by following a loop of edges with oriented labels $(\rho_2, -\tau_2, -\tau_3, \rho_3)$, the difference $(-1; 0, -1; 0, 1; 0, 0)$ corresponds to the grading of a periodic domain with boundary $\rho_{23} - \tau_{23}$.

Another value for $gr(x)$, and thus another element of $\mathcal{P}(x)$, can be found by consid-

ering the arrow from x to y. We have that

$$\begin{aligned} gr(x) &= \lambda gr(\sigma_1)gr(\tau_3)gr(y) \\ &= \lambda\left(-\frac{1}{2};0,0;\frac{1}{2},-\frac{1}{2};0,0\right)\left(-\frac{1}{2};0,0;0,0;-\frac{1}{2},\frac{1}{2}\right)\left(0;0,0;\frac{1}{2},\frac{1}{2};\frac{1}{2},\frac{1}{2}\right) \\ &= (0;0,0;1,0;0,1)\,. \end{aligned}$$

So $(0;0,0;1,0;0,1)$ is an element of $\mathcal{P}(x)$, corresponding to a periodic domain with boundary $\sigma_{12}+\tau_{23}$.

Consider the loop formed by the arrow from y to x, the $\rho_1\sigma_3\tau_{123}$ arrow from w to x, and the arrow from x to w. This loop corresponds to a periodic domain with boundary $\rho_{12}+\sigma_{23}+\tau_{12}$. As before, starting with $gr(x)=\vec{0}$ the arrow from y to x implies that $gr(y)=\left(0;0,0;\frac{1}{2},\frac{1}{2};\frac{1}{2},\frac{1}{2}\right)$. The arrow from w to y then implies that

$$\begin{aligned} gr(w) &= \lambda gr(\rho_1)gr(\sigma_3)gr(\tau_1)gr(y) \\ &= \lambda\left(-\frac{1}{2};\frac{1}{2},-\frac{1}{2};0,0;0,0\right)\left(-\frac{1}{2};0,0;-\frac{1}{2},\frac{1}{2};0,0\right)\left(-\frac{1}{2};0,0;0,0;\frac{1}{2},-\frac{1}{2}\right)gr(y) \\ &= \left(-\frac{1}{2};\frac{1}{2},-\frac{1}{2};-\frac{1}{2},\frac{1}{2};\frac{1}{2},-\frac{1}{2}\right)\left(0;0,0;\frac{1}{2},\frac{1}{2};\frac{1}{2},\frac{1}{2}\right) \\ &= \left(-\frac{1}{2};\frac{1}{2},-\frac{1}{2};0,1;1,0\right). \end{aligned}$$

The arrow from x to w then implies that

$$\begin{aligned} gr(x) &= \lambda gr(\rho_2)gr(w) \\ &= \lambda\left(-\frac{1}{2};\frac{1}{2},\frac{1}{2};0,0;0,0\right)\left(-\frac{1}{2};\frac{1}{2},-\frac{1}{2};0,1;1,0\right) \\ &= \left(-\frac{1}{2};1,0;0,1;1,0\right) \end{aligned}$$

is an element of $\mathcal{P}(x)$.

Since $\mathcal{Y}_{\mathcal{P}}$ has 3 boundary components, the space of periodic domains has dimension 3. Since the three elements of $\mathcal{P}(x)$ we have found are independent, they are enough to determine $\mathcal{P}(x)$:

$$\mathcal{P}(x)=\left\langle(-1;0,-1;0,1;0,0),(0;0,0;1,0;0,1),\left(-\frac{1}{2};1,0;0,1;1,0\right)\right\rangle$$

Chapter 4

Self Gluing

Any graph manifold which is represented by a tree with only genus zero vertices can be obtained by gluing together copies of $\mathcal{Y}_{\mathcal{P}}$, solid tori, and mapping cylinders of appropriate Dehn twists. Each time a new piece is glued on, the new bordered Heegaard Floer invariants can be obtained as a box tensor product by the pairing theorem.

To build up an arbitrary graph manifold from these building blocks, however, it is often necessary to glue two boundaries of one manifold together. The resulting bordered invariants are obtained by taking Hochschild homology. In this case, we must insert an additional bimodule, which corresponds to gluing a certain bordered Heegaard diagram $\mathcal{H}_{SG}$ (Figure 11) between the two boundary components that are being glued. Strictly speaking, $\mathcal{H}_{SG}$ is a bordered sutured diagram. This process is discussed in [11, Section 4.4], and a Heegaard diagram isotopic to $\mathcal{H}_{SG}$ is given there, but the bimodule associated to this Heegaard diagram is not computed. Let $\mathcal{Y}_{SG}$ denote the manifold represented by $\mathcal{H}_{SG}$. The focus of the present chapter is to compute $\widehat{CFDD}(\mathcal{Y}_{SG})$.

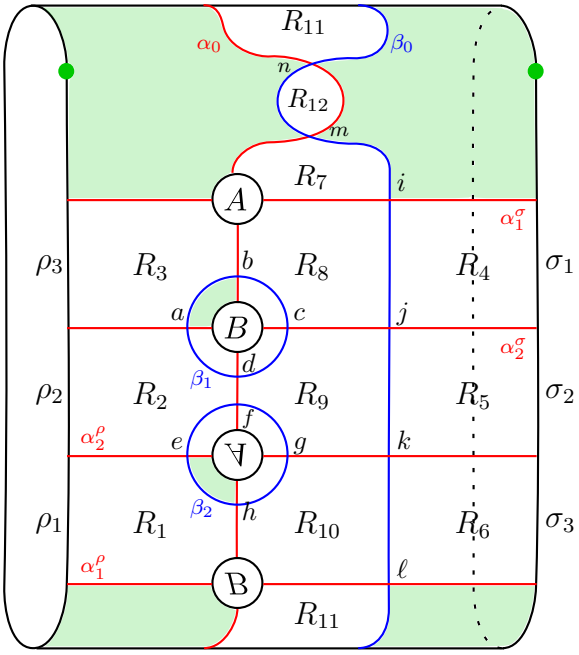

Figure 11: A Heegaard diagram $\mathcal{H}_{SG}$ for the self gluing bimodule.

4.1 Preliminaries

We first restrict our attention to the middle spin^c-structure, where exactly one α arc is occupied at each boundary component. In fact, this computation gives all of $\widehat{CFDD}(\mathcal{H}_{SG})$; it will be shown in Section 4.3 that the other summands for $\widehat{CFDD}(\mathcal{H}_{SG})$ are trivial.

4.1.1 Complex Structure

As always, the computation of $\widehat{CFDD}(\mathcal{H}_{SG})$ depends on the complex structure J chosen for the Heegaard surface Σ. We will make the following assumptions:

- $\Theta^{d,b}_{8,9} < \Theta^{i,k}_{8,9}$;
- $\Theta^{h,f}_{9,10} < \Theta^{j,l}_{9,10}$;
- $\Theta^{a,a}_{2,3,8,9} < \Theta^{i,k}_{2,3,8,9}$;

- $\Theta^{e,e}_{1,2,9,10} < \Theta^{j,l}_{1,2,9,10}$.

We will also assume that the following arcs are sufficiently pinched to apply Proposition 2.7.5 when necessary:

- an arc through R_1, R_2 and R_3 parallel to α_0 connecting β_2 in R_1 to β_1 in R_3;
- an arc in R_7 parallel to α_0, connecting β_0 to β_2;
- an arc in R_{11} parallel to α_0, connecting β_0 to β_1.

Finally, we will also assume that $\Theta^{h,b}_{2,5,8,9,9,10} < \Theta^{i,\ell}_{2,5,8,9,9,10}$, where here $\Theta_{2,5,8,9,9,10}$ refers to the appropriate ratio of α and β lengths for the annulus obtained from $R_2R_5R_8R_9R_9R_{10}$ by pinching along the arc through R_2 mentioned above (see Figure 13).

4.1.2 Generators

$\widehat{CFDD}(\mathcal{H}_{SG})$ has 20 generators in the middle spin^c structure: afi, afj, afk, afl, ahi, ahj, ahk, ahl, ang, amg, ebi, ebj, ebk, ebl, edi, edj, edk, edl, enc, and emc.

4.1.3 Domains

To list the domains that might contribute to $\widehat{CFDD}(\mathcal{H}_{SG})$, note that the multiplicities of the regions on the boundary $(R_1, \dots, R_6)$ are at most 1, and the region R_{12} cannot be combined with any other regions. Checking all positive connected domains which satisfy these conditions for appropriate corner multiplicity, we find 292 domains to consider. Of these, 200 can be eliminated by Proposition 2.7.2 or Proposition 2.7.1 (though we should make note of these domains, in case they come up when checking $\mathcal{A}_\infty$ relations). All of these steps are easy to perform with a computer program. The remaining 92 domains are listed in Table 4.

Regions	$\mathbf{x}$	$\mathbf{y}$
1	edi	ahi
1	edj	ahj
1	edk	ahk
1	edl	ahl
2	afi	edi
2	afj	edj
2	afk	edk
2	afl	edl
3	ebi	afi
3	ebj	afj
3	ebk	afk
3	ebl	afl
4	afj	afi
4	ahj	ahi
4	ebj	ebi
4	edj	edi
5	afk	afj
5	ahk	ahj
5	ebk	ebj
5	edk	edj
6	afl	afk
6	ahl	ahk
6	ebl	ebk
6	edl	edk
7	amg	ahi
11	ebl	enc
12	amg	ang
12	emc	enc
1,2,3	ebi	ahi
1,2,3	ebj	ahj
1,2,3	ebk	ahk

Regions	$\mathbf{x}$	$\mathbf{y}$
1,2,3	ebl	ahl
1,6,10	enc	ang
1,6,10	emc	amg
1,9,10	edj	afl
1,10,11	ebk	ang
2,5,9	ang	enc
2,5,9	amg	emc
2,8,9	afi	ebk
2,9,10	ahj	edl
3,4,8	enc	ang
3,4,8	emc	amg
3,7,8	emc	ahj
3,8,9	edi	afk
4,5,6	afl	afi
4,5,6	ahl	ahi
4,5,6	ebl	ebi
4,5,6	edl	edi
4,8,9	edj	ebk
4,8,11	afl	ang
5,8,9	edi	ebj
5,9,10	ahk	afl
6,7,10	emc	edi
6,9,10	ahj	afk
1,2,3,8,9	edi	ahk
1,2,3,9,10	ebj	afl
1,2,5,9,10	ebk	ebl
1,2,6,9,10	ebj	ebk
1,2,9,10,11	ebj	enc
1,5,6,9,10	edi	afi
1,8,9,10,11	edi	ang
2,3,4,8,9	ahj	ahk

Regions	$\mathbf{x}$	$\mathbf{y}$
2,3,5,8,9	ahi	ahj
2,3,7,8,9	amg	ahk
2,4,5,8,9	afl	ebl
2,5,6,9,10	ahi	edi
3,4,5,8,9	edl	afl
3,7,8,9,10	emc	afl
4,5,6,8,9	edl	ebk
4,5,6,9,10	ahj	afi
4,5,8,9,11	edl	enc
4,8,9,10,11	ahj	ang
5,6,7,9,10	amg	afi
6,7,8,9,10	emc	ebk
7,8,9,10,11	amg	ang
7,8,9,10,11	emc	enc
1,2,3,4,5,8,9	edl	ahl
1,2,3,5,6,9,10	ebi	afi
1,2,3,7,8,9,10	emc	ahl
1,2,3,8,9,10,11	ebi	ang
1,2,4,5,6,9,10	ebj	ebi
1,2,5,8,9,9,10	edi	ebl
2,3,4,5,6,8,9	ahl	ahk
2,3,5,8,9,9,10	ahi	afl
2,4,5,8,9,9,10	ahj	ebl
2,5,6,8,9,9,10	ahi	ebk
2,5,7,8,9,9,10	amg	ebl
2,5,8,9,9,10,11	ahi	enc
4,5,6,7,8,9,10	emc	ebi
4,5,6,8,9,10,11	ahl	ang
1,2,3,4,5,6,8,9,10	enc	ang
1,2,3,4,5,6,8,9,10	emc	amg

Table 4: List of 92 domains that might contribute to $\widehat{CFDD}(\mathcal{H}_{SG})$, with the corresponding initial generators $\mathbf{x}$ and final generators $\mathbf{y}$.

4.2 Analysis of Domains

4.2.1 Polygons

All of the single region domains are easily seen to be polygons, and thus contribute to the differential by Proposition 2.7.3. In addition, it is easy to check that the following domains are polygons: $R_1R_6R_{10}$, $R_1R_{10}R_{11}$, $R_2R_5R_9$, $R_3R_4R_8$, $R_3R_7R_8$, $R_4R_8R_{11}$, and $R_6R_7R_{10}$. Each domain has only one sequence of Reeb chords to consider. Thus by Proposition 2.7.3 each of these domains contributes, and we have quickly dispatched 38 of the entries in Table 4.

The domain $R_4R_5R_8R_9R_{11}$ is a polygon, though it may not be obvious at first glance. The only compatible sequence of Reeb chords is (σ_1, σ_2). To realize the domain as an immersed surface with boundary Reeb chords (σ_1, σ_2), we must cut along α_2^σ, which produces a polygon (see Figure 12). Similarly, the domain $R_5R_6R_7R_9R_{10}$ corresponds to a polygon with boundary (σ_2, σ_3) after cutting along α_1^σ. By Proposition 2.7.3, both of these domains contribute to the differential.

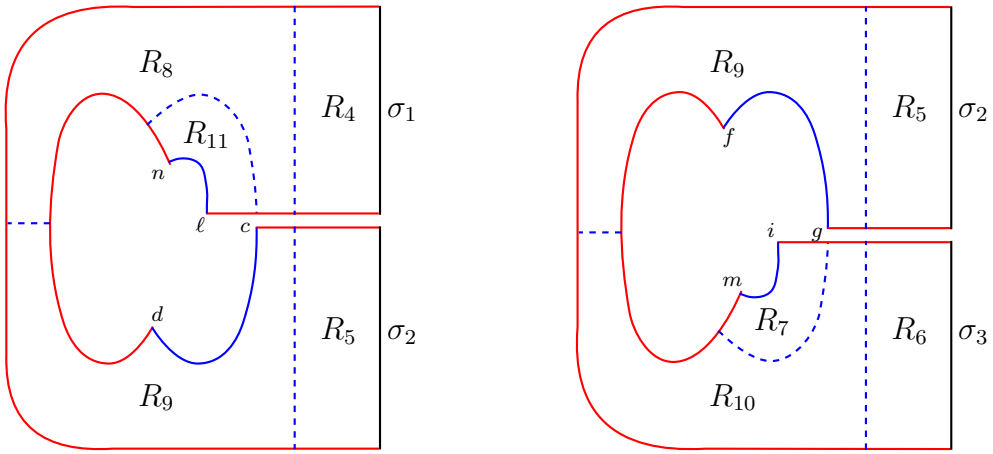

Figure 12: Regions $R_4R_5R_8R_9R_{11}$ and $R_5R_6R_7R_9R_{10}$ are both realized as immersed polygons when cut along α_2^σ and α_1^σ, respectively.

$R_1R_2R_3$ and $R_4R_5R_6$ can also be realized as polygons, and thus contribute with Reeb

chords (ρ_1, ρ_2, ρ_3) and (σ_{123}), respectively. Furthermore, $R_4R_5R_6$ can not contribute with its other sequence of compatible Reeb chords, $(\sigma_1, \sigma_2, \sigma_3)$, since cutting along the α^σ arcs from the boundary would produce a disconnected domain. Overall the domain $R_4R_5R_6$ contributes to the differential for each pair of generators it connects. The contribution of $R_1R_2R_3$ with (ρ_{123}) can be understood by examining the $\mathcal{A}_\infty$ relations for $(eb*, \rho_1, \rho_{23})$ and $(af*, \rho_2, \rho_3)$, where $*$ can be i, j, k, or l. The relations imply that

$$m(eb*, \rho_{123}) = m\left(m\big(m(eb*, \rho_1), \rho_2\big), \rho_3\right) = ah*.$$

Since the operation is nontrivial in $\widehat{CFAA}$, $(R_1R_2R_3, (\rho_{123}))$ contributes to the differential from $eb*$ to $ah*$ in $\widehat{CFDD}(\mathcal{H}_{SG})$ by Proposition 2.7.6, and the total mod 2 contribution of $R_1R_2R_3$ is zero.

4.2.2 Simple annuli

R_8R_9 is an index zero annulus analogous to A in Proposition 2.7.4. The four domains obtained by adding R_2, R_3, R_4, or R_5 to this annulus may or may not contribute to $\widehat{CFDD}(\mathcal{H}_{SG})$, depending on the choice of complex structure on R_8R_9. Since we have chosen J such that $\Theta^{d,b}_{8,9} < \Theta^{i,k}_{8,9}$, Proposition 2.7.4 asserts that none of these four domains contributes. Notice that since R_2 and R_3 are not bigons, we must first use Proposition 2.7.5 to pinch off the extra α portion of the boundary, and then we can apply Proposition 2.7.4. We specifically chose the complex structure J to be consistent with pinching the appropriate arcs in R_2 and R_3.

Similarly, R_9R_{10} is an index zero annulus to which the regions R_1, R_2, R_5, or R_6 may be added. Given the choice that $\Theta^{h,f}_{9,10} < \Theta^{j,l}_{9,10}$, none of the four corresponding domains contribute.

Two more direct applications of Proposition 2.7.4 involve the annuli $R_2R_3R_8R_9$ and $R_1R_2R_9R_{10}$. Given that $\Theta^{a,a}_{2,3,8,9} < \Theta^{i,k}_{2,3,8,9}$, $R_2R_3R_7R_8R_9$ contributes to $\widehat{CFDD}(\mathcal{H}_{SG})$, but $R_2R_3R_4R_8R_9$ and $R_2R_3R_5R_8R_9$ do not. The fact that $\Theta^{e,e}_{1,2,9,10} < \Theta^{j,l}_{1,2,9,10}$ implies that $R_1R_2R_9R_{10}R_{11}$ contributes to $\widehat{CFDD}(\mathcal{H}_{SG})$, but $R_1R_2R_5R_9R_{10}$ and $R_1R_2R_6R_9R_{10}$

do not. Note that for $R_2R_3R_7R_8R_9$ and $R_1R_2R_9R_{10}R_{11}$ we make use of Proposition 2.7.5 and the relevant assumptions about the complex structure on R_7 and R_{11}.

Finally, we will use Proposition 2.7.4 to account for the domain $R_2R_4R_5R_8R_9R_9R_{10}$, which connects ahj to ebl. There is only one way to piece together these regions so that there are no unwanted corners, which is shown in Figure 13. If we pinch R_2 along the arc connecting the two β curves, then this domain has exactly the form of D_2 in Proposition 2.7.4. Since we chose J such that $\Theta^{h,b}_{2,5,8,9,9,10} < \Theta^{i,\ell}_{2,5,8,9,9,10}$, it follows that this domain does not count.

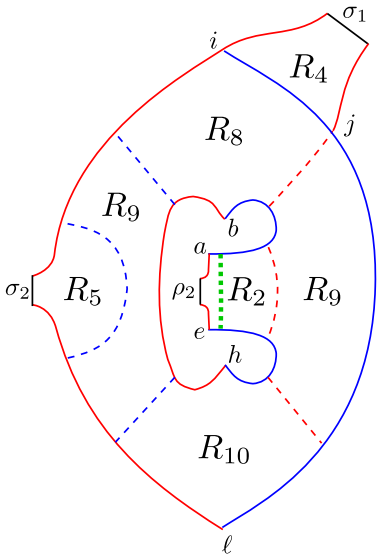

Figure 13: The domain $R_2R_4R_5R_8R_9R_9R_{10}$. It is just like the annulus $A + B_2$ in Figure 2, except that the inner boundary has too many α and β segments. To fix this, we pinch along the green dotted arc in R_2.

4.2.3 More annuli

The domain $R_1R_2R_3R_8R_9$, with the Reeb chords (ρ_1, ρ_2, ρ_3), is an annulus with one obtuse corner. If we pinch along the the arc through R_1, R_2, and R_3 parallel to α_0, the modified annulus has one α and one β segment on each boundary component. In this situation,

we can apply the same reasoning as the proof of Proposition 2.7.4 (the only difference is that the cuts from the obtuse corner do not leave the annulus through to the opposite boundary component). Cutting along β_1 from d makes the length of β on the boundary component containing d grow, so that as c approaches $+\infty$, $\theta^{d,a}_{1,2,3,8,9}(c)$ approaches $-\infty$, and $\theta^{d,a}_{1,2,3,8,9}(c) - \theta^{i,k}_{1,2,3,8,9}(c)$ is negative. On the other hand, cutting along α_0 from d pinches off $R_1R_2R_3$ from the annulus R_8R_9. In this extreme, $\theta^{d,a}_{1,2,3,8,9}(c) - \theta^{i,k}_{1,2,3,8,9}(c)$ approaches $\Theta^{d,b}_{8,9} - \Theta^{i,k}_{8,9} < 0$. Since the extremes are both negative, the mod 2 count of zeros, and thus the contribution of $R_1R_2R_3R_8R_9$ to $\widehat{CFDD}(\mathcal{H}_{SG})$, is zero. An analogous argument shows that $R_1R_2R_3R_9R_{10}$ does not contribute with (ρ_1, ρ_2, ρ_3).

$R_1R_2R_3R_8R_9$ may also contribute with the Reeb chord sequence (ρ_{123}). This contribution can be checked with the $\mathcal{A}_\infty$ trick, using the relation for (edi, ρ_1, ρ_{23}). This relation implies that $m(edi, \rho_{123}) = m\left(m(edi, \rho_1), \rho_{23}\right)$. The only domain that could contribute a nontrivial operation $m(edi, \rho_1)$ is $R_3R_8R_9$. As discussed above, $R_3R_8R_9$ does not contribute for our choice of complex structure J, and therefore $R_1R_2R_3R_8R_9$ does not contribute with $\vec{\rho} = (\rho_{123})$. An analogous argument also shows that $R_1R_2R_3R_9R_{10}$ does not contribute with (ρ_{123}).

The domain $R_4R_5R_6R_8R_9$ follows the same pattern. With Reeb chords $(\sigma_1, \sigma_2, \sigma_3)$ it is an annulus, and cuts in either direction split off the annulus R_8R_9 or the annulus $R_4R_5R_8R_9$. As we cut along β_0, $\theta^{l,k}_{4,5,6,8,9}(c) - \theta^{d,b}_{4,5,6,8,9}$ approaches $\Theta^{i,k}_{8,9} - \Theta^{d,b}_{8,9} > 0$. As we cut along α^σ_1 toward the σ boundary, $\theta^{l,k}_{4,5,6,8,9}(c)$ approaches ∞, and so $\theta^{l,k}_{4,5,6,8,9}(c) - \theta^{d,b}_{4,5,6,8,9}$ becomes positive. As a result, there is no contribution to the differential. The $\mathcal{A}_\infty$ relation for $(edl, \sigma_{12}, \sigma_3)$ reveals that $R_4R_5R_6R_8R_9$ also does not contribute with (σ_{123}). A similar argument shows that the domain $R_4R_5R_6R_9R_{10}$ does not contribute with either compatible sequence of Reeb chords.

4.2.4 Corners

Consider the domain $R_1R_2R_3R_4R_5R_8R_9$, which connects edl to ahl. Any compatible sequence of Reeb chords must contain (σ_1, σ_2), since (σ_{12}) would not be strongly bound-

ary monotonic with respect to the σ boundary. For the domain to have the chords (σ_1, σ_2) along the σ boundary, there must be a cut along α_1^σ. However, such a cut would leave corners at the point c. Since neither the initial generator edl nor the final generator ahl contain c, it is impossible to have a corner at c. As a result, the domain $R_1R_2R_3R_4R_5R_8R_9$ can not contribute to $\widehat{CFDD}(\mathcal{H}_{SG})$. The same reasoning applies to the domains $R_2R_4R_5R_8R_9$ and $R_3R_4R_5R_8R_9$.

Similarly, $R_1R_2R_3R_5R_6R_9R_{10}$ is only compatible with Reeb chord sequences containing (σ_2, σ_3). This Reeb chord sequence requires a cut along α_1^σ, which leaves corners at the point g. Since the initial generator ebi and the final generator afi do not contain g, this domain can not contribute to the differential. The same is true for the domains $R_1R_5R_6R_9R_{10}$ and $R_2R_5R_6R_9R_{10}$, so these also do not contribute.

The domain $R_2R_5R_8R_9R_9R_{10}R_{11}$ connects the generators ahi and enc. However, there is no way to piece together these seven regions without having corners at points other than a, h, i, e, n, and c. Therefore, this domain can not contribute to the differential.

4.2.5 $\mathbf{R_1R_2R_3R_4R_5R_6R_8R_9R_{10}}$

This domain has four compatible sequences of Reeb chords. It is possible to use $\mathcal{A}_\infty$ relations and analyze the contribution of each one. However, it is easier to notice that this domain contributes if an only if the shaded domain contributes in the Heegaard diagram for the mapping cylinder of the identity map shown in Figure 14. The computation of $\widehat{CFDD}(\mathbb{I})$ in [9, Proposition 10.1] reveals that this domain must contribute.

4.2.6 Using $\partial^2 = 0$

We can deduce the contribution of other domains using the fact that $\widehat{CFDD}(\mathcal{H}_{SG})$ must satisfy $\partial^2 = 0$. At this point, we have enough information to deduce the contribution of all domains but one using ∂^2. Table 5 gives the differential on $\widehat{CFDD}(\mathcal{H}_{SG})$ as computed so far, with coefficients $\lambda_{i_1,\dots,i_k}$ representing unknown contributions. $\lambda_{i_1,\dots,i_k}$ is 1 if the

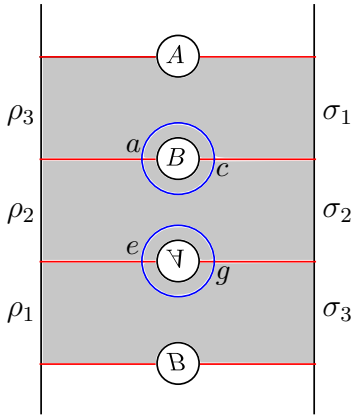

Figure 14: A bordered Heegaard diagram for the identity bimodule, $\widehat{CFDD}(\mathbb{I})$. $R_1R_2R_3R_4R_5R_6R_8R_9R_{10}$ contributes to $\widehat{CFDD}(\mathcal{H}_{SG})$ if and only if the shaded region contributes to the differential from ec to ag in $\widehat{CFDD}(\mathbb{I})$.

domain $R_{i_1}\cdots R_{i_k}$ contributes to the differential, and 0 otherwise.

Consider the generator ahj. $\partial(ahj) = \sigma_1(ahi) + \lambda_{4,8,9,10,11}\sigma_1(ang)$, and so

$$\begin{aligned} 0 = \partial^2(ahj) &= \sigma_1\big(\lambda_{2,3,5,8,9,9,10}\rho_{23}\sigma_2(afl) + \lambda_{2,5,6,8,9,9,10}\rho_2\sigma_{23}(ebk)\big) \\ &\quad +\lambda_{4,8,9,10,11}\sigma_1\big(\rho_2\sigma_2(enc)\big). \end{aligned}$$

It follows that $\lambda_{2,3,5,8,9,9,10} = \lambda_{2,5,6,8,9,9,10} = \lambda_{4,8,9,10,11} = 0$. Given these values, we find that

$$\begin{aligned} 0 = \partial^2(edi) &= \rho_1\big(0\big) + \lambda_{1,8,9,10,11}\rho_1\big(\rho_2\sigma_2(enc)\big) \\ &\quad +\lambda_{1,2,5,8,9,9,10}\rho_{12}\sigma_2\Big(\rho_3(afl) + \sigma_{123}(ebi) + \sigma_3(ebk) + (enc)\Big) \\ &= \big(\lambda_{1,8,9,10,11} + \lambda_{1,2,5,8,9,9,10}\big)\rho_{12}\sigma_2(enc) \\ &\quad +\lambda_{1,2,5,8,9,9,10}\rho_{123}\sigma_2(afl) \\ &\quad +\lambda_{1,2,5,8,9,9,10}\rho_{12}\sigma_{23}(ebk). \end{aligned}$$

The coefficient of afl implies that $\lambda_{1,2,5,8,9,9,10} = 0$, and the coefficient of enc implies that $\lambda_{1,8,9,10,11} = 0$.

$$
\begin{aligned}
\partial(afi) &= \rho_2(edi)\\
\partial(afj) &= \sigma_1(afi) + \rho_2(edj)\\
\partial(afk) &= \sigma_2(afj) + \rho_2(edk)\\
\partial(afl) &= \sigma_{123}(afi) + \sigma_3(afk) + \sigma_1 ang + \rho_2 edl\\
\partial(ahi) &= \lambda_{2,3,5,8,9,9,10}\rho_{23}\sigma_2(afl) + \lambda_{2,5,6,8,9,9,10}\rho_2\sigma_{23}(ebk)\\
\partial(ahj) &= \sigma_1(ahi) + \lambda_{4,8,9,10,11}\sigma_1(ang)\\
\partial(ahk) &= \sigma_2(ahj)\\
\partial(ahl) &= \sigma_{123}(ahi) + \sigma_3(ahk) + \lambda_{2,3,4,5,6,8,9}\rho_{23}\sigma_{123}(ahk) + \lambda_{4,5,6,8,9,10,11}\sigma_{123}(ang)\\
\partial(ang) &= \rho_2\sigma_2(enc)\\
\partial(amg) &= \sigma_{23}(afi) + (ahi) + \rho_{23}(ahk) + \lambda_{7,8,9,10,11}(ang) + (ang)\\
&\quad + \lambda_{2,5,7,8,9,9,10}\rho_2\sigma_2(ebl) + \rho_2\sigma_2(emc)\\
\partial(ebi) &= \rho_3(afi) + \lambda_{1,2,3,8,9,10,11}\rho_{123}(ang)\\
\partial(ebj) &= \rho_3(afj) + \sigma_1(ebi) + \lambda_{1,2,4,5,6,9,10}\rho_{12}\sigma_{123}(ebi) + \rho_{12}(enc)\\
\partial(ebk) &= \rho_3(afk) + \rho_1(ang) + \sigma_2(ebj)\\
\partial(ebl) &= \rho_3(afl) + \sigma_{123}(ebi) + \sigma_3(ebk) + (enc)\\
\partial(edi) &= \rho_1(ahi) + \lambda_{1,8,9,10,11}\rho_1(ang) + \lambda_{1,2,5,8,9,9,10}\rho_{12}\sigma_2(ebl)\\
\partial(edj) &= \rho_1(ahj) + \sigma_1(edi)\\
\partial(edk) &= \rho_1(ahk) + \sigma_2(edj)\\
\partial(edl) &= \rho_1(ahl) + \sigma_{123}(edi) + \sigma_3(edk) + \sigma_{12}(enc)\\
\partial(enc) &= \rho_3\sigma_1(ang) + \rho_1\sigma_3(ang) + \rho_{123}\sigma_{123}(ang)\\
\partial(emc) &= \lambda_{3,7,8,9,10}\rho_3(afl) + \rho_3(ahj) + \lambda_{1,2,3,7,8,9,10}\rho_{123}(ahl)\\
&\quad + \rho_3\sigma_1(amg) + \rho_1\sigma_3(amg) + \rho_{123}\sigma_{123}(amg) + \lambda_{4,5,6,7,8,9,10}\sigma_{123}(ebi)\\
&\quad + \lambda_{6,7,8,9,10}\sigma_3(ebk) + \sigma_3(edi) + \lambda_{7,8,9,10,11}(enc) + (enc)
\end{aligned}
$$

Table 5: The differential on $\widehat{CFDD}(\mathcal{H}_{SG})$. λ is used for coefficients that have yet to be determined; they are 0 or 1 depending on the contribution of the corresponding domain.

The coefficient of the enc term of $\partial^2(amg)$ is $\lambda_{2,5,7,8,9,9,10}\rho_2\sigma_2$, which implies that $\lambda_{2,5,7,8,9,9,10} = 0$. Then the afl term of $\partial^2(amg)$ becomes $\lambda_{3,7,8,9,10}\rho_{23}\sigma_2(afl)$, and the ebk term becomes $\lambda_{6,7,8,9,10}\rho_2\sigma_{23}(ebk)$, implying that $\lambda_{3,7,8,9,10} = \lambda_{6,7,8,9,10} = 0$. Similarly the ang term of $\partial^2(edl)$ reveals that $\lambda_{4,5,6,8,9,10,11} = 1$ and the ahk term of $\partial^2(edl)$ implies that $\lambda_{2,3,4,5,6,8,9} = 0$. The afi term of $\partial^2(ebj)$ implies that $\lambda_{1,2,4,5,6,9,10} = 0$, and the ang term implies that $\lambda_{1,2,3,8,9,10,11} = 1$. Finally, the ang term of $\partial^2(emc)$ implies that $\lambda_{4,5,6,7,8,9,10} = 1$, and the ahi term implies that $\lambda_{1,2,3,7,8,9,10} = 1$. The only coefficient in Table 5 that remains undetermined is $\lambda_{7,8,9,10,11}$.

4.2.7 $\mathbf{R_7R_8R_9R_{10}R_{11}}$

We have determined that $\widehat{CFDD}(\mathcal{H}_{SG})$ is one of two possibilities, depending on the value of $\lambda_{7,8,9,10,11}$. We will deduce the right choice by showing that one of these possible bimodules does not behave correctly under tensoring with type A modules for the solid torus.

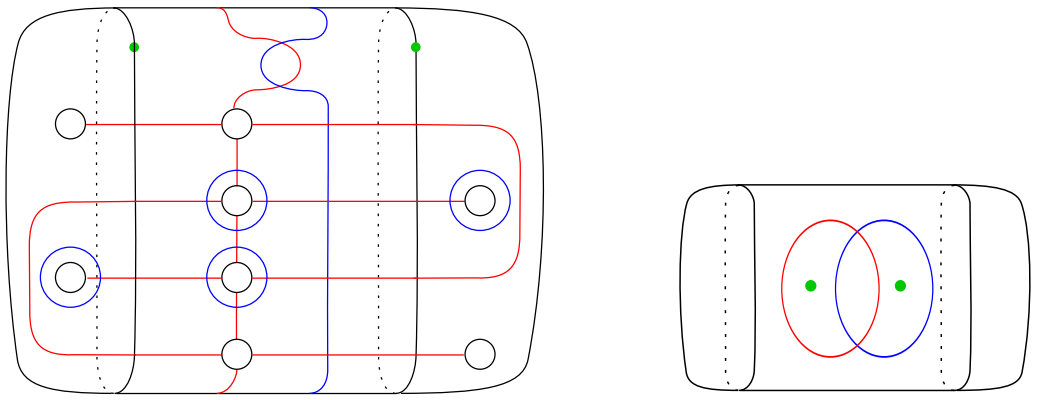

(a) (b)

Figure 15: The manifold obtained from the self-gluer by capping off both ends with identical 0-framed solid tori.

Consider the closed, doubly basepointed Heegaard diagram in Figure 15(a), which is obtained from the bordered Heegaard diagram $\mathcal{H}_{SG}$ by gluing bordered Heegaard dia-

grams for solid tori to each boundary component. A sequence of isotopies and destabilizations leads to the diagram in Figure 15(b), so it is easy to check that $\widehat{HF}$ of the manifold represented by this diagram has rank 2. $\widehat{HF}$ can also be obtained by taking the box tensor product of $\widehat{CFDD}(\mathcal{H}_{SG})$ with two copies of the type A module for the solid torus. A bounded version of the solid torus module has three generators x, y, and z and the following operations:

$$m_1(x) = z, \quad m_2(x, \rho_1) = y, \quad m_2(x, \rho_2) = z, \quad m_2(x, \rho_{12}) = z.$$

It is routine to perform the tensor products, and we find that the homology of the resulting chain complex is rank 2 if $\lambda_{7,8,9,10,11} = 1$, and rank 4 if $\lambda_{7,8,9,10,11} = 0$. Thus, the domain $R_7R_8R_9R_{10}R_{11}$ must contribute, and we have completed the computation of $\widehat{CFDD}(\mathcal{H}_{SG})$ in the middle spin^c-structure. The result is pictured in Figure 16.

4.3 Extremal spin^c-structures

First consider the spin^c-structure in which both α^ρ arcs are occupied and neither α^σ arc is occupied. There are only two generators with those conditions: aem and aen. There are two domains which have the right corner count to connect aem and aen. The bigon R_{12} contributes a differential from aem to aen. The domain $R_7R_8R_9R_{10}R_{11}$, as an element of $\pi_2(aem, aen)$, has index -1 and thus does not contribute. Canceling the differential and two generators, we find that $\widehat{CFDD}(\mathcal{Y}_{SG})$ in this extremal spin^c structure has no generators.

The other extremal spin^c-structure has more generators (given the choice of Heegaard diagram $\mathcal{H}_{SG}$), but the corresponding summand of $\widehat{CFDD}(\mathcal{Y}_{SG})$ is still trivial. Indeed, we could handleslide β_0 across the handles in Figure 11 to produce a new Heegaard diagram with only two generators in this spin^c structure. This diagram is a mirror image of $\mathcal{H}_{SG}$, so the reasoning above applies and shows that the two generators are canceled by the single differential between them.

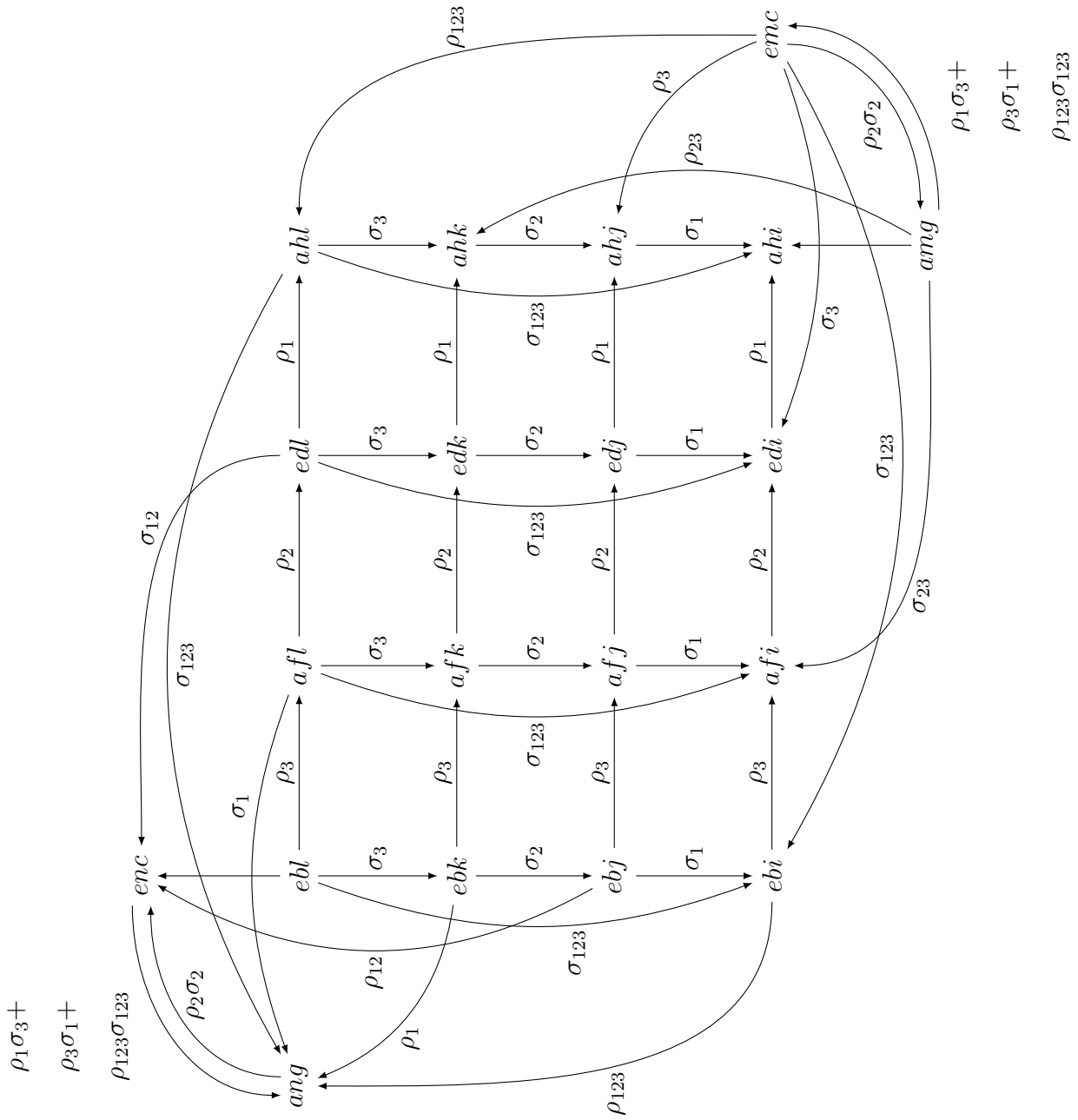

Figure 16: $\widehat{CFDD}(\mathcal{Y}_{SG})$ in the middle spin^c-structure.

4.4 Gradings

As described in Section 2.8, $\widehat{CFDD}(\mathcal{Y}_{SG})$ is graded by a set which is a quotient of the noncommutative group $G_{2,0}$. We will compute this (relative) grading using Figure 16.

We choose ebl to be the preferred generator and set $gr(ebl) = \vec{0} = (0;0,0;0,0)$. The arrow labelled ρ_3 from ebl to afl determines the grading of afl.

$$gr(afl) = \lambda^{-1}gr(\rho_3)^{-1}gr(ebl) = \lambda^{-1}\left(\frac{1}{2};\frac{1}{2},-\frac{1}{2};0,0\right)\vec{0} = \left(-\frac{1}{2};\frac{1}{2},-\frac{1}{2};0,0\right)$$

Similarly, the successive arrows labelled ρ_2 and ρ_1 (moving right from afl in Figure 16) determine the gradings of edl and ahl.

$$\begin{aligned} gr(edl) &= \lambda^{-1}gr(\rho_2)^{-1}gr(afl) = \lambda^{-1}\left(\frac{1}{2};-\frac{1}{2},-\frac{1}{2};0,0\right)\left(-\frac{1}{2};\frac{1}{2},-\frac{1}{2};0,0\right) \\ &= \left(-\frac{1}{2};0,-1;0,0\right) \\ gr(ahl) &= \lambda^{-1}gr(\rho_1)^{-1}gr(edl) = \lambda^{-1}\left(\frac{1}{2};-\frac{1}{2},\frac{1}{2};0,0\right)\left(-\frac{3}{2};0,-1;0,0\right) \\ &= \left(-\frac{1}{2};-\frac{1}{2},-\frac{1}{2};0,0\right) \end{aligned}$$

Working down the chain of σ labelled arrows starting from ebl determines the gradings of ebk, ebj, and ebi.

$$\begin{aligned} gr(ebk) &= \lambda^{-1}gr(\sigma_3)^{-1}gr(ebl) = \left(-\frac{1}{2};0,0;\frac{1}{2},-\frac{1}{2}\right) \\ gr(ebj) &= \lambda^{-1}gr(\sigma_2)^{-1}gr(ebk) = \left(-\frac{1}{2};0,0;0,-1\right) \\ gr(ebi) &= \lambda^{-1}gr(\sigma_1)^{-1}gr(ebj) = \left(-\frac{1}{2};0,0;-\frac{1}{2},-\frac{1}{2}\right) \end{aligned}$$

The vertical chains of σ labelled arrows from afl, edl, and ahl determine the following

gradings:

$$\begin{aligned}
gr(afk) &= \lambda^{-1}gr(\sigma_3)^{-1}gr(afl) = \left(-1;\frac{1}{2},-\frac{1}{2};\frac{1}{2},-\frac{1}{2}\right)\\
gr(afj) &= \lambda^{-1}gr(\sigma_2)^{-1}gr(afk) = \left(-1;\frac{1}{2},-\frac{1}{2};0,-1\right)\\
gr(afi) &= \lambda^{-1}gr(\sigma_1)^{-1}gr(afj) = \left(-1;\frac{1}{2},-\frac{1}{2};-\frac{1}{2},-\frac{1}{2}\right)\\
gr(edk) &= \lambda^{-1}gr(\sigma_3)^{-1}gr(edl) = \left(-1;0,-1;\frac{1}{2},-\frac{1}{2}\right)\\
gr(edj) &= \lambda^{-1}gr(\sigma_2)^{-1}gr(edk) = (-1;0,-1;0,-1)\\
gr(edi) &= \lambda^{-1}gr(\sigma_1)^{-1}gr(edj) = \left(-1;0,-1;-\frac{1}{2},-\frac{1}{2}\right)\\
gr(ahk) &= \lambda^{-1}gr(\sigma_3)^{-1}gr(ahl) = \left(-1;-\frac{1}{2},-\frac{1}{2};\frac{1}{2},-\frac{1}{2}\right)\\
gr(ahj) &= \lambda^{-1}gr(\sigma_2)^{-1}gr(ahk) = \left(-1;-\frac{1}{2},-\frac{1}{2};0,-1\right)\\
gr(ahi) &= \lambda^{-1}gr(\sigma_1)^{-1}gr(ahj) = \left(-1;-\frac{1}{2},-\frac{1}{2};-\frac{1}{2},-\frac{1}{2}\right)
\end{aligned}$$

The two unlabeled arrows in the diagram determine the gradings so *enc* and *amg*.

$$\begin{aligned}
gr(enc) &= \lambda^{-1}gr(ebl) = (-1;0,0;0,0)\\
gr(amg) &= \lambda gr(ahi) = \left(0;-\frac{1}{2},-\frac{1}{2};-\frac{1}{2},-\frac{1}{2}\right)
\end{aligned}$$

Finally, the two arrows labelled $\rho_2\sigma_2$ determine the gradings of *ang* and *emc*.

$$\begin{aligned}
gr(ang) &= \lambda gr(\rho_2)gr(\sigma_2)gr(enc) = \left(-1;\frac{1}{2},\frac{1}{2};\frac{1}{2},\frac{1}{2}\right)\\
gr(emc) &= \lambda gr(\rho_2)gr(\sigma_2)gr(amg) = (0;0,0;0,0)
\end{aligned}$$

It remains to compute the indeterminacy $\mathcal{P}(ebl)$. We compute equivalent values for the grading of *ebl* by using the loop *ebl* to afl to *edl* to *enc* to *ebl* and the loop *ebl* to *ebk* to *ebj* to *enc* to *ebl*. The first loop gives the element of $\mathcal{P}(ebl)$ corresponding to a

periodic domain with boundary $\rho_{23} + \sigma_{12}$.

$$\begin{aligned} gr(afl) &= \lambda^{-1} gr(\rho_3)^{-1} gr(ebl) = \left(-\frac{1}{2}; \frac{1}{2}, -\frac{1}{2}; 0, 0\right) \\ gr(edl) &= \lambda^{-1} gr(\rho_2)^{-1} gr(afl) = \left(-\frac{1}{2}; 0, -1; 0, 0\right) \\ gr(enc) &= \lambda^{-1} gr(\sigma_{12})^{-1} gr(afl) = (-1; 0, -1; -1, 0) \\ gr(edl) &= \lambda gr(enc) = (0; 0, -1; -1, 0) \end{aligned}$$

The second loop gives the element of $\mathcal{P}(ebl)$ corresponding to a periodic domain with boundary $\rho_{12} + \sigma_{23}$.

$$\begin{aligned} gr(ebk) &= \lambda^{-1} gr(\sigma_3)^{-1} gr(ebl) = \left(-\frac{1}{2}; 0, 0; \frac{1}{2}, -\frac{1}{2}\right) \\ gr(ebj) &= \lambda^{-1} gr(\sigma_2)^{-1} gr(ebk) = \left(-\frac{1}{2}; 0, 0; 0, -1\right) \\ gr(enc) &= \lambda^{-1} gr(\rho_{12})^{-1} gr(ebj) = (-1; -1, 0; 0, -1) \\ gr(edl) &= \lambda gr(enc) = (0; -1, 0; 0, -1) \end{aligned}$$

Thus $\mathcal{P}(ebl)$ is the subgroup of $G_{2,0}$ generated by $(0; 0, -1; -1, 0)$ and $(0; -1, 0; 0, -1)$.

Chapter 5

Computing $\widehat{HF}$ of graph manifolds

In this chapter we describe the procedure for computing $\widehat{HF}$ of an arbitrary graph manifold given a connected plumbing graph Γ and give some example applications. For simplicity, we will assume that every vertex of Γ has nonnegative genus. The manifold can be constructed from simpler bordered pieces using two types of gluing: *extension* glues fibers to fibers and base surface to base surface, and *plumbing* glues a fiber of one bundle to a curve in the base of the other bundle. Gluing two S^1-bundles by extension produces an S^1-bundle over the surface obtained by gluing the two bases.

Recall that in the Heegaard Diagram for $\mathcal{Y}_\mathcal{P}$, α_1^ρ, α_2^σ, and α_1^τ parametrize curves in the base surface $\mathcal{P}$, while α_2^ρ, α_1^σ, and α_2^τ parametrize fibers. If we glue two type D boundaries together, α_1 glues to α_2 and vice versa (to combine the relevant modules we would first change one of the boundaries to type A, which switches α_1 and α_2). Thus gluing the ρ boundary of one copy of $\mathcal{Y}_\mathcal{P}$ to the σ boundary of another is extension. Gluing the ρ boundary to the τ boundary is plumbing.

It will be convenient to introduce the bordered manifold $\bar{\mathcal{Y}}_\mathcal{P}$, the mirror image of $\mathcal{Y}_\mathcal{P}$. The trimodule $\widehat{CFD^3}(\bar{\mathcal{Y}}_\mathcal{P})$ can be obtained from $\widehat{CFD^3}(\mathcal{Y}_\mathcal{P})$ by interchanging 1's with 3's for all algebra elements and reversing the direction of the arrows. α_1 and α_2 are also interchanged on each boundary component.

5.1 Algorithm of computing $\widehat{HF}$

5.1.1 Trivial bundles over surfaces

Recall that each vertex of Γ represents a particular S^1-bundle over a surface $S_{g,b}$ with genus g and b boundary components. We first construct the trivial bundle over $S_{g,b}$.

If $g = 0$ and $b \geq 3$, then we simply glue copies of $\mathcal{Y}_{\mathcal{P}}$ by extension until we have the right number of boundary components. The multimodule $\widehat{CFD^b}$ is obtained by taking box tensor products, inserting copies of $\widehat{CFAA}(\mathbb{I})$ when two type D boundaries are glued. For intance, $\widehat{CFD^4}(S^1 \times S_{0,4})$ is given by

$$\left(\widehat{CFAA}(\mathbb{I}) \boxtimes \widehat{CFD^3}(\mathcal{Y}_{\mathcal{P}})\right) \boxtimes \widehat{CFD^3}(\mathcal{Y}_{\mathcal{P}}),$$

where the tensor products are with respect to the ρ and σ boundaries on the two copies of $\widehat{CFD^3}(\mathcal{Y}_{\mathcal{P}})$. The trivial bundle over $S_{0,1}$ is just the solid torus, which has bordered invariant

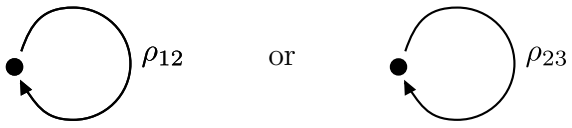

depending on whether α_1 parametrizes a curve in the base (left) or a fiber (right) [8, Section 11.2]. The trivial bundle over $S_{0,2}$ is the same as the mapping cylinder of the identity map on the torus. The corresponding bimodule $\widehat{CFDD}(\mathbb{I})$ is computed in [9, Proposition 10.1]. Here either α arc can be the fiber, but α_1 on one boundary is the same as α_2 on the other boundary.

We construct a Heegaard diagram for the trivial bundle over $S_{1,2}$ as indicated in Figure 17. Notice that we must insert a copy of $\mathcal{H}_{SG}$ when we glue two components of $\partial\bar{\mathcal{Y}}_{\mathcal{P}}$ to each other. The bimodule $\widehat{CFDD}(S^1 \times S_{1,2})$ can be computed as follows:

- Change $\widehat{CFD^3}(\bar{\mathcal{Y}}_{\mathcal{P}})$ to a type DDA trimodule by tensoring with $\widehat{CFAA}(\mathbb{I})$ along the σ boundary;

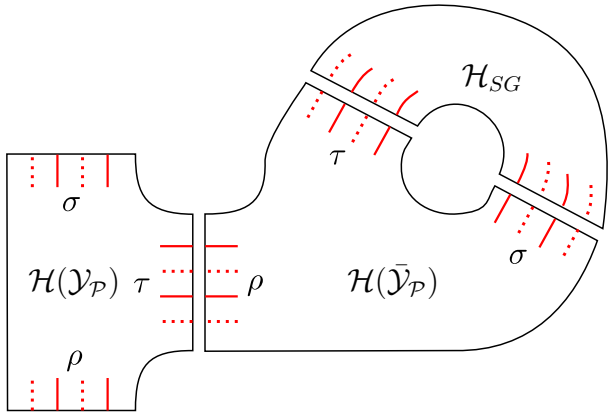

Figure 17: A Heegaard diagram for $S_{1,2}\times S^1$ can be obtained by gluing $\mathcal{H}_{SG}$ and Heegaard diagrams for $\mathcal{Y}_\mathcal{P}$ and $\bar{\mathcal{Y}}_\mathcal{P}$. Solid red lines indicate α arcs in the base of each bundle, while dotted red lines correspond to fibers.

- Tensor the type A boundary of the resulting trimodule with $\widehat{CFDD}(\mathcal{H}_{SG})$;
- Change the τ boundary to type A by tensoring with $\widehat{CFAA}(\mathbb{I})$, and then take the Hochschild homology with respect to the appropriate boundary components, resulting in a type D module.
- Change this module to type A by tensoring with $\widehat{CFAA}(\mathbb{I})$ and tensor with the τ boundary of $\widehat{CFD^3}(\mathcal{Y}_\mathcal{P})$;
- The result is a type DD bimodule with 16 generators. Note that it is still the case that α_2^ρ and α_1^σ represent fibers.

For $b>0$, the trivial bundle over $S_{g,b}$ can now be obtained easily by extending $S_{0,b}$ with g copies of $S_{1,2}$. For the case of $b=0$, we simply extend the trivial bundle over $S_{g,1}$ by capping off the boundary with the trivial bundle over $S_{0,1}$.

5.1.2 Nontrivial bundles

In general the bundle associated to a vertex of Γ is nontrivial, with a specified Euler number e. The Euler number of a circle bundle over a surface with boundary is well defined once a trivialization is chosen on the boundary. Choosing the trivialization over the boundary of an S^1-bundle is equivalent to choosing the α arcs to parametrize the boundary on a bordered Heegaard diagram of the total space. A trivialization over the boundary specifies two curves in the boundary $S^1 \times S^1$: a fiber γ_f, and a curve γ_b meeting each fiber in one point. These in turn can specify a boundary parametrization by letting one be α_1 and the other be α_2.

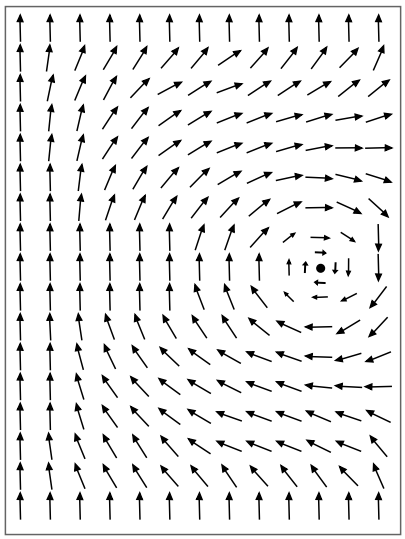

Figure 18: A section of a D^2-bundle over the cylinder, where the top and bottom edges are identified. The section specifies a trivialization of the boundary on each end of the cylinder. The signed number of zeros indicates that the euler number is -1. The boundary S^1-bundle is equivalent to a the mapping cylinder of a Dehn twist.

Consider changing the trivialization over one boundary component of an S^1-bundle from the trivialization on the left to the trivialization on the right in Figure 18. On one hand, this change corresponds to gluing on the S^1-bundle over the cylinder which is

the boundary of the D^2 bundle represented by Figure 18. The figure shows a section of this D_2 bundle, which has a zero of sign -1. Since the Euler number can be defined as the signed number of zeros of such a section, it follows that attaching the corresponding S^1-bundle to a bundle over a surface decreases the Euler number by 1. On the other hand, this change of trivialization corresponds to the change in parametrization which fixes γ_f and takes γ_b to $\gamma_b \pm \gamma_f$ (depending on the orientation on $S^1 \times S^1$). This change is accomplished by attaching the mapping cylinder of a negative Dehn twist about γ_f.

In the same way, attaching a positive Dehn twist about the fiber γ_f has the effect of increasing the Euler number of a circle bundle by 1. The bimodules for Dehn twists about α_1 and α_2 are known [9, Section 10.2]. By tensoring with enough of these bimodules we can obtain the bordered invariants for arbitrary S^1-bundles over arbitrary (oriented) surfaces with boundary.

5.1.3 Combining vertices

Once multimodules have been determined for each vertex of Γ, they can be combined according to the edges of Γ. If vertices v_1 and v_2 are connected by an edge, chose a boundary component of each circle bundle such that both boundaries have fiber α_1 or both have fiber α_2. Take the box tensor product (after changing one boundary component to type A) to compute the new multimodule. If there is no way to choose a boundary component with the desired α arc as fiber, the fiber direction can be changed as follows:

- To change the fiber from α_1 to α_2, extend the bundle by $\mathcal{Y}_{\mathcal{P}}$, attached along the ρ boundary, with the σ boundary capped off by a solid torus as in Figure 19(a);
- To change the fiber from α_2 to α_1, extend the bundle by $\bar{\mathcal{Y}}_{\mathcal{P}}$, attached along the ρ boundary, with the σ boundary capped off by a solid torus as in Figure 19(b).

For acyclic graphs any plumbing will work when combining vertices along an edge. In general, however, there is an additional consideration: edges are decorated by a sign,

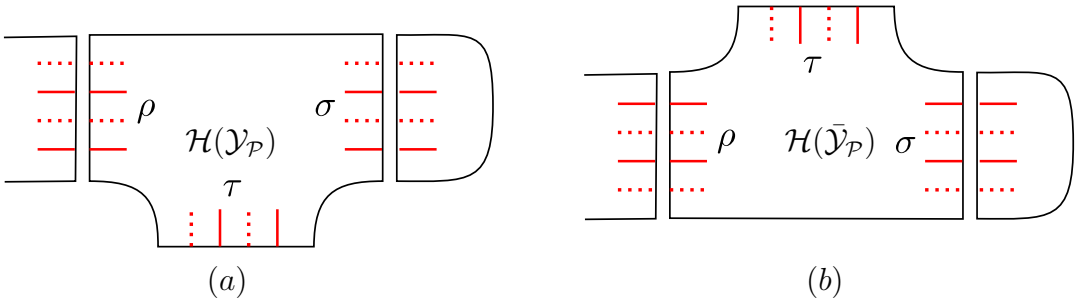

Figure 19: The fiber direction can be be changed by extending at a boundary with $\mathcal{Y}_\mathcal{P}$ or $\bar{\mathcal{Y}}_\mathcal{P}$ and an appropriate solid torus. Dotted lines indicate α arcs which are fibers. The arrangement in (a) changes the fiber from α_1 to α_2, while the arrangement in (b) does the opposite.

which distinguishes between two plumbing options. In terms of bordered Heegaard diagrams, the difference is between gluing two type D boundaries with fiber α_1 or gluing two boundaries with fiber α_2. Suppose we orient each boundary component so that the positive fiber direction is to the left of the positive base direction at a fiber-base intersection. Then a type D boundary with α_1 a fiber has oriented fiber $-\alpha_1$ and oriented base $+\alpha_2$. Since gluing type D boundaries glues α_1 to $-\alpha_2$, this corresponds to the map $\begin{pmatrix} 0 & 1 \\ 1 & 0 \end{pmatrix}$ in the standard {base, fiber} basis. That is, gluing two boundaries with α_1 fibers corresponds to a $+$ edge. A type D boundary with fiber α_2 has oriented fiber $+\alpha_2$ and oriented base $+\alpha_1$, so gluing two of these boundaries corresponds to the map $\begin{pmatrix} 0 & -1 \\ -1 & 0 \end{pmatrix}$.

Once the bundles of two adjacent vertices have been plumbed, the result is no longer an S^1-bundle. However, continue to keep track of which α arc is the "fiber" at each boundary component. Repeat the process above to add on successive vertices. If at any point an edge connects to a vertex that has already been incorporated, insert the bimodule $\widehat{CFDD}(\mathcal{H}_{SG})$ and take the appropriate Hochshchild homology instead of a tensor product.

5.2 Example computations

The author has implemented a program[1] using the techniques described above to compute the total rank of $\widehat{HF}$ of a closed graph manifold, or the bordered invariant of a graph manifold with boundary, from a plumbing graph. It can be used, for example, to see that the rank of $\widehat{HF}$ of the manifold represented by the negative definite plumbing tree in Figure 20 is 213,312. It is easy to compute $|H_1|$ from the plumbing graph and see that this manifold is an L-space. This is as expected; the fact that this plumbing graph corresponds to an L-space follows from [16, Theorem C].

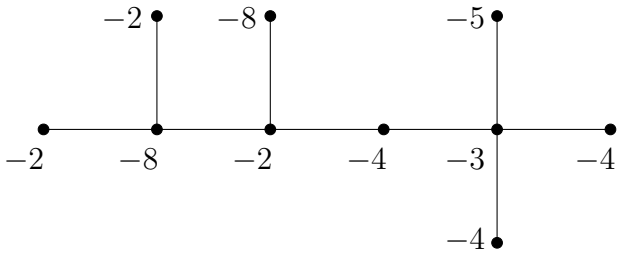

Figure 20: Plumbing graph for a graph manifold with $\mathrm{rk}(\widehat{HF}) = 213,312$. The weights on the vertices correspond to Euler numbers; the genus is zero for every vertex and we omit it from the notation.

With this algorithm, we can quickly run computations for large sets of graph manifolds and check, for instance, which are L-spaces. Consider as an example the plumbing graph Γ below, with weights in the range $-5 \leq a, b \leq 5$ and $-5 \leq c, d, e, f \leq -2$ (the bound of -2 on the weights of the outer vertices is so that we only consider graphs in normal form, in the notation of [18]).

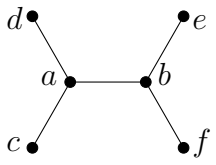

[1] Available at http://math.columbia.edu/~jhansel/graph_manifolds_program.html

There are 6106 distinct graphs of this form. Of the corresponding 3-manifolds, 5643 are L-spaces. Some of these trees are negative definite, but most are not. To the author's knowledge, there is currently no other way to compute $\widehat{HF}$ for these non-definite examples. Results for a few examples are in Figure 21.

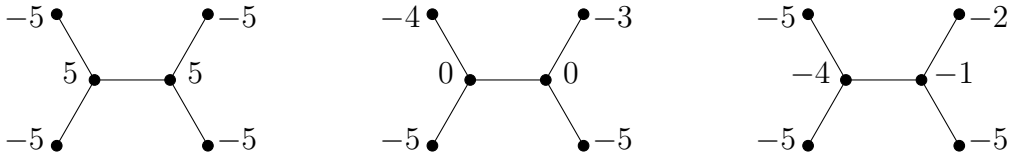

$\text{rk}(\widehat{HF}) = 17{,}600$ $|H_1| = 17{,}600$

$\text{rk}(\widehat{HF}) = 230$ $|H_1| = 228$

$\text{rk}(\widehat{HF}) = 72$ $|H_1| = 20$

Figure 21: The manifold corresponding to the graph on the left has the largest $\widehat{HF}$ of the 6106 examples tested, and it is an L-space. The graph in the middle gives the smallest difference between $rk(\widehat{HF})$ and $|H_1|$ possible for a non L-space, and the third gives the largest difference among this set of examples.

The plumbing graphs in the above examples are all trees with only genus zero vertices. For a more general example, consider the boundary of the 4-manifold represented by the Kirby diagram in Figure 22. This diagram is presented in [2] as a typical example of a 4-manifold obtained by plumbing D^2-bundles. The boundary is thus a typical example of graph manifold, which can be represented by the graph in Figure 23. We can apply the algorithm described above to this graph, and we find that the the rank of $\widehat{HF}$ of the corresponding 3-manifold is 13,788.

Our final example is the manifold $\Sigma \times S^1$, where Σ is the surface of genus two. This manifold can be represented by a plumbing graph with just one vertex and no edges. The vertex carries the weights 2 and 0 for the genus and Euler number, respectively. Evaluating the rank of $\widehat{HF}$ from this graph gives 24, which agrees with the result in [5].

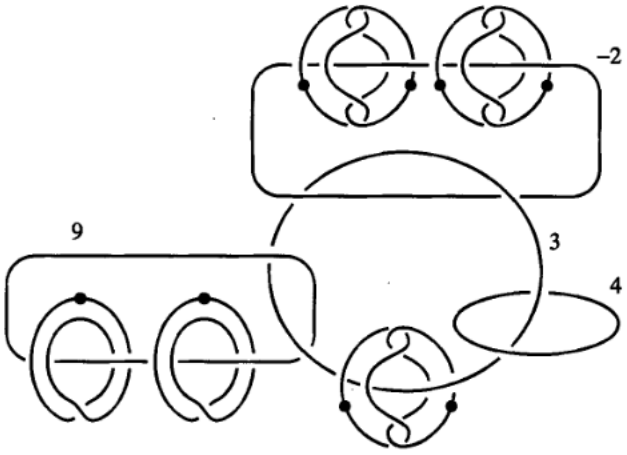

Figure 22: A typical example of a plumbed 4-manifold. The boundary of this 4-manifold is a graph manifold. This example is Figure 6.5 in [2].

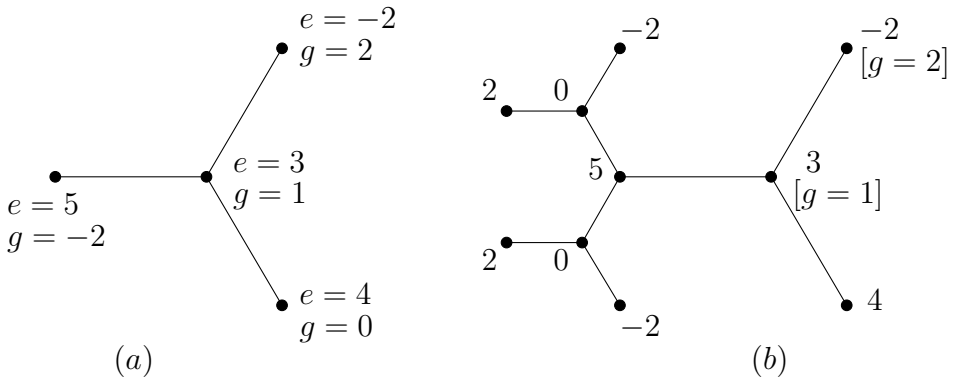

Figure 23: Two graphs representing the manifold which is the boundary of the plumbing of D^2-bundles represented in Figure 22. The graph in (a) is most directly obtained from Figure 22, but it contains a vertex with negative genus. To apply the algorithm described in this section we can use the plumbing calculus in [18] to rewrite the graph as shown in (b). For vertices in (a), e denotes the euler number and g denotes the genus. In (b), the genus is 0 unless noted in brackets, and the remaining numbers are the euler numbers.

5.3 Bordered graph manifolds with good vertices

We have seen that the methods of this chapter are effective in computing $\widehat{HF}$ for specific graph manifold examples. For sufficiently nice graph manifolds, we can also prove general results about the structure of Heegaard Floer invariants. Consider the special case of plumbing trees, that is, graph manifolds whose plumbing graph Γ is acyclic and has only genus zero vertices. For any vertex v_i of Γ, let d_i denote the number of edges incident to v_i and let e_i denote the euler weight associated to v_i. We say that v_i is a *good vertex* if $d_i + e_i \leq 0$. We say that v_i is a *bad vertex* if it is not a good vertex. Plumbed manifolds with only good vertices are particularly simple, and the Heegaard Floer homology of these manifolds is easy to understand (they are all L-spaces, as proved in [21, Corollary 1.4]). In this section, we show that the same is true of the bordered Heegaard Floer homology of plumbed manifolds with boundary.

Recall that a graph manifold is obtained from a plumbing tree Γ by associating to each vertex v_i the euler number e_i circle bundle over a sphere with d_i boundary components and gluing the torus boundary components of these bundles together according to the edges of Γ. We can produce a graph manifold with boundary by adding additional boundary components to the bundles associated with certain vertices. More specifically, each vertex v_i of Γ carries an additional weight $b_i \geq 0$, and we associate to v_i the euler number e_i circle bundle over the sphere with $d_i + b_i$ boundary components. When these bundles are glued according to the edges of Γ, the result is a graph manifold with $\sum_i b_i$ boundary components. We will record this extra boundary information in the weighted tree Γ by adding b_i "half edges" (denoted by dotted lines) to the vertex v_i. We extend the notion of good vertices by requiring that $d_i + b_i + e_i \leq 0$ for each vertex of Γ. In other words, we count half edges as edges when determining if a vertex is good.

To discuss the type D bordered Heegaard Floer module associated to a plumbed manifold with boundary, we must first fix a parametrization of the boundary. We will assume that each boundary associated to the vertex v_i is parametrized such that α_2

represents a fiber of the bundle associated to v_i and α_1 represents a curve in the base. Gluing two manifolds of this form along a torus boundary takes fiber to base and base to fiber. Thus gluing manifolds corresponds to gluing the corresponding plumbing graphs by replacing a half edge in each by an edge.

Consider the class of one-boundary component plumbed 3-manifolds which are represented by a plumbing tree with only good vertices. The following theorem says that the bordered Heegaard Floer invariants $\widehat{CFD}$ of such manifolds are quite restricted in form:

Theorem 3. *Let Γ be a plumbing tree with one half edge and let Y_Γ be the corresponding bordered 3-manifold. Let G denote the labeled, directed graph representing $\widehat{CFD}(Y_\Gamma)$, as in Remark 2.1.1. If Γ has no bad vertices then there exists a basis for $\widehat{CFD}(Y_\Gamma)$ such that G has the following form:*

- *Every vertex of G has exactly two incident edges. In fact, each vertex looks locally like one of the following five options:*

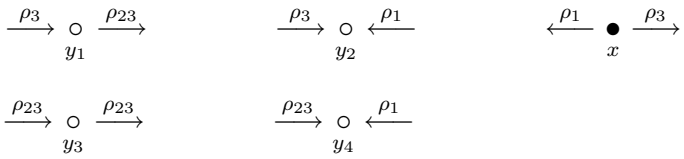

- *Equivalently, G is a disjoint union of loops, which are composed of segments of the form*

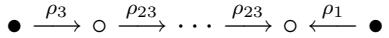

  concatenated front to back.

Proof. Let e be the euler weight associated to the boundary vertex of Γ, and let $n \geq 0$ be the number of edges at this vertex, not counting the boundary half edge. Note that since all vertices of Γ are good, we have $e \leq -(n+1)$. Let $\Gamma_1, \ldots, \Gamma_n$ denote the corresponding subtrees which are attached by edges to the boundary vertex, as pictured below. We can think of each Γ_i as a plumbing tree with one half edge.

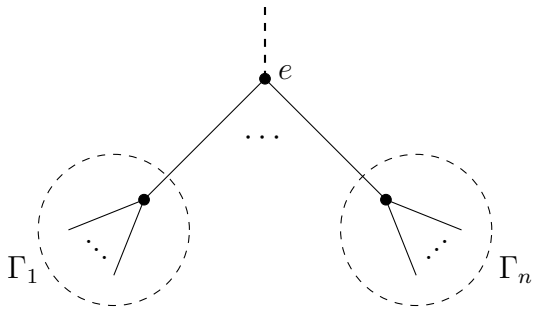

We will use induction on the number of vertices of Γ and on e. The key will be proving the following inductive step:

Inductive step: Let Γ' and Γ'' be plumbing trees with one half edge. Suppose that the conclusion of the theorem is true for Γ' and Γ'', that is, that the graphs representing $\widehat{CFD}(Y_{\Gamma'})$ and $\widehat{CFD}(Y_{\Gamma''})$ have the form described above. Then the conclusion of the theorem also holds for the following three plumbing trees:

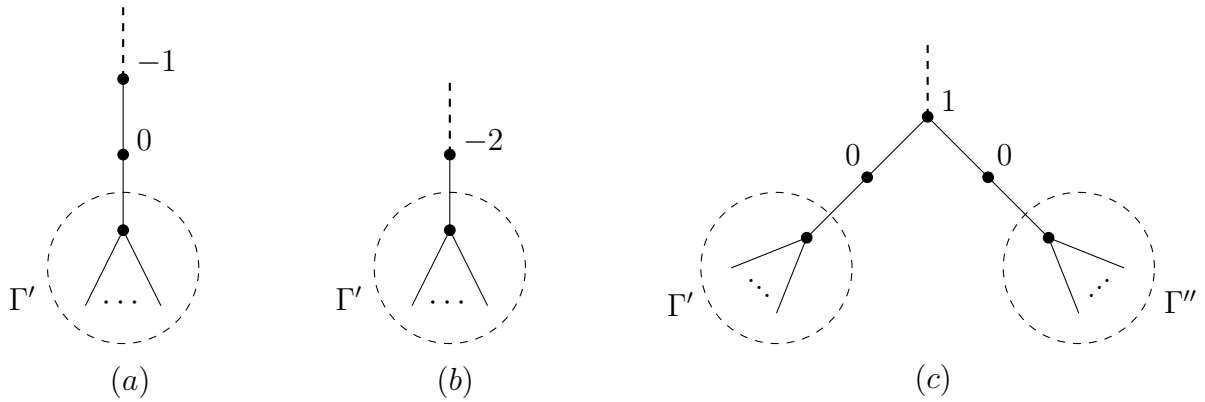

Assuming the inductive step, the proof proceeds as follows. We assume by induction that the theorem holds for all plumbing trees with fewer vertices than Γ, or with the same number of vertices and larger e. We now wish to prove the statement for Γ.

If $e < -(n+1)$, let Γ' be the tree obtained from Γ by replacing e with $e' = e + 1$. Since all $e' \leq -(n+1)$ and all other vertices are the same as Γ, Γ' has only good vertices. By the inductive hypothesis, $\widehat{CFD}(Y_{\Gamma'})$ has the desired form. Γ can be obtained from Γ' by subtracting one from the euler weight of the boundary vertex, which is equivalent to

attaching the two-boundary plumbing tree Γ_a shown below (the equivalence comes from rule R3 of [18, Proposition 2.1]).

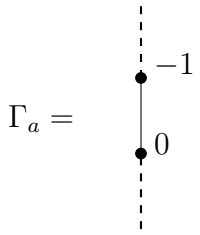

Thus by part (a) of the inductive step, the theorem holds for Γ.

If $e = -(n+1)$ and $n = 1$, take Γ' to be Γ_1, the subtree obtained by removing the -2 framed boundary vertex. Γ' still has only good vertices and has fewer vertices than Γ, so by the inductive assumption the result holds for Γ'. By part (b) of the inductive step, it also holds for Γ.

If $e = -(n+1)$ and $n > 1$, let Γ' be the tree obtained from Γ by removing the subtree Γ_n and increasing the euler weight of the boundary vertex by 1, and let Γ'' be the tree obtained from Γ by removing the subtrees Γ_1 through Γ_{n-1} and replacing e with -2.

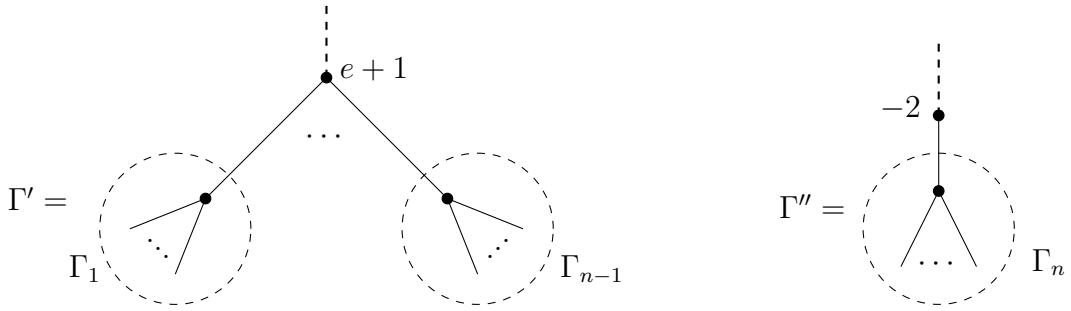

Γ' and Γ'' have fewer vertices than Γ and have only good vertices, so by the inductive hypothesis $\widehat{CFD}(Y_{\Gamma'})$ and $\widehat{CFD}(Y_{\Gamma''})$ have the desired form. Furthermore, Γ is equivalent to the tree obtained from Γ' and Γ'' as in part (c) of the inductive hypothesis (we again us rule R3 of [18, Proposition 2.1] to eliminate the vertices with weight 0). Therefore by the inductive step $\widehat{CFD}(Y_\Gamma)$ has the desired form.

Finally, if $e = -(n+1)$ and $n = 0$, we have the base case of induction. In this case, Γ has only a single vertex. The corresponding bordered manifold Y_Γ is a -1 framed solid

torus. The invariant $\widehat{CFD}(Y_\Gamma)$, pictured below, has the required form.

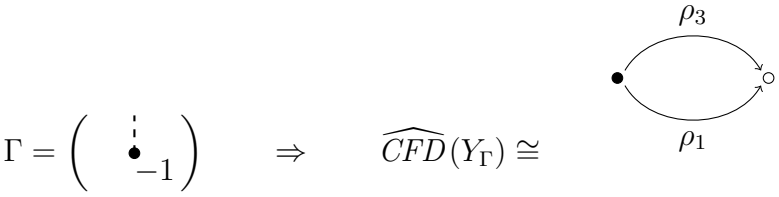

Proof of the inductive step: Suppose Γ has the form of one of the graphs in the inductive step. Thus Γ is obtained from the graphs Γ' and Γ'' by attaching them to one of the following three graphs in the appropriate way:

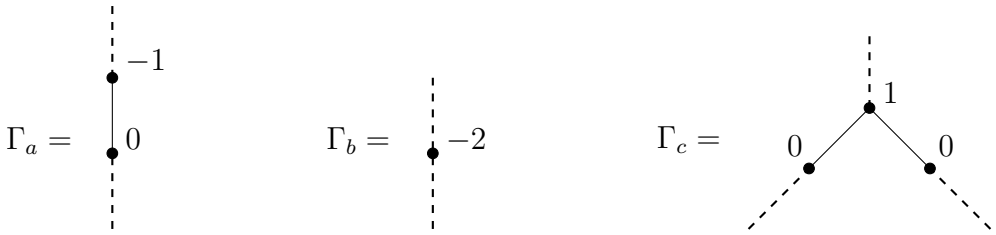

This means that the bordered manifold Y_Γ is obtained from the bordered manifolds $Y_{\Gamma'}$ and $Y_{\Gamma''}$ by gluing with one of the the bordered manifolds Y_{Γ_a}, Y_{Γ_b}, or Y_{Γ_c}. Accordingly, the module $\widehat{CFD}(Y_\Gamma)$ is obtained from $\widehat{CFD}(Y_{\Gamma'})$ and $\widehat{CFD}(Y_{\Gamma''})$ by tensoring with an appropriate multimodule. Tensoring with these modules can be viewed as operations which input a type D module over the torus algebra (or two such modules in the case of Γ_c) and output a type D module over the torus algebra. We will compute the relevant modules and show that if the input modules have the form specified in the theorem then the output module does as well.

Bimodule for Γ_a: We need to compute the type DA bimodule $\widehat{CFDA}(Y_{\Gamma_a})$, where the type A boundary is the one corresponding to the weight 0 vertex of Γ_a. Recall that by convention the bordered manifold Y_{Γ_a} is parametrized so that α_2 parametrizes a fiber at each boundary for type D boundaries. For type A boundaries, α_1 parametrizes the fiber. It is easy to see that Y_{Γ_a} is exactly the mapping cylinder of the negative Dehn twist about α_2. The bimodule for this manifold is computed in [9, Section 10.2], where the manifold is called τ_m^{-1}.

The bimodule $\widehat{CFDA}(Y_{\Gamma_a})$ has three generators: p, q, and r. Since we only need to tensor this bimodule with type D modules which satisfy the conditions of the theorem, we can ignore bimodule operations which have ρ_2, ρ_{12}, or ρ_{123} as $\mathcal{A}_\infty$ inputs. There are four relevant operations for $\widehat{CFDA}(Y_{\Gamma_a})$:

$$m_1(p) = \rho_3\, r \qquad m_2(p, \sigma_1) = \rho_1\, q \qquad m_2(r, \sigma_3) = \rho_{23}\, q \qquad m_2(q, \sigma_{23}) = \rho_{23}\, q$$

Let M be a module over the torus algebra of the form described in the statement of the theorem. Let x, y_1, y_2, y_3, and y_4 be arbitrary generators of M of the five types specified above. We will show that the generators $p \otimes x$, $r \otimes x$, and $q \otimes y_i$ of the type D module $\widehat{CFDA}(Y_{\Gamma_a}) \boxtimes M$ have one of the five forms required by the theorem.

The generator $p \otimes x$ has one outgoing ρ_1 arrow coming from the second bimodule operation and the fact that x has one outgoing ρ_1 arrow. $p \otimes x$ also has an outgoing ρ_3 arrow ending at $r \otimes x$, coming from the first bimodule operation. There are no other arrows in or out of $p \otimes x$, since p appears in no other bimodule operations. Thus $p \otimes x$ has the same form as x.

The generator $r \otimes x$ has an incoming ρ_3 arrow coming from the first bimodule operation. Since r has an outgoing ρ_3 arrow, the third multimodule operation implies that $r \otimes x$ also has an outgoing ρ_{23} arrow. There are no other incoming or outgoing differentials, so $r \otimes x$ has the form of a type y_1 generator.

The generators y_i have two arrows each, either outgoing ρ_{23} arrows or incoming ρ_1 or ρ_3 or ρ_{23} arrows. The bimodule operation $m_2(q, \sigma_{23}) = \rho_{23}\, q$ implies that an ingoing or outgoing ρ_{23} arrow at y_i gives rise to the same arrow at $q \otimes y_i$. The operation $m_2(r, \sigma_3) = \rho_{23}\, q$ implies that an incoming ρ_3 arrow at y_i gives rise to an incoming ρ_{23} arrow at $q \otimes y_i$, and the operation $m_2(p, \sigma_1) = \rho_1\, q$ implies that an incoming ρ_1 arrow at y_i gives rise to an incoming ρ_1 arrow at $q \otimes y_i$. There are no other incoming or outgoing arrows at $q \otimes y_i$ for any i. It follows that $q \otimes y_1$ has the form of y_3, $q \otimes y_2$ has the form of y_4, $q \otimes y_3$ has the form of y_3, and $q \otimes y_4$ has the form of y_4.

The effect of $\widehat{CFDA}(Y_{\Gamma_a})$ on a representative sequence of generators in M is pictured

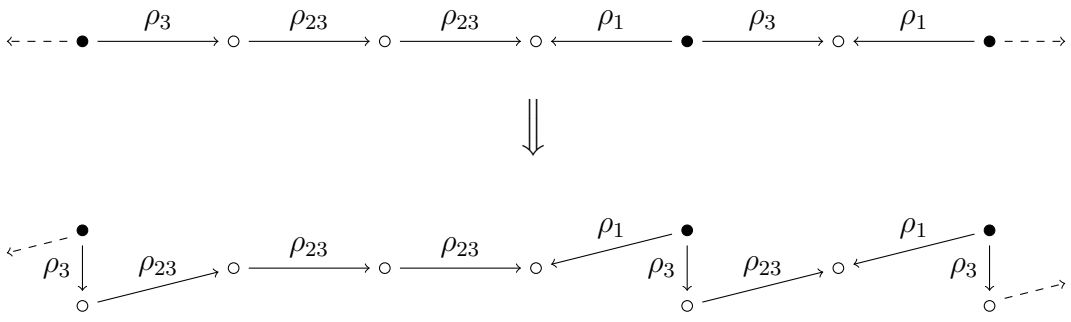

Figure 24: The effect of tensoring with $\widehat{CFDA}(Y_{\Gamma_a})$ on a typical sequence of generators of a module M which satisfies the conclusion of Theorem 3. Each generator gives rise to one or two generators in the tensor product, depending on the idempotent of the original generator. The generators of the tensor product still have the form required in Theorem 3.

in Figure 24.

Bimodule for Γ_b: We first find the type D module for the trivial S^1-bundle over the cylinder parametrized so that α_2 is the fiber on each boundary. This bordered manifold can be obtained from $\mathcal{Y}_{\mathcal{P}}$ by capping off one boundary with a solid torus as in Figure 19(a). The bimodule $\widehat{CFDA}(Y_{\Gamma_b})$ is obtained from this by twice tensoring with the Dehn twist bimodule $\widehat{CFDA}(\tau_m^{-1})$ and tensoring with $\widehat{CFAA}(\mathbb{I})$ to change one boundary to type a. The result has six generators, which we label a, b, c, d, e, and f. Once again, we can ignore operations with ρ_2, ρ_{12}, or ρ_{123} as inputs. There are nine relevant operations:

$$\begin{array}{ccc} m_1(a) = \rho_3\, c & m_1(c) = \rho_2\, b & m_1(a) = \rho_3\, c \\ m_1(e) = \rho_{23}\, f & m_2(a, \rho_1) = d & m_2(b, \rho_1) = \rho_3\, f \\ m_2(b, \rho_3) = \rho_1\, f & m_2(c, \rho_1) = e & m_2(d, \rho_{23}) = \rho_1\, f \end{array}$$

If M is a module of the form described in the theorem, then every generator of $\widehat{CFDA}(Y_{\Gamma_b}) \boxtimes M$ has the form of $a \otimes x$, $b \otimes x$, $c \otimes x$, $d \otimes y_i$, $e \otimes y_i$, or $f \otimes y_i$. We must show that each of these generators either is canceled by a differential or has one of the five types specified in the theorem after unlabeled arrows are canceled.

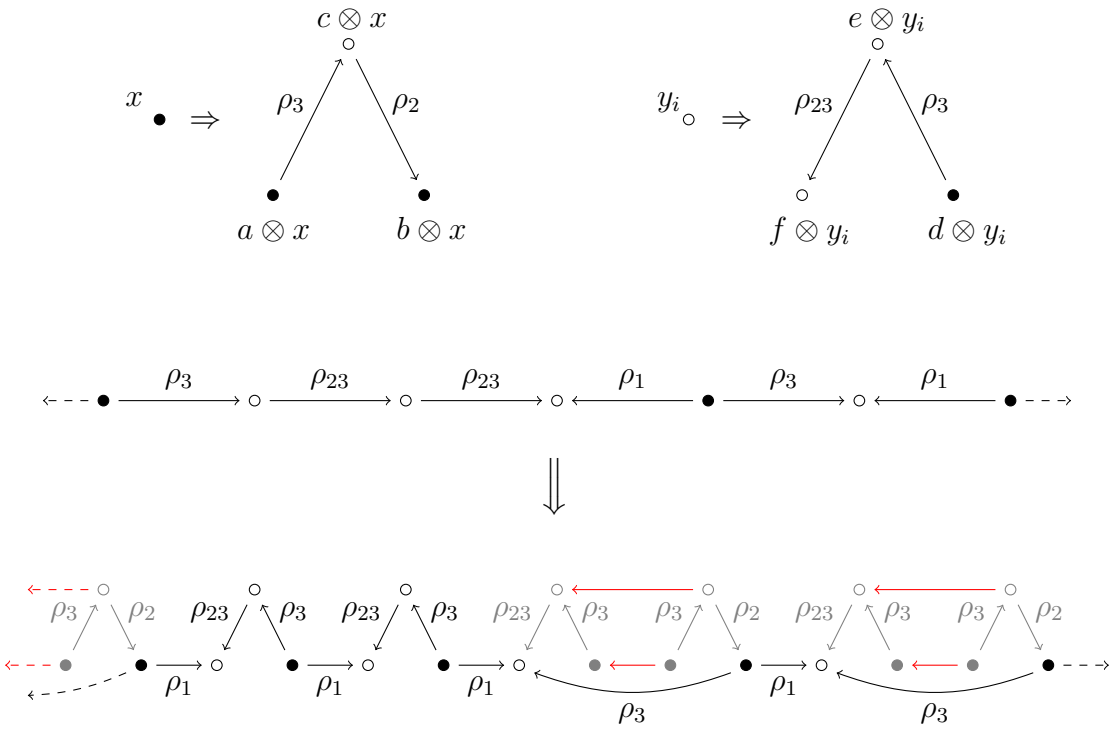

Figure 25: The effect of tensoring with $\widehat{CFDA}(Y_{\Gamma_b})$ on a typical sequence of generators of a module M which satisfies the conclusion of Theorem 3. Red arrows represent differentials. Gray indicates generators and arrows that are canceled when the differential is cancelled. In the resulting module (black), every generator is of the form required in Theorem 3.

The operations $m_2(a, \rho_1) = d$ and $m_2(c, \rho_1) = e$ imply that there are unlabeled arrows from $a \otimes x$ to $d \otimes y_i$ and from $c \otimes x$ to $e \otimes y_i$ for $i \in \{2, 4\}$. There are no other unlabeled arrows. Furthermore, there are no other arrows coming from generators of the form $a \otimes x$, so we can cancel the unlabeled arrows from $a \otimes x$ to $d \otimes y_i$ without adding extra arrows. Once this is done, there are no arrows into $e \otimes y_i$ except for the unlabeled one from $c \otimes x$, so this differential may be cancelled without introducing new arrows as well.

After canceling unlabeled arrows to eliminate all generators of the form $a \otimes x$, $c \otimes x$, $d \otimes y_2$, $d \otimes y_4$, $e \otimes y_2$, or $e \otimes y_4$, it is straightforward to check that the remaining generators have the desired form. This is pictured for a typical segment of M in Figure 25.

Trimodule for Γ_c: Recall that $\bar{\mathcal{Y}}_{\mathcal{P}}$ denotes the mirror of the bordered manifold $\mathcal{Y}_{\mathcal{P}}$,

and the type D trimodule for $\bar{\mathcal{Y}}_{\mathcal{P}}$ can be easily obtained from that of $\mathcal{Y}_{\mathcal{P}}$. The type DAA trimodule associated to Γ_c can be obtained from $\widehat{CFD^3}(\bar{\mathcal{Y}}_{\mathcal{P}})$ by tensoring with $\widehat{CFDA}(\tau_m)$ to increase the euler number by one. This represents a single valence three vertex with euler number 1. Adding the 0-weighted vertices in Γ_c has the same effect as changing the parametrization of the corresponding boundary component so that α_1 is the fiber instead of α_2. This agrees with the given parametrization of the ρ and τ boundaries of $\bar{\mathcal{Y}}_{\mathcal{P}}$, so we simply tensor with $\widehat{CFAA}(\mathbb{I})$ on these boundaries to change them to type A. The resulting trimodule has 6 generators.

Let M_1 and M_2 be type D modules of the form described in Theorem 3. We need to show that $\widehat{CFDAA}(Y_{\Gamma_c}) \boxtimes M_1 \boxtimes M_2$ also has the form described in the theorem. Once again, to compute this tensor product we may ignore operations which have ρ_2, ρ_{12}, or ρ_{123} as inputs. The relevant operations of $\widehat{CFDAA}(Y_{\Gamma_c})$ are listed below. Inputs of $\mathcal{A}_\infty$ operations are written as ρ or τ, depending on which type A boundary they represent.

$$
\begin{array}{lll}
m_1(b) = \rho_2\, a & m_2(d, \tau_{23}) = \rho_{23}\, d & m_2(f, \tau_{23}) = \rho_{23}\, f \\
m_2(b, \tau_3) = c & m_2(d, \rho_{23}) = f & m_3(a, \tau_3, \tau_{23}) = \rho_3\, c \\
m_2(b, \rho_3) = e & m_2(e, \tau_3) = f & m_3(a, \rho_1, \tau_1) = \rho_1\, d \\
m_2(c, \rho_3) = f & m_2(e, \tau_3) = \rho_{23}\, d & m_3(a, \rho_3, \tau_3) = \rho_3\, d \\
m_2(c, \tau_{23}) = \rho_{23}\, c & m_2(e, \rho_{23}) = \rho_{23}\, e & m_3(a, \rho_3, \rho_{23}) = \rho_3\, e \\
m_2(d, \tau_{23}) = f & &
\end{array}
$$

Note that there is only one operation involving ρ_1 or τ_1. If we exclude this operation, then the box tensor product $\widehat{CFDAA}(Y_{\Gamma_c}) \boxtimes M_1 \boxtimes M_2$ can be be understood by restricting to the connected components of the graphs obtained from M_1 and M_2 by removing ρ_1 and τ_1 arrows. Let M_1' and M_2' be such components. Thus M_1' is a chain of arrows consisting one ρ_3 arrow followed by any number of ρ_{23} arrows, and similarly for M_2'. Consider the module $\widehat{CFDAA}(Y_{\Gamma_c}) \boxtimes M_1' \boxtimes M_2'$. The result of this tensor product is depicted in Figure 26. If M_1' has at least one ρ_{23} arrow (as in the figure), then after canceling unlabeled arrows the result is a chain of arrows consisting of a ρ_3 arrow and some ρ_{23} arrows (vertical in the diagram) followed more ρ_{23} arrows (horizontal in the diagram). If M_1' does not have

a ρ_{23} arrow then the vertical ρ_3 arrow in the diagram does not exist, but the diagonal ρ_3 arrow is not eliminated when differentials are canceled. In this case the result is a ρ_3 arrow (diagonal) followed by a chain of ρ_{23} arrows (horizontal). In either case, the result is a chain of arrows with each generator of the form required by the theorem.

If we ignore the ρ_1 and τ_1 arrows in M_1 and M_2, we find that $\widehat{CFDA}(Y_{\Gamma_c}) \boxtimes M_1 \boxtimes M_2$ is a disjoint union of chains of ρ_3 and ρ_{23} arrows. When we consider the ρ_1 and τ_1 arrows, the operation $m_3(a, \rho_1, \tau_1)$ in $\widehat{CFDA}(Y_{\Gamma_c})$ determines how these chains are connected. It follows that they are connected by ρ_1 arrows in a way that forms loops of the type required.

□

The inductive step in the proof of Theorem 3 can be used to quickly compute $\widehat{CFD}$ for one boundary graph manifolds with no bad vertices. The theorem implies that we can record $\widehat{CFD}$ as a collection of lists of nonnegative integers, each defined up to cyclic permutation; each list of integers represents a loop in the graph of $\widehat{CFD}$ and each integer k represents a sequence of one ρ_3 arrow and k ρ_{23} arrows followed by a backwards ρ_1 arrow. Note that for the bordered graph manifold represented by a single -1 weighted vertex, the base case of induction in Theorem 3, $\widehat{CFD}$ is represented by the single list (0). We only need to determine the effect of the three inductive operations on these loops.

Tensoring with the bimodule in part (a) of the inductive step adds a ρ_{23} to each segment in a loop. Thus, in the cyclic lists of integers notation, the effect is simply to add one to each integer in each list.

$$(k_1, \ldots, k_n) \longmapsto (k_1 + 1, \ldots, k_n + 1)$$

Tensoring with the bimodule in part (b) of the inductive step replaces a segment with k ρ_{23}'s with a segment with no ρ_{23}'s followed by k segments with one ρ_{23}. It also reverses the orientation of the loop. Thus for each cyclic list of integers we reverse the order of

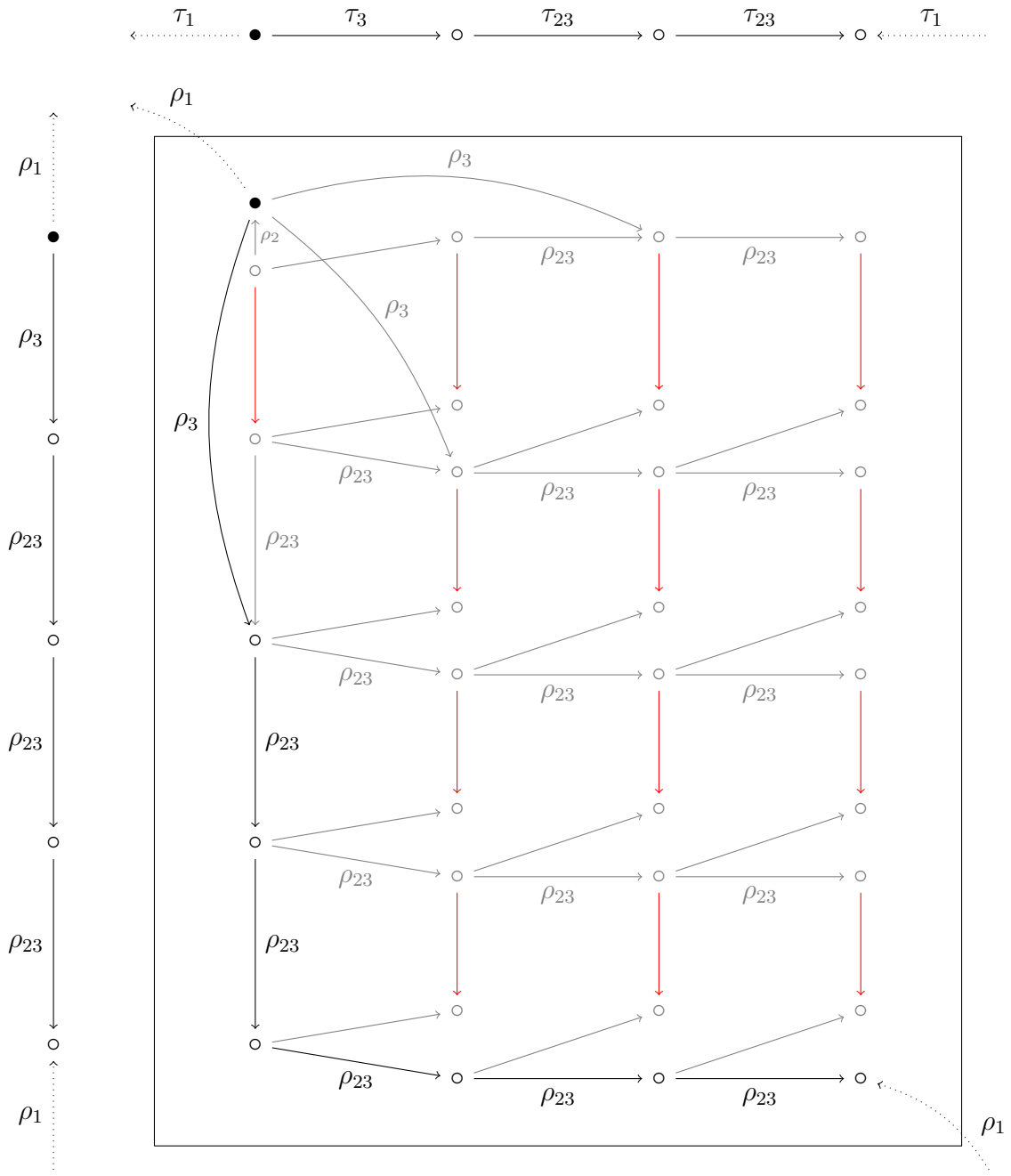

Figure 26: The portion of $\widehat{CFDA}(Y_{\Gamma_b}) \boxtimes M_1 \boxtimes M_2$ coming from a typical piece of M_1 (left) and a typical piece of M_2 (top). Red arrows represent differentials that can be canceled. Gray indicates generators and arrows that are eliminated when the differentials are cancelled.

the list and replace each integer k with a 0 followed by k 1's.

$$(k_1, \ldots, k_n) \longmapsto (0, \underbrace{1, \ldots, 1}_{k_n}, 0, \ldots, 0, \underbrace{1, \ldots, 1}_{k_1})$$

Finally, tensoring with the trimodule in part (c) of the inductive step pairs a segment with k ρ_{23}'s and a segment with ℓ $\rho'_{23}s$ to produce a segment with $(k+\ell)$ ρ_{23}'s. These segments are connected diagonally. Given a cyclic list $(k_1, \ldots, k_n)$ for the first input and $(\ell_1, \ldots, \ell_m)$ for the second inputs, we produce new list(s) for the tensor product by taking $(k_1 + \ell_1, k_2 + \ell_2, \ldots)$. The indices of both k and ℓ increase by one for each term and are counted mod n and mod m, respectively. The loop ends after $lcm(n, m)$ terms, when it will return to $k_1 + \ell_1$. If the term $k_2 + \ell_1$ does not appear in this first loop then we form a second loop in the same way starting $(k_2 + \ell_1, k_3 + \ell_2, \ldots)$. There will be loops starting with $k_i + \ell_1$ for i up to $gcd(n, m)$. In all there will be $gcd(n, m)$ cyclic lists of length $lcm(n, m)$. For example, if $\widehat{CFD}(\Gamma')$ and $\widehat{CFD}(\Gamma'')$ are represented by the lists $(0, 2, 1, 2)$ and $(0, 1)$, respectively, then $\widehat{CFD}(\Gamma)$ will be represented by the lists $(0, 3, 1, 3)$ and $(2, 2, 2, 1)$.

	0	2	1	2
0	**0**	2	**1**	2
1	1	**3**	2	**3**

By using this cyclic list notation and the three operations described above, we can compute $\widehat{CFD}$ for plumbing trees with no bad vertices without computing any tensor products. This approach gives a very efficient method for computing $\widehat{CFD}$ in this special case.

Bibliography

[1] Steven Boyer, Cameron McA. Gordon, and Liam Watson, *On L-spaces and left-orderable fundamental groups*, Math. Ann. **356** (2013), no. 4, 1213–1245. MR3072799

[2] Robert Gompf and András Stipsicz, *4-manifolds and kirby calculus*, Amer. Math. Soc., Providence, RI, 1999.

[3] Jonathan Hales, Dmytro Karabash, and Michael T. Lock, *A modification of the Sarkar-Wang algorithm and an analysis of its computational complexity*, 2007.

[4] Matthew Hedden and Adam Simon Levine, *Splicing knot complements and bordered Floer homology*, 2012.

[5] Stanislav Jabuka and Thomas E. Mark, *On the Heegaard Floer homology of a surface times a circle*, Adv. Math. **218** (2008), no. 3, 728–761. MR2414320 (2010j:57044)

[6] Adam Simon Levine, *Knot doubling operators and bordered Heegaard Floer homology*, 2010.

[7] Robert Lipshitz, *A cylindrical reformulation of Heegaard Floer homology*, Geom. Topol. **10** (2006), 955–1097. MR2240908 (2007h:57040)

[8] Robert Lipshitz, Peter S. Ozsváth, and Dylan P. Thurston, *Bordered Heegaard Floer homology: Invariance and pairing*, 2008.

[9] ———, *Bimodules in bordered Heegaard Floer homology*, 2010.

[10] ———, *Computing $\widehat{HF}$ by factoring mapping classes*, 2010.

[11] Robert Lipshitz and David Treumann, *Noncommutative Hodge-to-de Rham spectral sequence and the Heegaard Floer homology of double covers*, 2012.

[12] Paolo Lisca and András I. Stipsicz, *On the existence of tight contact structures on Seifert fibered 3-manifolds*, Duke Math. J. **148** (2009), no. 2, 175–209. MR2524494 (2010c:53127)

[13] Ciprian Manolescu, Peter Ozsváth, and Sucharit Sarkar, *A combinatorial description of knot Floer homology*, Ann. of Math. (2) **169** (2009), no. 2, 633–660. MR2480614 (2009k:57047)

[14] Ciprian Manolescu and Peter S. Ozsváth, *Heegaard Floer homology and integer surgeries on links*, 2010.

[15] Ciprian Manolescu, Peter S. Ozsváth, and Dylan P. Thurston, *Grid diagrams and Heegaard Floer invariants*, 2009.

[16] Mauro Mauricio, *On lattice cohomology and left–orderability*, 2013.

[17] András Némethi, *Lattice cohomology of normal surface singularities*, Publ. Res. Inst. Math. Sci. **44** (2008), no. 2, 507–543. MR2426357 (2009m:32053)

[18] Walter D. Neumann, *A calculus for plumbing applied to the topology of complex surface singularities and degenerating complex curves*, Trans. Amer. Math. Soc. **268** (1981), no. 2, 299–344. MR632532 (84a:32015)

[19] ———, *Graph 3-manifolds, splice diagrams, singularities*, Singularity theory, 2007, pp. 787–817. MR2342940 (2008k:32085)

[20] Peter Ozsváth, András I. Stipsicz, and Zoltán Szabó, *Combinatorial Heegaard Floer homology and nice Heegaard diagrams*, Adv. Math. **231** (2012), no. 1, 102–171. MR2935385

[21] Peter Ozsváth and Zoltán Szabó, *On the Floer homology of plumbed three-manifolds*, Geom. Topol. **7** (2003), 185–224 (electronic). MR1988284 (2004h:57039)

[22] ———, *Holomorphic disks and knot invariants*, Adv. Math. **186** (2004), no. 1, 58–116. MR2065507 (2005e:57044)

[23] ———, *Holomorphic disks and topological invariants for closed three-manifolds*, Ann. of Math. (2) **159** (2004), no. 3, 1027–1158. MR2113019 (2006b:57016)

[24] ———, *Holomorphic triangles and invariants for smooth four-manifolds*, Adv. Math. **202** (2006), no. 2, 326–400. MR2222356 (2007i:57029)

[25] Peter S. Ozsváth, András Stipsicz, and Zoltán Szabó, *Knot lattice homology in L-spaces*, 2012.

[26] ———, *Knots in lattice homology*, 2012.

[27] ———, *A spectral sequence on lattice homology*, 2012.

[28] Peter S. Ozsváth, András I. Stipsicz, and Zoltán Szabó, *A combinatorial description of the $U^2 = 0$ version of Heegaard Floer homology*, Int. Math. Res. Not. IMRN **23** (2011), 5412–5448. MR2855074

[29] Thomas Peters, *On l-spaces and non left-orderable 3-manifold groups*, 2009.

[30] Jacob Andrew Rasmussen, *Floer homology and knot complements*, ProQuest LLC, Ann Arbor, MI, 2003. Thesis (Ph.D.)–Harvard University. MR2704683

[31] Sucharit Sarkar and Jiajun Wang, *An algorithm for computing some Heegaard Floer homologies*, Ann. of Math. (2) **171** (2010), no. 2, 1213–1236. MR2630063 (2012f:57032)